(4)

The University of Texas at Dallas
Center for Quantum Electronics
The Gamma-Ray Laser Project
Quarterly Report
July-September 1988

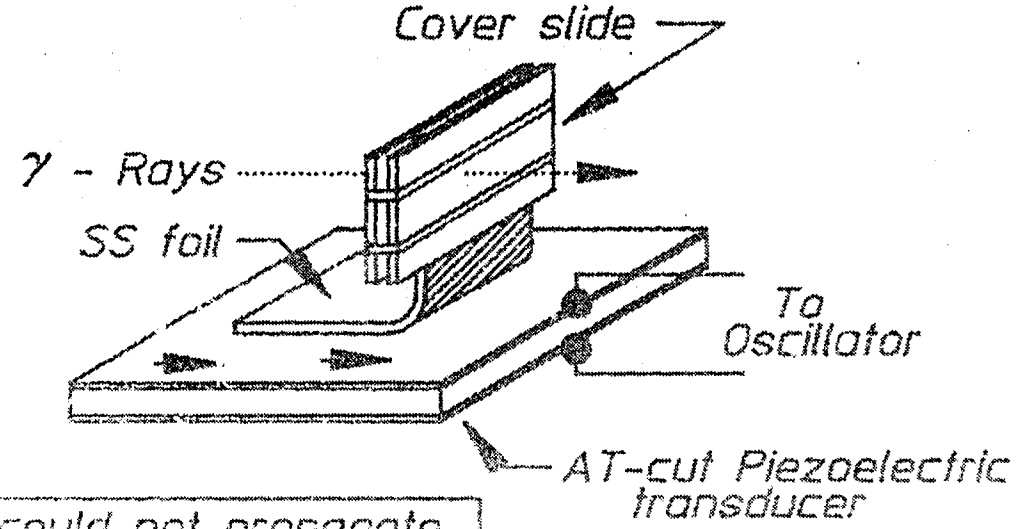

Phonons could not propagate far enough to make sidebands at the point of observation.

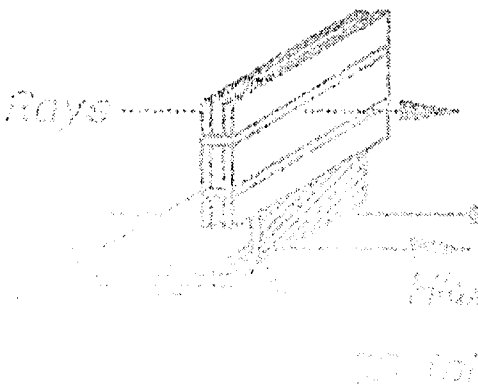

REPORT GRL/8802

PROOF OF THE FEASIBILITY OF COHERENT AND INCOHERENT SCHEMES FOR PUMPING A GAMMA-RAY LASER

Principal Investigator: Carl B. Collins
The University of Texas at Dallas
Center for Quantum Electronics
P.O. Box 830688
Richardson, Texas 75083-0688

October 1988

Quarterly Technical Progress Report
1 July 1988 through 30 September 1988
Contract Number N00014-86-C-2488

Prepared for
INNOVATIVE SCIENCE AND TECHNOLOGY DIRECTORATE
OF STRATEGIC DEFENSE INITIATIVE ORGANIZATION

Contracting Officer's Technical Representative
Dr. Paul Kepple, Code 4720
Naval Research Laboratory
4555 Overlook Avenue, SW
Washington, DC 20375-5000

SECURITY CLASSIFICATION OF THIS PAGE (When Data Entered)

REPORT DOCUMENTATION PAGE

READ INSTRUCTIONS BEFORE COMPLETING FORM

1. REPORT NUMBER: GRL/8802	2. GOVT ACCESSION NO.
3. RECIPIENT'S CATALOG NUMBER	
4. TITLE (and Subtitle): PROOF OF THE FEASIBILITY OF COHERENT AND INCOHERENT SCHEMES FOR PUMPING A GAMMA-RAY LASER	5. TYPE OF REPORT & PERIOD COVERED: Quarterly Technical Progress 7/1/88 - 9/30/88
	6. PERFORMING ORG. REPORT NUMBER
7. AUTHOR(s): C. B. COLLINS	8. CONTRACT OR GRANT NUMBER(s): N00014-86-C-2488
9. PERFORMING ORGANIZATION NAME AND ADDRESS: University of Texas at Dallas, Center for Quantum Electronics, P.O. Box 830688, Richardson, TX 75083-0688	10. PROGRAM ELEMENT, PROJECT, TASK AREA & WORK UNIT NUMBERS
11. CONTROLLING OFFICE NAME AND ADDRESS: INNOVATIVE SCIENCE AND TECHNOLOGY DIRECTORATE OF STRATEGIC DEFENSE INITIATIVE ORGANIZATION	12. REPORT DATE: October, 1988
	13. NUMBER OF PAGES: 126
14. MONITORING AGENCY NAME & ADDRESS (if different from Controlling Office): Dr. Paul Kepple, Code 4720, Naval Research Laboratory, 4555 Overlook Avenue, SW, Washington, DC 20375-5000	15. SECURITY CLASS. (of this report): Unclassified
	15a. DECLASSIFICATION/DOWNGRADING SCHEDULE

16. DISTRIBUTION STATEMENT (of this Report)

This document has been approved for public release and sale; its distribution is unlimited.

17. DISTRIBUTION STATEMENT (of the abstract entered in Block 20, if different from Report)

18. SUPPLEMENTARY NOTES

19. KEY WORDS (Continue on reverse side if necessary and identify by block number)

20. ABSTRACT (Continue on reverse side if necessary and identify by block number)

Recent approaches to the problem of the gamma-ray laser have focused upon upconversion techniques in which metastable nuclei are pumped with long wavelength radiation. At the nuclear level the storage of energy can approach tera-Joules (10^{12}J) per liter for thousands of years. However, any plan to use such a resource for a gamma-ray laser poses problems of a broad interdisciplinary nature requiring the fusion of concepts taken
(continued next page)

DD FORM 1 JAN 73 1473 EDITION OF 1 NOV 65 IS OBSOLETE

20. Abstract (continued)

from relatively unrelated fields of physics. Our research group has described several means through which this energy might be coupled to the radiation fields with cross sections for stimulated emission that could reach 10^{-17} cm^2. Such a stimulated release could lead to output powers as great as 3×10^{21} Watts/liter. Since 1978 we have pursued an approach for the upconversion of longer wavelength radiation incident upon isomeric nuclear populations that can avoid many of the difficulties encountered with traditional concepts of single photon pumping. Recent experiments have confirmed the general feasibility and have indicated that a gamma-ray laser is feasible if the right combination of energy levels and branching ratios exists in some real material. Of the 1886 distinguishable nuclear materials, the present state-of-the-art has been adequate to identify 29 first-class candidates, but further evaluation cannot proceed without remeasurements of nuclear properties with higher precision. A laser-grade database of nuclear properties does not yet exist, but the techniques for constructing one have been developed under this contract and are now being utilized. Resolution of the question of the feasibility of a gamma-ray laser now rests upon the determination of: 1) the identity of the best candidate, 2) the threshold level of laser output, and 3) the upconversion driver for that material.

This quarter's report focuses upon a breakthrough recently realized along the more complex direction toward the coherent pumping of a gamma-ray laser. In this process the intent is to mix the quantum properties of long-lived nuclear states with those able to radiate freely. In this way the metastability of an isomeric state could be "switched off". The critical experiment is to show that some laboratory level of coherent input power can affect the properties of a nuclear level. Reported here are the details of a series of experiments which clearly demonstrated that large levels of modulation of the phases of nuclear states can be obtained with relatively modest input powers. Now many more critical experiments become possible even along this more complex path toward a gamma-ray laser. Also reported here are the most recent advances we have made in the preparation of the thin film diamond materials. Efficacy of the unique laser plasma process we describe is so great that it already has become clear that applications will range far beyond the support of this gamma-ray laser project.

TABLE OF CONTENTS

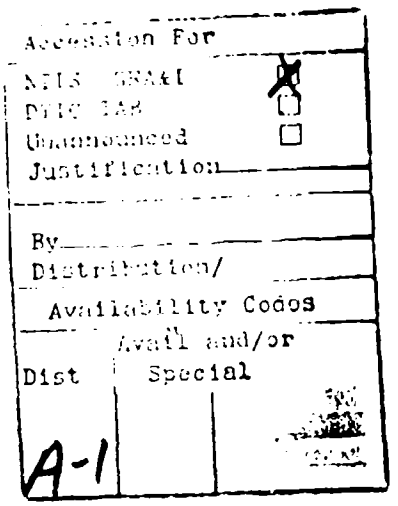

PREFACE

This report shares one of the great pleasures of conducting in an academic environment this research into the feasibility of a gamma-ray laser. Much of our work is done by graduate students who are able to incorporate their achievements into dissertations of the high quality required for the award of their Ph.D. degrees. The focus of our report this quarter is upon the most recent success of this type of synergism.

Previous reports have focused upon the most direct approach to the pumping of a gamma-ray laser, the nuclear analog of the ruby laser. Such excitement has been generated along that line that it has tended to eclipse the sustained progress enjoyed in our other approaches. One of the most difficult breakthroughs was recently realized along the more complex direction of coherent pumping. In this process the intent is to mix the quantum properties of long-lived nuclear states with those able to radiate freely. In this way the metastability of an isomeric state could be "switched off." The critical experiment is to show that some laboratory level of coherent input power can affect the properties of a nuclear level. Reported recently was the demonstration that large levels of modulation of the phases of nuclear states can be obtained with relatively modest input powers.

The conceptual key to this breakthrough lay in the realization that large amplitude spin waves could be transported from sources in ferromagnetic media into paramagnetic hosts containing the nuclei of interest. The long range ordering of the spins in ferromagnetic samples allows one to obtain with a few Watts of power the level of modulation of the magnetization in the material that would otherwise require gigawatts of applied power in the absence of these natural process of amplification. The essential demonstration was that these great levels of magnetic modulation could be transported as spin waves into less magnetic materials where they could couple directly to the nuclear magnetic moments. The resulting interaction energies experienced by the nuclear states were of a scale that would have required gigawatts of power be applied to the nonmagnetic material had the spin waves not been used. The development and proof of this technique are detailed in the dissertation by T. W. Sinor presented in this quarterly report because of

its importance; however, all usual copyrights are retained by the author. It is a pleasure to report that Dr. Sinor successfully defended this great accomplishment and was awarded the Ph.D.

Also presented in this report is the most recent advance we have made in the preparation of thin film diamond material. Efficacy of the unique process we describe is so great that it already appears applications will range far beyond the support of the Mössbauer studies we originally envisioned.

Continuing the preparation of this report as an "in-house" journal, this series presents material to reflect the individual contributions of the teams of research faculty and graduate students involved in these phases of the research. In this regard I wish to thank all our staff for their splendid efforts in supporting the preparation of these manuscripts to a rather demanding timetable.

C. B. Collins
Director
Center for Quantum Electronics

A LASER PLASMA SOURCE OF AMORPHIC DIAMOND

by C. B. Collins, F. Davanloo, E. M. Juengerman, W. R. Osborn, and D. R. Jander

The past few years have witnessed a renaissance in the preparation and study of thin films of carbon having diamond-like properties.[1] However, while natural diamond is a well-defined substance, these diamond-like films are not. In many cases different materials result from the different methods of preparation and this has contributed much complexity to the evaluation of the merits of the different techniques of growth.

From a structural viewpoint, Spencer[2] has identified six allotropes of carbon, two for each of the numbers of dimensions through which the carbon atoms may bond. The ones most important in the formation of thin films of diamond-like carbon (DLC) are the two dimensional sp^2 bonds which characterize graphite and the three dimensional sp^3 bonds which give cubic diamond its unique properties.

From the standpoint of mechanical and electrical properties the best results have been obtained with a class of DLC materials denoted as a-C:H, the "a" suggesting an amorphic structure. They can be grown by a variety of techniques for chemical vapor deposition (CVD) at rates practical for commercial applications. Surprisingly, these materials contain hydrogen in amounts which vary from about 20 to 60%. Within these limits the amount of hydrogen correlates with the proportions of sp^3 to sp^2 bondings and thus, with the prevalence of diamond-like properties. A reduction in the amount of hydrogen in such a film degrades it toward graphite. At 20% there is a discontinuity in stability and only pure carbon films can exist with less than this limiting amount of hydrogen.[1]

Denoted as a-C films, these unhydrogenated DLC films have received relatively little attention, although they have been known for quite some time. As early as 1971, Aisenberg and Chabot[3] reported the quenching of a beam of C^+ ions in the presence of Ar and Ar^+ on a cold substrate to form an amorphic layer containing no hydrogen, yet having some diamond-like properties. Spencer, et al.,[2] continued this line of development in 1976, attributing the favorable properties of the deposited layers to the selective destruction of exposed sp^2 bonds by the bombarding ions. However, with these early ion beam methods the

growth rates were extremely slow and the material they produced remained only a curiosity until relatively recent times.

With a high fluence ion source Miyazawa et al.[4] brought growth rates up to about 360 A/hr on a one cm^2 substrate, while Savvides[5,6] achieved 500 A/hr on a 20 cm^2 area with a sputtered source of carbon ions and atoms. Even higher growth rates were demonstrated at the cost of degraded film quality. The resulting availability of samples of a tangible scale together with the potential importance of such films in optical applications seems to have motivated an intensive study of their optical properties. Unlike the a-C:H materials these unhydrogenated DLC films were moderately clear in the visible wavelengths and Miyazawa recorded the observation of colored interference fringes.[4] The resulting indices of refraction reported by Miyazawa and Savvides[5] are collected in Fig. 1a and 1b.

While the real parts of the indices in Fig. 1a are interesting in their approaches to the value of 2.42 for natural diamond, the greatest diagnostic significance lies in the imaginary parts, shown in Fig. 1b. Savvides has shown[5,6] how at small values this extinction coefficient is reasonably proportional to the fraction of sp^2 bondings in the film, provided the real part is reasonably constant. Purely diamond-like sp^3 bonding would give no loss at these photon energies. The lower curve, identified by the 5 W of input power to the sputtering source in Savvides' system, provides a calibration that is identified with a 25% content of graphitic, sp^2 bonds. Though not computed previously, it can be seen that Miyazawa's films should have contained only about 10% of the sp^2 bonding. This compares favorably with the best results[1] attained by using hydrogen to minimize to 14% the proportions of sp^2 bonds in a-C:H. Since the latter material is black in the visible because of the hydrogen bonding, the a-C films might be the preferred choice for applications, were the growth rates of practical magnitudes. Moreover, if the residual sp^2 bonds could be shown to be an artifact of the production, as opposed to being a necessary ingredient for stability, then the direction would be shown toward the development of truly amorphic diamond containing only sp^3 bonds.

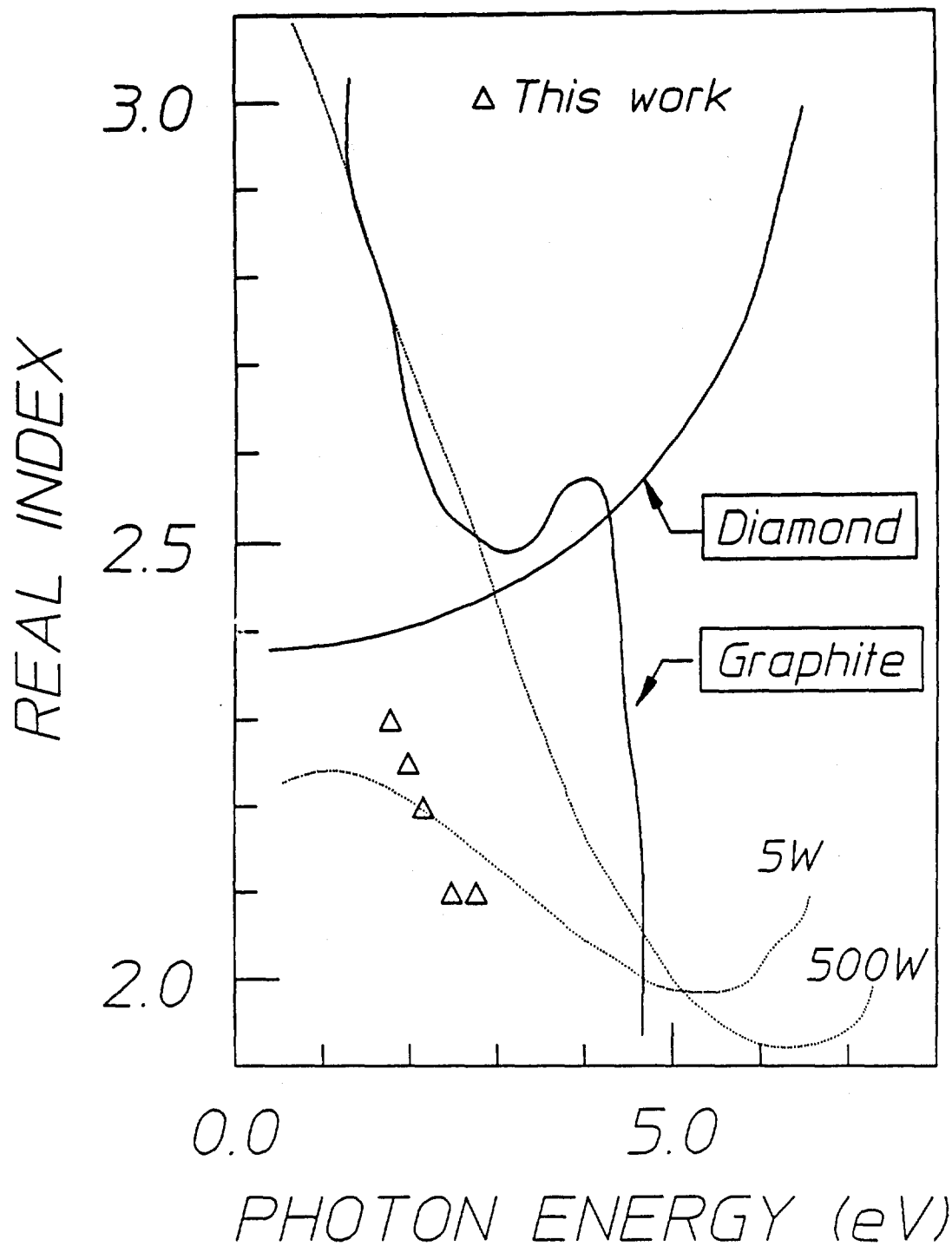

Fig.1(a): Symbols plot the real parts of the refractive indices of a-C films produced by the laser plasma source described in this work as functions of photon energy together with comparative values for diamond and graphite as indicated. Dotted curves show the results reported in Ref. 6 for films prepared with a sputter ion source operated at the powers shown.

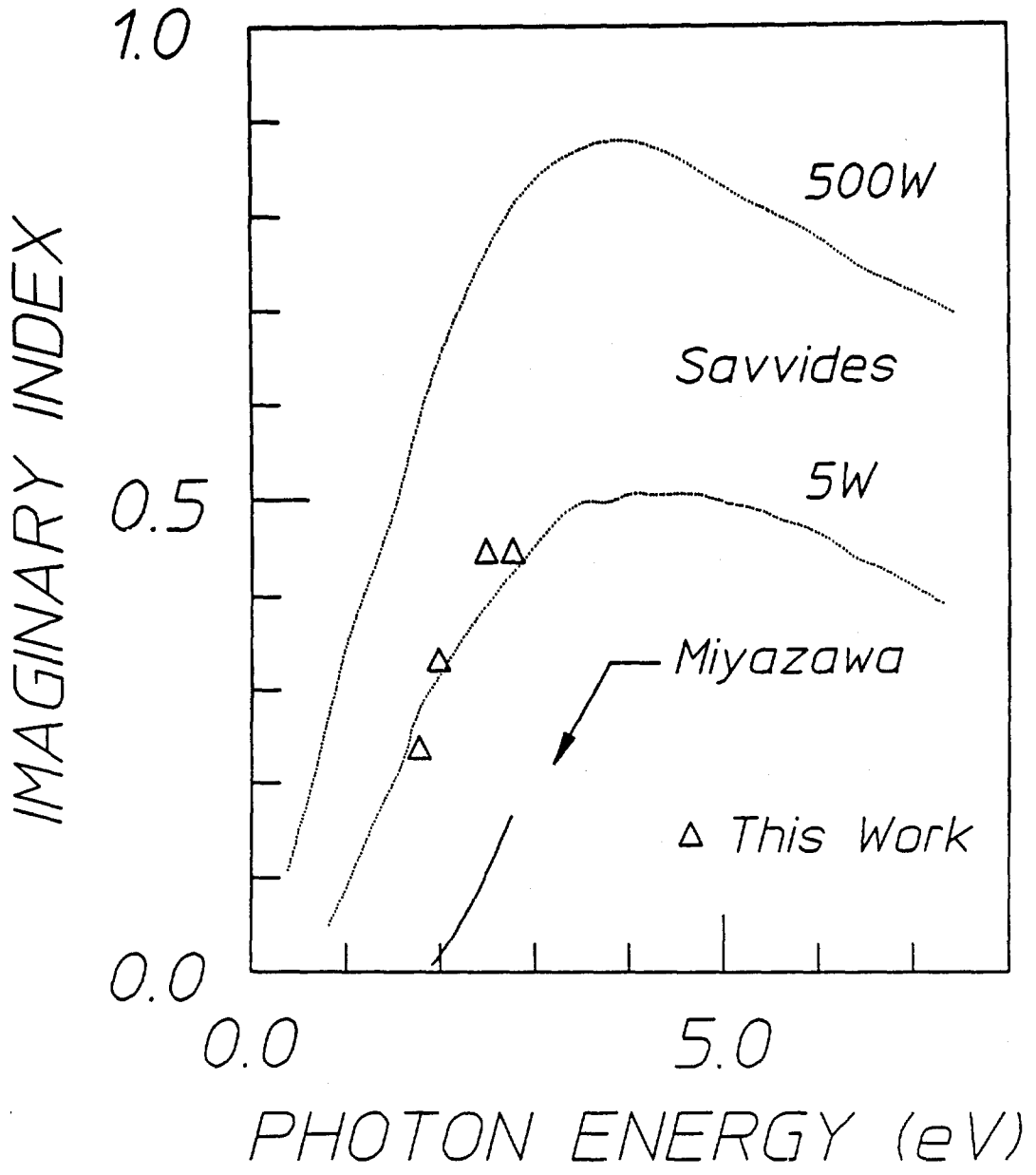

Fig.(1)b: Symbols plot the imaginary parts of the refractive indices of a-C films produced by the laser plasma source described in this work as functions of photon energy. Comparable values of the refractive indices of a-C films reported by Savvides in Ref.6 are shown by the dotted lines for the two powers used in his process while results reported by Miyazawa in Ref. 4 are plotted by the solid curve.

Reported here is the deposition and characterization of several a-C films grown at rates of 3000 A/hr on 30 cm^2 areas with a laser plasma source. Losses indicate that the proportion of sp^2 bonding is comparable to the best of Savvides samples and can be reduced further with lasers of higher power that are commercially available. It is believed that this material can be reasonably described as amorphic diamond with 25% impurities and that the sp^2 inclusions serve no necessary role.

The experimental arrangement is shown in Fig. 2. As can be seen it represents a substantial evolution from the laser plasma device we described earlier,[7] both in the electronics and in the laser. The laser plasma source of Wagal[7], together with the earlier sources of Richter[8] and Sato[9], had been limited to peak intensities at the graphite feedstock of a few $\times 10^{10}$, 10^8, and 10^9 W/cm^2, respectively. The system shown in Fig. 2 delivers 5×10^{11} W/cm^2 in a 15 nsec pulse to the graphite target. While Sato[9] and Wagal[7] used supplementary electrodes for cleaning the substrate and for steering the ions, respectively, the system in Fig. 2 incorporates an auxiliary discharge to further increase the plasma temperature by Joule heating in the small volume of the ablation plume.

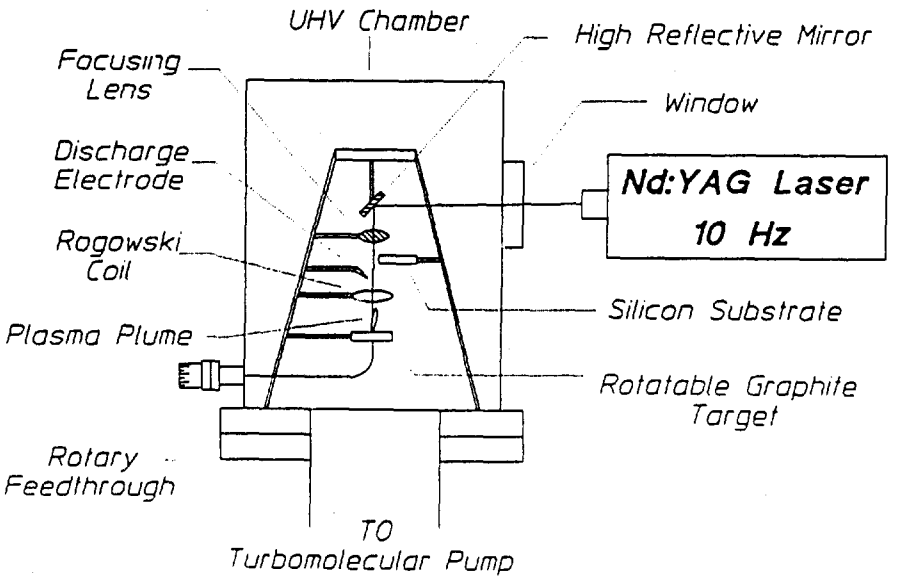

Fig.2: Schematic representation of the laser plasma source used in this work to prepare amorphic diamond films.

The current which was passed from electrode to the ablation plume was measured with a Ragowski coil, electrically isolated from the deposition system. A typical result is shown in Fig. 3 where it can be seen that currents peak in the 1-10 A range in a pulse found to have FWHM of the order of 2 μsec. From the time-dependence of the current it appears that it flows only when the ejected material is filling the space between the point of ablation and the electrode, as would be expected.

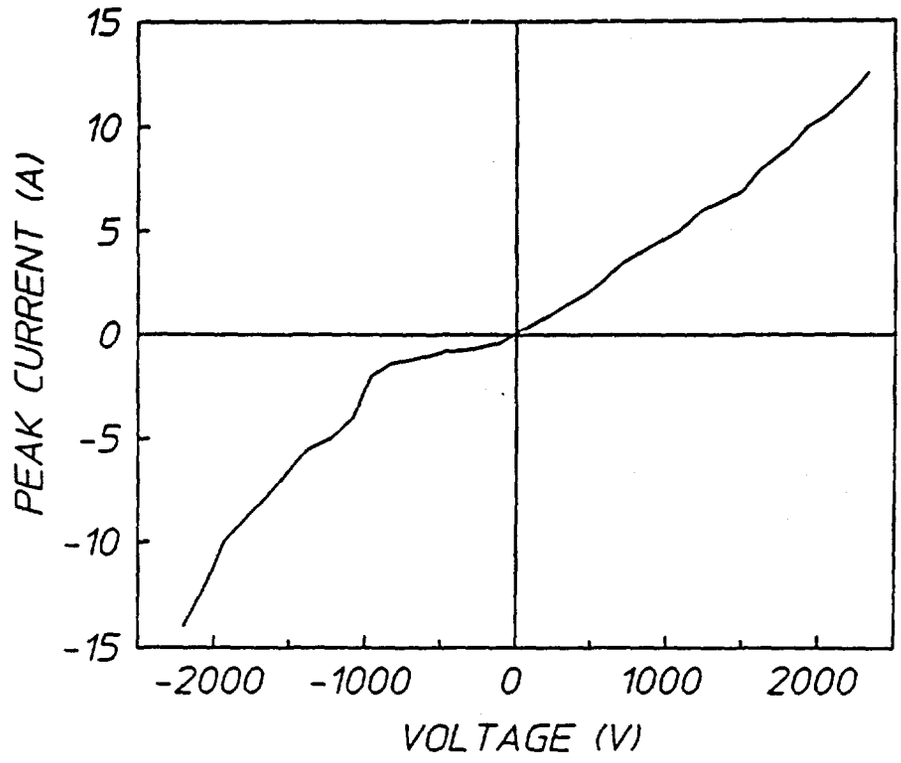

Fig.3: Plot of the current and voltage characteristics of the diode formed by the graphite target and the grid containing the conductive plasma ablated from the graphite by the laser.

The V-I characteristics seen in Fig. 3 are typical for a gas-filled diode with the "forward" direction for conduction being established when the plume is negative and so able to function as a hot filament. Voltages and currents in Fig. 3 are referred to the collecting electrode, so characteristics of "forward" conduction are found in the

positive (first) quadrant. In the "reverse" direction current is lessened until the potential difference is sufficiently elevated to cause a glow discharge. The selection of either positive or negative voltages to give the same absolute values of current generally yields very similar depositions on Si(100) substrates. There was no particular sensitivity of the results to the placement of the collecting electrode but no effect of the discharge current unless it passed through the small volume at the laser focus.

The characterization of such thin lossy films as produced in this work requires particular attention to the fact that ellipsometry, as customarily employed, does not give a unique result, when both real, n_o and imaginary indices, n_i are to be measured together with the thickness, z. In our experiments, ellipsometry was used at 632.8 nm and reflectance spectroscopy was employed to obtain uniqueness.

In these experiments films were deposited on Si(100) wafers. The relative indices of air, a-C and Si differ enough that strong reflections are developed, in-phase, at both the air/a-C and a-C/Si interfac-

Simple bookkeeping of the multiply reflected field strengths yields an expression for the relative intensity, R reflected at normal incidence from the coated Si which can be written,

$$R = \frac{1}{|\beta|} \frac{(\beta-\alpha)^2 + 4\alpha\beta \sin^2 \delta/2}{(1-\alpha)^2 + 4\alpha \sin^2 \delta/2} \quad . \qquad (1)$$

where δ - phase shift resulting from one round trip through the film,

β - product of reflection coefficients for the fields from the inside and outside at the air/a-C interface,

α - product of the reflection coefficients for the fields from the inside at both a-C interfaces multiplied by $\exp(-\delta n_i/n_o)$.

Fitting this expression to reflectance spectra gave values of $(n_o z)$ and (n_i/n_o) and with these a unique result could be obtained from the ellipsometry data.

Phenomenology was examined over a wide range of process variables. All experiments were conducted in a UHV environment operated around 10^{-6} Torr, as residual pressures seemed of little actual importance. The laser was a Q-switched NdYAG delivering 250 mJ to the focus at a repetition rate of 10 Hz. The only variables of particular importance was the peak laser intensity in the ablation plume and the peak discharge current. Generally, lower current could be compensated by higher laser power. Consistent with this was the observation that cratering the graphite or defocusing the laser gave larger plumes and higher growth rates at the substrate but the resulting a-C film had much greater loss. Characteristics of films deposited at the lower power densities of Wagal,[7] Richter,[8] and Sato[9] could not be plotted on the scale of Fig. 1b.

Optical constants for a typical film prepared at 5×10^{11} w/cm^2 are plotted in Figs. 1a and 1b. Peak discharge currents were 10 A. In each case the substrate was 5.5 cm from the laser plasma source and radial expansion of the ejected material produced a domed profile of thickness which could be appreciated by the visual appearance of bright Newton's rings of interference. Optical constants were measured to be consistent across the 30 cm^2 over which thickness varied from 0.1 to 0.2 μm.

As can be seen, the high power densities at the ablation source give a relatively smaller n_1 which in turn implies low fraction of sp^2 bonding. The data points in Fig. 1b correspond to a graphitic, sp^2 concentration of about the same as the value of 25% characterizing Savvides best films. The fact that a higher power density at the same total energy gives a smaller deposited volume supports the expectations that a tighter focus gives a higher temperature to a smaller amount of carbon material. This in turn strengthens the perception of Miyazawa[4] that the carbon ions are the critical precursors of sp^3 bonding, but refute his conclusion that the concurrent transport of electrons is detrimental. At these densities the ablated material must be traveling as largely neutral plasma. However, in agreement with Savvides[5] these results suggest that such sputtering techniques depending upon ion beam sources may be intrinsically limited by the inability to reach high power densities at high enough values of fluence to be practical. With the higher process temperatures and greater ionization fractions achieved with our laser plasma source there does not seem to be a

necessary component of sp^2 bonding in the resulting a-C material. It may be reasonably considered to be amorphic diamond.

The authors gratefully acknowledge the contributions of R. Krause in arranging the deposition system.

References

1. An excellent review can be found in J. C. Angus and C. C. Hayman, Science, 241, 913 (1988).

2. E. G. Spencer, P. H. Schmidt, D. C. Joy, and F. J. Sansalone, Appl. Phys. Lett. 29, 118 (1976).

3. S. Aisenberg and R. Chabot, J. Appl. Phys. 53, 2953 (1971).

4. T. Miyazawa, S. Misawa, S. Yoshida, and S. Gonda, J. Appl Phys. 55, 188 (1984).

5. N. Savvides and B. Window, J. Vac. Sci. Technol. A3, 2386 (1985).

6. N. Savvides, J. Appl. Phys. 58, 518 (1985); J. Appl. Phys. 59, 4133 (1986).

7. S. S. Wagal, E. M. Juengerman, and C. B. Collins, Appl. Phys. Lett. 53, 187 (1988).

8. A. Richter, H. J. Scheibe, W. Pompe, K. W. Brzezinka, and I. Muhling, J. Non-Cryst. Solids 88, 131 (1986).

9. T. Sato, S. Furuno, S. Iguchi, and M. Hanabusa, Jpn. J. Appl. Phys. 26, L1487 (1987).

OBSERVATION OF LARGE SCALE NUCLEAR PHASE MODULATION EFFECTS

by

TIMOTHY WAYNE SINOR, B. S., M. S.

DISSERTATION

Presented to the Faculty of

The University of Texas at Dallas

in Partial Fulfillment

of the Requirements

for the Degree of

DOCTOR OF PHILOSOPHY IN PHYSICS

THE UNIVERSITY OF TEXAS AT DALLAS

FALL, 1988

TABLE OF CONTENTS

Chapter

CHAPTER 1

INTRODUCTION

The discovery by Mössbauer[1] that gamma-rays can be resonantly emitted and absorbed by nuclei bound in a crystal made possible the direct observation of many phenomena formerly thought to be unmeasurable. The terrestrial measurement of the gravitational red shift,[2,3] the testing of the equivalence principle for rotating systems,[4] and the observation of nuclear hyperfine interactions[5,6] are but a few of the experiments made feasible by the Mössbauer effect.

Mössbauer's observation is attributed to the fact that in the case of a nucleus bound in a crystal a gamma-ray can be emitted or absorbed without any transfer of energy to or from the lattice. This means that neither thermal motion nor recoil can broaden or displace such transitions in energy. The high Q of such resonances, approximately 10^{12} for ^{57}Fe, provides photons of well defined energy which are useful for probing phenomena involving very small energies. In this way Mössbauer spectroscopy can provide a highly detailed account of the way in which the nucleus interacts with its environment. It is only through the existence of the Mössbauer effect that a practical source of very narrow line radiation can be produced, and with such a source very small changes in frequency can be measured.

With Mössbauer techniques there is sufficient frequency resolution that spectral changes produced by ultrasonic and magnetic perturbations to the nucleus can be observed in the short wavelength limit where quantum effects are dominant. For example, consider a classical emitter of radiation which has a negligible recoil energy. If the source is made to oscillate harmonically about some point with an amplitude x_0 and a frequency Ω, the emitted electromagnetic wave can be Fourier analyzed into a component with frequency ω_0 and "sidebands" at frequencies $\omega_0 \pm n\Omega$ where n

= 1, 2,...,. From a quantum viewpoint, this mechanical vibration of the nuclei generates a sharp peak in the phonon spectra of the solid at the oscillation frequency. The emission of the Mössbauer gamma-ray is then accompanied by the emission or absorption of n phonons, with the resulting gamma-ray spectrum consisting of a central absorption line accompanied by equally spaced sidebands.

In 1960, during their efforts to utilize Mössbauer spectroscopy as a tool to study the phonon spectra of solids, Ruby and Bolef[7] demonstrated the feasibility of producing ultrasonic sidebands to the single absorption line of ^{57}Fe in stainless-steel. These ultrasonic sidebands were produced by mounting the Mössbauer source onto a quartz transducer which was excited at megahertz frequencies. In addition, the source-transducer assembly was simultaneously driven at low frequencies (15 Hz) to tune the absorption in and out of resonance with the Doppler shifts produced by the lower frequency motion. With the use of a stainless-steel absorber, they were able to obtain spectra which consisted of a central unshifted absorption line accompanied by symmetrically located sidebands occurring at integral multiples of the ultrasonic driving frequency. Subsequent experiments similiar to those of Ruby and Bolef's have been performed by Burov et al.,[8] using ^{119}Sn and by Cranshaw and Reivari[9] with ^{57}Fe. Classical frequency modulation theory successfully predicts both the intensity and position of these ultrasonically induced sidebands as will be presented in Chapter 2.

Eight years after the initial observation of ultrasonic sidebands it was found that when either a ferromagnetic source or absorber was subjected to a magnetic field oscillating at radio-frequencies additional lines appeared in the gamma ray spectra. The resulting pattern of lines strongly resembled the sidebands that had been produced earlier by the ultrasonic effects. Since these rf sidebands were initially observed in ferromagnetic materials, they were incorrectly explained as ultrasonic sidebands driven

by the magnetostrictive oscillations of the source or absorber foils when exposed to an oscillating rf magnetic field.

More recently, some variations in the recoilless gamma-ray spectra have been reported[10] to result from direct modulation of the interaction energies arising from the couplings of the nuclear magnetic moments to the hyperfine fields. Described in terms of the phase modulation of the nuclear states involved in the transition,[10] those results demonstrate that even the earlier rf effects reported in ferromagnetic materials could have been the result of this type of phase modulation. It was not necessary to associate them with the time dependent magnetostrictive oscillations of the source or absorber foils.

This dissertation reports a reexamination of the question of radiofrequency sidebands and demonstrates that the effect arises from a direct interaction of the rf magnetic field with the energy levels of the nucleus and that magnetostriction effects produce a negligible contribution to the sideband intensities.

Literature Survey

Radiofrequency (rf) sidebands in Mössbauer spectroscopy, a well documented yet poorly understood phenomena, was first proposed in 1967 by Mitin,[11,12] who predicted that Mössbauer transitions could be excited as the result of a multiphoton interaction for nuclei immersed in intense radiofrequency fields. In cases where there was the simultaneous absorption of a gamma ray quantum under Mössbauer conditions and a quantum of the external radiofrequency field, the Mössbauer spectrum was predicted to show each recoilless gamma transition to be accompanied by sum and difference frequency lines displaced from it by integral multiples of the frequency of the applied rf field. In appearance these multiphoton spectra were expected to strongly resemble the transmission spectra obtained by Ruby and

Bolef[7] by imposing periodic Doppler shifts of mechanical origin on the source. This unfortunate similiarity between two phenomena arising from completely different origins subsequently provided years of critical controversy.

When radiofrequency sidebands were initially observed, they were seen only in ferromagnetic materials where there exists a coupling between the magnetic and elastic energy of the lattice. In such materials there are time dependent magnetostrictive oscillations when they are subjected to rf magnetic fields. Therefore, sidebands observed in ferromagnetic materials could possibly contain a certain contribution due to mechanical frequency modulation, as well as to multiphoton gamma-transitions. It is precisely this combination of effects which has led to considerable controversy as to the dominant mechanism producing the rf sidebands which have been observed in ferromagnetic media.

The earliest experiment investigating the influence of radiofrequency magnetic fields on Mössbauer transitions was reported by Perlow[13] in 1968. In this experiment, Perlow subjected several ^{57}Co sources which radiated the 14.4-keV transition of ^{57}Fe to intense magnetic fields oscillating at radiofrequencies. He was able to demonstrate the destruction of the Mössbauer hyperfine pattern by the action of the rf field. Even though rf sidebands were unresolved, Perlow attributed the observed change in the recoilless absorption to the random flipping of the hyperfine field due to domain wall motion.

It was later in 1968 that Heiman, Pfeiffer, and Walker[14] reported the first clear evidence of radiofrequency sidebands in ^{57}Fe as a result of subjecting an iron foil absorber rather than a source to an rf field. In addition to the usual six-line Zeeman pattern of ^{57}Fe, a set of sidebands were observed at energies $\hbar\omega_\gamma \pm m\hbar\omega_{rf}$, where $\hbar\omega_\gamma$ is the energy of the resonant gamma-radiation. Heiman et al.,[14] interpreted the additional lines as acoustically modulated sidebands arising from time-dependent

magnetostrictive oscillation within the foil and dismissed the possibility that the sidebands resulted from multiphoton processes. A later paper by the same authors[15] provided considerable experimental evidence supporting the magnetostrictive hypotheses. However, these results were challenged by other researchers in the field because the magnetostrictive-acoustic theory did not quantitatively predict the observed sidebands intensities in terms of a single modulation index which would be a measure of the sideband development.[16] In order to get reasonable predictions of the sideband intensities, it was necessary to postulate a large acoustic Q for these samples that provided a remarkable amplification of the vibrational amplitude of the acoustic vibrations inside the foil.[17]

It was the experiment reported by Chien and Walker[18] which gave the most compelling evidence in favor of the magnetostrictive-acoustic theory as an explanation of rf sidebands in ferromagnetic materials. In that experiment a composite absorber composed of ferromagnetic and nonmagnetic layers was used to study the transport of the causitive agent from the ferromagnetic layer into the nonmagnetic region where the sidebands were observed upon Mössbauer transitions of the ^{57}Fe nuclei. Very clear evidence showed that the cause did arise in the ferromagnetic nickel layers producing sidebands in the nonmagnetic stainless steel layers. The most ready explanation at that time was a transport of phonons from one layer to the next with a high acoustic Q, but as will be shown in this dissertation, this explanation is inadaquate and does not explain the new experimental evidence to be presented.

The possibility that rf sidebands might be produced by modulating the interaction energies of the nucleus with an rf field were all but dismissed until 1978 when West and Mattias[19] observed first-order sidebands from a single parent line by subjecting a non-magnetic ^{181}W Mössbauer source of the 6.2-keV line of ^{181}Ta to a strongly oscillating field of up to 230 Oe amplitude at a frequency of about one megahertz. The appearance of the

sidebands was due to the modulation of the interaction energy between the applied radiofrequency magnetic field and the nuclear magnetic moments of the two states of ^{181}Ta, linked by the 6.2-keV transition. The sideband positions, and intensities agreed well with theoretical analysis, assuming a pure magnetic interaction, and successfully yielded the g-factor ratio of the nuclear states involved in the transition that was in good agreement with values obtained by other techniques.[19] The results of that experiment, however, have not been widely accepted because the sidebands were obscured by the dispersive shape of the unperturbed Mössbauer resonance.

More recently, time-resolved Mössbauer spectroscopy[10] (TMS) has been used to analyze the influence of a periodically varying magnetic field on the high resolution Mössbauer resonance of ^{67}Zn in order to unambiguously demonstrate the pure magnetic phase modulation of the nuclear Zeeman levels in diamagnetic ZnO. This benchmark experiment required magnetic field amplitudes as large as 13.4 mT for sinusoidal modulation at applied frequencies, ω, of 10 kHz. In a complimentary frequency domain experiment where the time average of the recoilless gamma-radiation was measured, the Mössbauer spectrum resulting from magnetic phase modulation effects showed each absorption line to be split into an infinite set of sidebands displaced apart from it by integral multiples of the applied driving frequency. In essence, a Mössbauer spectrum resulting from magnetic phase modulation effects is identical in appearence to the ultrasonic and radiofrequency sidebands previously reported in the gamma-resonance spectrum of ^{57}Fe.

Since magnetic phase modulation effects were reported to scale as $(H_0/\omega)^2$, it would appear that such studies cannot be extended to nuclear systems with transition widths much greater than that of ^{67}Zn through a simple extension of efforts. The conceptual key to orders-of-magnitude enhancement of the phase modulation effects was developed in a series of three papers by Depaola and Collins[20-22] in 1984. In a critical reexamina-

tion of the phenomenology of rf sidebands in a ferromagnetic material, they suggested that the effect could be enhanced by the use of smaller powers used to manipulate the hyperfine magnetic fields arising from the natural correlations of the individual spins in ferromagnetic materials. The magnetization of the sample was then controlled by the internal magnetic field B_0 and by a perpendicular radiofrequency field B_{rf}. In this way the applied radiofrequency field could be enhanced at the nuclear sites by the ratio of the hyperfine magnetic field to the static field B_0.

Summary

Even though a tremendous amount of literature has been published on radiofrequency sidebands in ferromagnetic materials, a comprehensive understanding of their origins remains elusive. It has been the goal of this work to investigate and characterize certain phenomenological aspects of radiofrequency sidebands in two Mössbauer isotopes, ^{57}Fe and ^{119}Sn, in an effort to provide new insights into the origins of these controversial sidebands. To this end three specific series of experiments were performed.

In the first set of experiments, use was made of the well known fact that foils composed of alternating layers of ferromagnetic and nonmagnetic materials immersed in a radiofrequency field will display sidebands on the Mössbauer nuclei contained in the nonmagnetic layer (following the technique of Chien and Walker[18]). Using the concept of a modulation index, which is a measure of the strength of sideband development, this first experiment demonstrated that the sideband intensity measured as a function of the applied rf power scaled as the square of the number of sources, an observation not consistent with the magnetostrictive hypothesis.

Continuing this series, the next experiment was another direct attack of the magnetostrictive hypothesis. In this experiment we presented clear

evidence of radiofrequency modulation of the hyperfine fields of ^{57}Fe in a nonmagnetostrictive iron-nickel alloy. Such alloys, or permalloys as they are called, are of great scientific and technical interest because of their unusual magnetic properties. In particular, the magnetostriction of a polycrystaline permalloy passes through zero when the composition of the permalloy approaches 81 percent nickel.[23,24] At this critical composition in well annealed alloys, hystersis losses are at a minimum and the permeability is nearly maximum. Making use of two professionally prepared permalloy foils with compositions near the magnetostrictive null, this experiment demonstrated that the appearence of sidebands in these ferromagnetic iron-nickel alloys correlated with their permeability and not with their magnetostrictive properties.

The second series of experiments was performed using ^{119}Sn as the Mössbauer isotope. Pure tin, which is diamagnetic, can be readily alloyed with nickel and iron to form ferromagnetic and antiferromagnetic compounds. These alloys allowed a direct comparision of sideband behavior in materials with different magnetic properties.

The third and final series of experiments dealt with the transport properties of ultrasonic and radiofrequency sidebands. Here it was demonstrated conclusively that rf sidebands induced in paramagnetic materials via an interaction with a ferromagnetic driver are the result of spin waves propagating in the absorber foil. These spin waves interact with the nucleus and the net effect is to induce sidebands upon the Mössbauer transitions of the nucleus by modulating the phases of the nuclear states.

REFERENCES

1. R. L. Mössbauer, Z. Physik 151, 124 (1958).
2. R. V. Pound and G. A. Rebka, Jr. Phys. Rev. Letters 4, 337 (1960).
3. T. Katila and K. J. Riski, Phys. Lett. 83A, 51 (1981).
4. H. J. Hay, J. P. Schiffer, T. E. Cranshaw and P. A. Egelstaff, Phys. Rev. Letters 4, 165 (1960).
5. R. V. Pound and G. A. Rebka, Jr. Phys. Rev. Letters 3, 554 (1959).
6. S. S. Hanna, J. Heberle, C. Littlejohn, G. J. Perlow, R. S. Preston and D. H. Vincent, Phys. Rev. Letters 4, 177 (1960).
7. S. L. Ruby and D. I. Bolef, Phys. Rev. Lett. 5, 5 (1960).
8. V. A. Burov, V. A. Krasil'nikov, and O. Yu. Sukharevskaya, Sov. Phys. JETP 43, 837 (1962).
9. T. E. Cranshaw and P. Reivari, Proc. Phys. Soc., 90, 1059 (1967).
10. E. Ikonen, P. Helistö, J. Hietanieni, and T. Katila, Phys. Rev. Lett. 60, 643 (1988).
11. A. V. Mitin, Sov. Phys. JETP 25, 1062 (1967).
12. A. V. Mitin, Sov. Phys. Dok. 15, B27 (1971).
13. G. L. Perlow, Phys. Rev. 172, 319 (1968).
14. N. D. Heiman, L. Pfeiffer, and J. C. Walker, Phys. Rev. Lett. 21, 93 (1968).
15. L. Pfeiffer, N. D. Heiman, and J. C. Walker, Phys. Rev. B 6, 74 (1972).
16. G. Asti, AB. Albanese, and C. Bucci, Phys. Rev. 184, 260 (1969).
17. N. Heiman, R. K. Hester, and S. P. Weeks, Phys. Rev. B 8, 8 (1973).
18. C. L Chien and J. C. Walker, Phys. Rev. B 13, 1876 (1976).
19. P. J. West and E. Matthias, Z. Phys. A 288, 369 (1978).
20. C. B. Collins and B. D. DePaola, Optics Lett. 10, 25 (1985).
21. B. D. DePaola and C. B. Collins, J. Opt. Soc. Am. B 1, 812 (1984).

22. B. D. DePaola, S. S. Wagal, and C. B. Collins, J. Opt. Soc. Am. B 2, 541 (1985).

23. L. W. McKeehan and P. P. Cioffi, Phys. Rev. 28, 146 (1926).

24. M. Kersten, Z. tech Physik, 12, 665 (1931).

CHAPTER 2

THEORY

THE MÖSSBAUER EFFECT: AN OVERVIEW

The Mössbauer effect can be readily described by considering a nucleus which decays from some excited state to its ground state by the emission of a gamma-ray. The recoil energy of the nucleus, E_r, reduces the energy of the gamma-ray and also serves to increase the Doppler broadening of the line due to the thermal motions of the nuclei. The recoil energy of the nucleus is given by

$$E_r = E_\gamma^2/2Mc^2 \quad , \tag{2.1}$$

where E_γ is the transition energy, M is the mass of the nucleus, and c is the speed of light.

According to the Debye theory of specific heat,[1] a solid may be considered to consist of a large number of linear oscillators with a distribution of frequencies ranging from zero to some maximum frequency ω_D; the total number of oscillators being equal to 3N, where N is the number of atoms in the solid. If the recoil energy of the nucleus is less than the quantum of energy necessary to excite the oscillator to the next higher energy level, the gamma-ray may be emitted without recoil. The probability of such recoilless emission is, in most cases, governed by the Debye-Waller factor, a familiar quantity in the theory of x-ray and neutron scattering. The Debye-Waller fraction[2,3] is given by the Debye model as

$$f = \exp\ (-3E_r/2k_B\theta_D);\ T \ll \theta_D \quad , \tag{2.2}$$

$$f = \exp\ (-6E_rT/k_B\theta_D);\ T > \theta_D \quad , \tag{2.3}$$

where T is the absolute temperature, k_B is the Boltzman constant and Θ_D is the Debye temperature. The Debye temperature, which is a measure of the stiffness of the lattice, is defined by the expression $\hbar\omega_D = k_B\Theta_D$.

Practical considerations dictate that to observe the Mössbauer effect it is necessary to have $E_\gamma < k\Theta_D$, where $k = 2\pi/\lambda$. This condition requires the emitted gamma-rays to be of relatively low energy and the material in which the Mössbauer nuclei are embedded to have a high Debye temperature. Typical Debye temperatures are on the order of a few hundred degrees Kelvin (Θ_D = 470 K for Fe and 200 K for Sn) while typical gamma-ray energies used in Mössbauer spectroscopy lie between 10-100-keV (E_γ = 14.4-keV for ^{57}Fe and 23.875-keV for ^{119}Sn). To date the Mössbauer effect has been observed in over 100 nuclei.[3] The best known are ^{57}Fe and ^{119}Sn, both of which have large recoilless fractions at room temperature.

Although experiments involving the Mössbauer effect can be performed with either a transmission or a scattering geometry, only the former is of interest for the current research. A typical transmission experiment consists of measuring the intensity of the resonance radiation passing through the absorber as a function of the relative velocity between the source and absorber. Because of the Doppler shift in energy produced by such a velocity, a resonance line shape is traced out.

In the work being presented here, two Mössbauer isotopes were used: ^{57}Fe and ^{119}Sn. The energy level diagram of the nuclear emission for ^{57}Fe is shown in Figure 2.1a. The gamma-ray source is ^{57}Co, in either a Pd or Rh lattice. It decays by electron capture into an excited state of ^{57}Fe, with its 3/2 - 1/2 transition emitting a 14.4-keV gamma-ray as seen in Figure 2.1a. This transition is very long-lived by nuclear standards with a mean lifetime, τ of 1.4×10^{-7} sec. From Heisenberg's uncertainty principle; $\Delta E \cdot \Gamma \approx \hbar/\tau$, the natural line width of the transition is $\Gamma = 5 \times 10^{-9}$ eV. Since the ratio of the natural line width and the photon energy, E_γ/Γ is a measure of the accuracy of the determination of the relative frequency or

energy changes of the system, the 14.4-keV transition is sharply defined with $E_\gamma/\Gamma = 2.9 \times 10^{12}$.

In Pd or Rh lattices the 14.4-keV transition can emit its gamma-ray without recoil in about 80% of the cases; therefore, resonant absorption can occur when the nuclear energy levels of the source and absorber match. With the frequency of the photon so well-defined, the Doppler effect (i.e., moving the source relative to the absorber) can be used to tune the absorption in and out of resonance with respect to the source. The relative velocity of the source to the absorber in order to scan a full width, 2Γ, of the gamma-ray line is given by the Doppler shift

$$E_0 = (v/c)E_\gamma \cos\alpha \quad , \tag{2.4}$$

where E_γ is the gamma-ray energy, v is the relative velocity of the source and absorber, and α is the angle between the velocity direction and the direction of the gamma-ray propagation.

Since a Mössbauer spectrum is obtained by determining the intensity of the gamma radiation that reaches the detector as a function of the Doppler modulating velocity, the spectrum can be represented by a plot of intensity verses velocity. Under ideal conditions the velocity-dependent intensity is given by

$$I(v) = I(0) \frac{\Gamma^2/4}{(v-v_0)^2 + \Gamma^2/4} \quad , \tag{2.5}$$

where I(0) is the intensity of the resonance peak when the energies of the emitted and absorbed gamma-ray are equal, v is the Doppler velocity, v_0 is the velocity at the resonance maximum and Γ is the full width of the absorption peak at one-half the maximum intensity (FWHM).

Figure 2.1

Energy level diagram for a ^{57}Co source and ^{57}Fe absorber showing (a) the emission process for the 14.4-keV gamma-ray and (b-d) static perturbations of the nuclear energy levels. Note: In (b-d) the energy scale is about 10^{13} smaller than in (a).

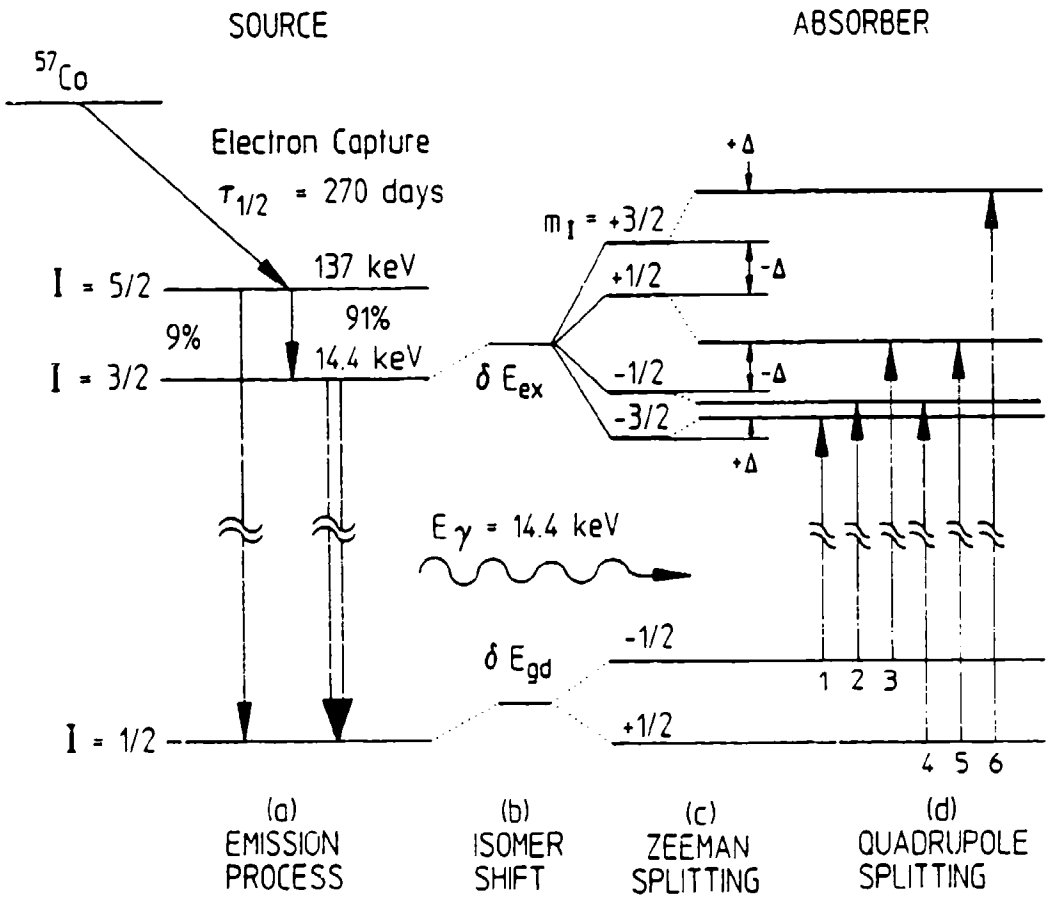
SOURCE
ABSORBER
^{57}Co
Electron Capture
$\tau_{1/2}$ = 270 days
137 keV
I = 5/2
9%
91%
14.4 keV
I = 3/2
δE_{ex}
+Δ
m_I = +3/2
+1/2
-Δ
-1/2
-Δ
-3/2
+Δ
E_γ = 14.4 keV
δE_{gd}
-1/2
+1/2
I = 1/2
1 2 3
4 5 6
(a) EMISSION PROCESS
(b) ISOMER SHIFT
(c) ZEEMAN SPLITTING
(d) QUADRUPOLE SPLITTING

In terms of the resonant cross-section the energy distribution of the emission or absorption line has a Breit-Wigner or Lorenzian line shape given by

$$\sigma(E) = \sigma_0 \frac{(\Gamma^2/4)}{(E-E_\gamma)^2 + (\Gamma^2/4)} \quad . \tag{2.6}$$

The total cross section, σ_0, for the absorption of nuclear radiation is given by

$$\sigma_0 = \frac{\lambda}{2\pi} \frac{2I_e+1}{2I_g+1} \frac{1}{\alpha_t+1} \quad , \tag{2.7}$$

where $k = 2\pi/\lambda$, and α is the total internal conversion coefficient for the gamma transition. The quantity $(2I_e+1)/(2I_g+1)$ is a statistical factor which is simply the ratio of the degeneracy of the excited to the ground state where I_e and I_g are the spins of the excited and ground states of the gamma transition. The quantity $1/(1+\alpha)$ gives the fraction of transitions which occur by the emission of a gamma photon. Since the emission and absorption resonances have the same line shape, the experimentally observed spectrum is a convolution of the source and absorber lines with a full width at half maximum (FWHM) of 2Γ.

In order to extract as much information as possible from a Mössbauer spectrum, there are two important features that must be understood. The first is why the resonance may be shifted between source and absorber by some finite, non-zero value of the velocity. The second is why the spectra from two level transitions are often composed of a number of resonance lines instead of just a single line.

In a Mössbauer spectrum the change in the position of a resonance line, or the center of a resonance pattern, is called the isomer shift. It is due to the electrostatic interaction of the nucleus with the electron charge density at the nucleus and can be considered an electric monopole interaction as shown in Figure 2.1b. More specifically, the excited and ground state nuclei differ in radius by a small yet significant amount (about 0.02% in ^{57}Fe). It is this change in the radius of the nucleus which causes the electrostatic interaction between the nucleus and the surrounding electrons to change upon excitation of the nucleus. If the Mössbauer nuclei in the source and absorber are in different chemical environments so that different electron distributions are experienced, the isomer shift is given by

$$I.S. = \frac{2\pi}{5} Ze^2[|\Psi_a(0)|^2 - |\Psi_s(0)|^2](R_e^2 - R_g^2) \quad , \quad (2.8)$$

where $|\Psi(0)|^2$ is the electron charge density at the nucleus, and R_e and R_g are the effective radii of the excited and ground state nuclei, respectively.

The fine structure of the Mössbauer spectrum arises from two principle static interactions; the magnetic dipole and electric quadrupole interactions, as shown in Fig. 2.1c and 2.1d, respectively. Since both the excited and ground states of ^{57}Fe and ^{119}Sn have non-zero nuclear spin, the magnetic dipole moment of the nucleus can interact with a magnetic field H, to produce a nuclear Zeeman effect, splitting the nuclear levels with spin I ($I > 0$) into $(2I + 1)$ sublevels, with eigenvalues

$$E_m = -\mu_N Hm_I/I = -g_N\beta_N Hm_I \quad , \quad (2.9)$$

where m_I is the magnetic quantum number with values m_I = I, I-1,..., -I, H is the magnetic field intensity at the site of the nucleus and μ_N is the nuclear magnetic dipole moment. The nuclear magnetic moment is related to the nuclear Bohr magneton, β_N by the Lande' factor, g_N defined by the relation $\mu_N = g_N\beta_N I$. In the case of ^{57}Fe, which has a 330 kOe internal magnetic field, the absorption spectrum is split into six lines as shown in Figure 2.2. One of the most important applications of the Mössbauer effect has been the observation of this nuclear Zeeman interaction which can, in principle, be studied in practically all cases simply by placing either the source or the absorber in a field of convenient size while observing the splitting of the resonant line.

The electric quadrupole interaction is the interaction of the nuclear quadrupole moment, Q, with the gradient of the electrostatic field at the nucleus as shown in Figure 2.1d. The nuclear quadrupole moment arises from the deviation of the nucleus from a spherical symmetry;[2] hence, Q = 0 for nuclear spin states I = 0 or 1/2, but Q is non-zero for the 14.4-keV state of ^{57}Fe. However, the quadrupole interaction is much smaller than the magnetic splitting of interest in this work and, therefore, can be neglected.

MECHANICAL FREQUENCY MODULATION

Ruby and Bolef[4] were the first to produce frequency modulated sidebands in Mössbauer spectra. They did so by mechanically vibrating the source with a piezoelectric quartz transducer which was made to oscillate at megahertz frequencies. Several other investigations of frequency modulated sidebands have since been reported.[5-8]

The formalism of frequency modulated sidebands produced by periodic Doppler shifts is as follows. Consider a source of electromagnetic radiation which is made to execute a simple harmonic motion with frequency,

Ω, and amplitude x_0. The time dependent displacement of the nucleus from its equilibrium position is given by

$$x(t) = x_0 \sin\Omega t \quad . \tag{2.10}$$

The resulting time dependence of the recoilless gamma radiation as observed in the transmission through a resonant absorber has been given to be[9]

$$E(t,t_0) = \lambda^{1/2}\exp[i(\omega_0 t + a\sin\Omega t) - (\lambda/2)(t-t_0) \quad , \quad \begin{matrix} t \geq t_0 \\ t<t_0 \end{matrix} \tag{2.11}$$

where the constant $\lambda(= \tau^{-1} = \Gamma/\hbar)$ is the reciprocal of the mean lifetime of the decaying state, ω_0 is the frequency of the unperturbed radiation and $a = \omega_0 x_0/c$ is called the modulation index. Choosing the formation of the excited state to occur at time $t_0 = 0$ the observed intensity of the emitted radiation is proportional to the absolute square of the its amplitude: Eq. (2.11) shows that I(t) is given by

$$I(t) \propto |E(t)|^2 = \lambda e^{-\lambda t} = \lambda e^{-\Gamma t/2\hbar} \quad , \tag{2.12}$$

However, since the wave is not monotonic, the frequency distribution of the wave is obtained by expanding E(t) as

$$E(t) = (2\pi)^{-1/2} \int_{-\infty}^{\infty} d\omega \Phi(\omega) e^{i\omega t} \quad . \tag{2.13}$$

The term $\Phi(\omega)$ gives the weight with which the frequency ω appears in E(t).

Fourier inversion gives

Figure 2.2

Mössbauer absorption spectrum of an iron foil enriched with ^{57}Fe. The six lines observed are the result of a magnetic dipole interaction. The separation of the outermost lines is ± 5.3 mm/sec while the innermost lines are separated by ± 0.84 mm/sec.

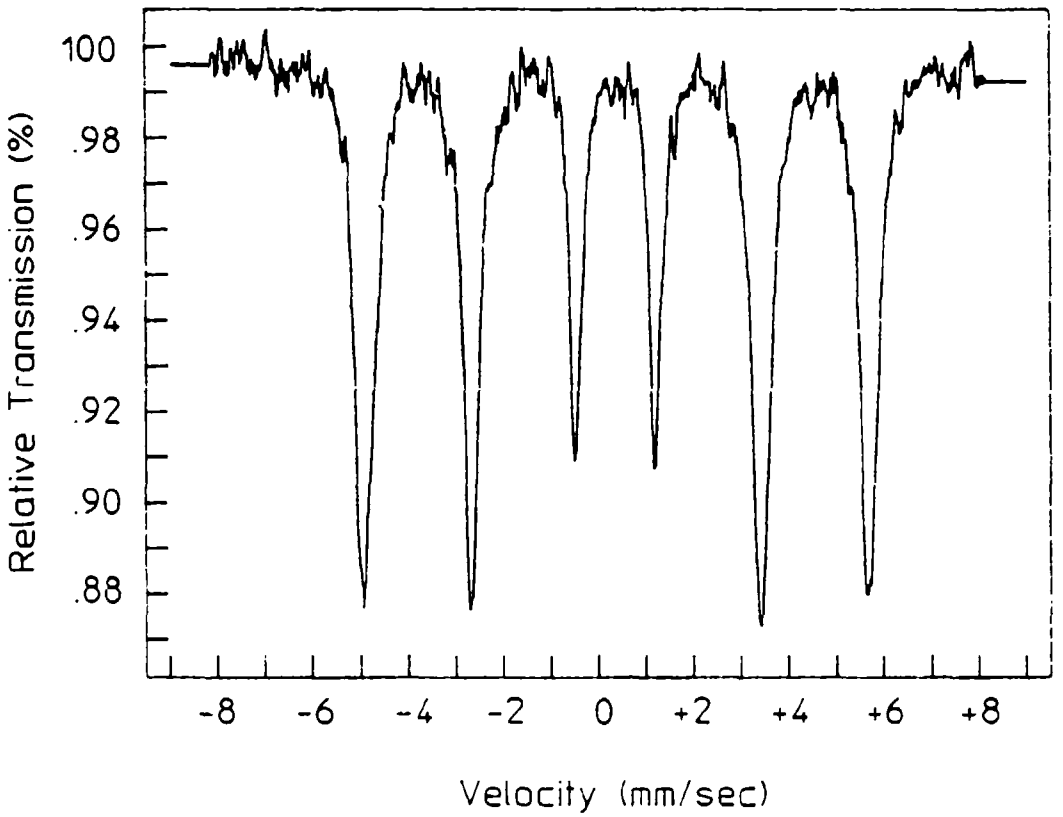
100
.98
.96
.94
.92
.90
.88
Relative Transmission (%)
-8
-6
-4
-2
0
+2
+4
+6
+8
Velocity (mm/sec)

$$\Phi(\omega) = (2\pi)^{-1/2} \int_{-\infty}^{\infty} dt E(t) e^{i\omega t} \quad , \tag{2.14}$$

or with Eq. (2.11), along with the Jacobi-Anger Bessel function identity;

$$e^{ia\sin\Omega t} = \sum_{n=0}^{\infty} J_n(a) e^{in\Omega t} \quad , \tag{2.15}$$

after integeration yields

$$\Phi(\omega) = -\lambda^{1/2} i \exp[-i(\omega t + a\sin\Omega t)] \sum_{n=0}^{\infty} \frac{J_n(a)\exp[in\Omega t]}{\omega - \omega_0 - n\Omega - i(\lambda/2)} \quad , \tag{2.16}$$

The intensity distribution of the wave is then

$$I(\omega) = \lambda \sum_{n=0}^{\infty} \frac{J_n^2(a)}{[(\omega - (\omega_0 - n\Omega)^2 + \lambda^2/4]} \quad , \tag{2.17}$$

where $J_n(a)$ is a Bessel function of the first kind.

The spectrum of Eq. (2.17) reveals that the electromagnetic wave is a superposition of partial waves with frequencies $\omega_0 \pm n\Omega$ where n = 0, 1, 2,...,. Since the intensity of the Mössbauer absorption line goes as the square of the electric field vector, the intensity of the n^{th} sideband is related to the square of the n^{th} Bessel coefficient

$$J_n^2(x_0/\bar{\lambda}) \quad . \tag{2.18}$$

The argument of the Bessel function, $x_0/\bar{\lambda}$ where $\bar{\lambda}$ is the normalized wavelength of the gamma-ray, is usually referred to as the modulation index

and is denoted by a. The intensity of the unperturbed absorption line is given by

$$f = |E_{n=0}(\omega,t)|^2 = J_0^2(x_0/\chi) \quad . \tag{2.19}$$

Since E_0 is normalized, f is the fraction of the radiated energy with frequency ω_0.

MAGNETIC PHASE MODULATION

Magnetic phase modulation theory[10] was derived to analyze the influence of a periodically varying magnetic field on the Mössbauer resonance of ^{67}Zn in diamagnetic ZnO. Pure magnetic modulation of the nuclear Zeeman levels by an alternating magnetic field was observed to produce phase changes of the nuclear states which were manifested as time-dependent oscillation of the transmission intensity measured as a function of the oscillating magnetic field.

For cases in which there is no static magnetic field[11] or in which the modulation is parallel to the static field,[12] the effect of the time varying component, $H_0 f(t)$ upon an eigenstate of the nucleus, $\psi^{(o)}_{\alpha,m}$ can be written,

$$\Psi_{\alpha,m} = e^{-i\varphi_\alpha(t)}\, \psi^{(o)}_{\alpha,m} \quad , \tag{2.20}$$

where $\varphi_\alpha(t)$ is the modulation angle of the phase,

$$\varphi_\alpha(t) = m_I \omega_\alpha \int_0^t f(t')dt' \quad , \tag{2.21}$$

and the Larmor frequency, ω_α is,

$$\omega_\alpha = \mu_N g_\alpha H_o/\hbar \quad , \tag{2.22}$$

where μ_N is the nuclear magneton, g_α is the gyromagnetic ratio for the α-th excited or ground state of the nucleus, and m_I is the magnetic quantum number of the eigenstates.

In principle, the difference in phase modulation between the ground state, g, and an excited state, e, may be observed during an absorption transition because the Fourier components of $\Delta\varphi(t) = \varphi_e(t) - \varphi_g(t)$ will be manifested as sidebands. However, since the transition will have a width, Γ associated with the time-dependent decay of the states, unless,

$$\hbar\omega_\alpha \geq \Gamma \quad , \tag{2.23}$$

the sidebands will be buried in the natural wings of the probing transition.

The modulation angle of the phase is easily calculated for a nucleus with spin I under the influence of a sinusoidally oscillating magnetic field, $B(t) = B_0\cos\Omega t$. The nuclear magnetic dipole moment interacts with the magnetic field according to

$$\mu_N \cdot B = g_N \frac{e}{2m_p} \beta_N I \cdot B \quad . \tag{2.24}$$

The modulation angle of the phase $\varphi_\alpha(t)$ is calculated as the integral of the time-dependent Zeeman energy, hence by Eq. (2.18) we have

$$\Delta\varphi(t) = \frac{1}{\hbar}\int_0^t g_e\mu_N I_e \cdot B(t)dt - \frac{1}{\hbar}\int_0^t g_g\mu_N I_g \cdot B(t)dt \quad , \tag{2.25}$$

$$= \pm\, a_i \sin\Omega t$$

where $a_i = g_e\mu_N B_0/2\hbar\Omega$ is the amplitude of the phase modulation.

This last expression may be expanded as a Fourier series by using Eq. (2.15). The Fourier coefficient $C_n(a_i)$ is calculated from $\varphi_\alpha(t)$ over the period of the oscillating magnetic field ($T = 2\pi/\Omega$):

$$C_n(a_i) = \frac{1}{T}\int_0^T dt \exp[i(\varphi(t) - n\Omega t)] \quad , \tag{2.26}$$

for sinusodial modulation $C_n(a) = J_n(a)$.

Equation (2.27) indicates that the radiation consists of sidebands which are separated by the modulation frequency with relative amplitudes given by $|C_n(a_i)|^2$:

$$|C_n(a_i)|^2 = \frac{16a_i^2}{[n^2\pi^2 - 4a_i^2]^2}\sin^2 a_i \quad , \tag{2.27}$$

for even n. For odd indices the sine function is replaced by cosine.[10]

Large Scale Magnetic Phase Modulation Effects

The phase modulation theory presented in the last section was specifically developed to explain the response of a diamagnetic material to a rapidly oscillating rf magnetic field. Next, it is interesting to address the question of what happens when these same fields are applied to paramagnetic and ferromagnetic materials.

It is well known that when an external magnetic field is imposed on a diamagnetic material, there is an induced atomic EMF which opposes the externally applied field in accordance with Lenz's law. The induced

magnetization of the material is directed opposite to the imposed field; therefore, the magnetic field seen by the nucleus within a diamagnetic material is smaller than the applied field would be in a vacuum.

When an atomic system has a permanent magnetic moment due to the presence of unpaired electrons, the material is either paramagnetic or ferromagnetic. In paramagnetic materials these moments are weakly coupled together and undergo random fluctuations due to thermal agitations. In ferromagnetic materials the unpaired electron spins are coupled together throughout the lattice producing strong magnetic fields at the nuclear sites. For example, in ^{57}Fe the unpaired electrons are in the 3d orbital and produce the 330 kOe internal magnetic field.

If an external field is applied to a paramagnetic material it becomes energetically favorable for the moments to align with the field, but this energy gain has to compete with the loss of entropy that would be associated with the loss of the random movement of the atomic moments.

With the application of an alternating magnetic field it is possible to excite spin waves in materials possessing a permanant magnetic moment. Spin waves which are oscillations in the relative orientations of the spins in a material provide a mechanism through which phase modulation effects can be propagated from ferromagnetic materials; where spin wave excitations are strong, into paramagnetic materials where the individual spins are weakly coupled.

The conceptual key to orders-of-magnitude of enhancement of phase modulation effects has been reported[11-13] to lie in the use of smaller powers to manipulate the greater magnetic fields arising from the natural correlations of individual spins in ferromagnetic materials. However, the modulation, $\partial M/\partial t$ of the magnetization, M of a ferromagnetic material is rarely parallel to either the applied field, H_o or even to M, itself.[14] For such cases of nuclei in ferromagnetic media, the modulation angle of Eq. (2.20) takes a more complex form;[11] and one which causes a mixing of the

eigenstates, $\psi^{(o)}_{\alpha,m}$. Nevertheless, the principal parameter is still a Larmor frequency, Ω_α which for magnetic environments becomes,

$$\Omega_\alpha = \mu_N g_\alpha M/\hbar \quad , \tag{2.28}$$

a value much larger than that found in Eq. (2.19) for nonmagnetic samples. Unfortunately, magnetic materials are almost invariably magnetostrictive and the concern has lingered that even the enhanced effects of phase modulation might always be overwhelmed by the periodic Doppler shifts produced by vibration in the lattices excited by magnetostriction.

The propagation of magnetoelastic waves is a complex problem which has been intensively studied since 1958.[15] For many magnetic media the dispersion equation for such waves displays several branches[16,17] which can be individually identified with spin waves, magnetostatic waves or elastic waves. Mixed waves coupling magnons and phonons occur principally when branches intersect, so that the frequencies and wavelengths for both are nearly equal.[15] Away from those values of parameters magnetic and acoustic waves can be separated. In principle this offers a means to propagate only the former to a sample in which it is desired to magnetically modulate the phases of the states of the nuclei to be observed there without the concomitant introduction of acoustic noise. This possibility was realized in the third set of experiments reported in this dissertation and seems to provide the key for separating phase modulation effects from those of acoustic origin.

REFERENCES

1. G. Burns, Solid State Physics, (Academic Press, New York, 1985).
2. H. Frauenfelder, The Mössbauer Effect, (Benjamin, New York, 1962).
3. U. Gonser, Topics in Applied Physics Vol. 5: Mössbauer Spectroscopy, (Springer-Verlag, New York, 1975).
4. S. L. Ruby and D. I. Bolef, Phys. Rev. Letters 5, 5 (1960).
5. V. Burov, V. Krasilnikov, and O. Sukharevskaya, Sov. Phys. JETP 16, 837 (1963).
6. T. E. Cranshaw and P. Reivari, Proc. Phys. Soc. (London) 90, 1059 (1967).
7. L. Mishory and D. Bolef, in Mossbauer Effect Methodology, edited by I. Gruverman (Plenum, New York, 1968), Vol. 4, p. 13.
8. R. P. Vardapetyan and A. H. Mkrtchyan, Solid State Commun. 60, 357, (1986).
9. J. E. Monahan and G. J. Perlow, Phys. Rev. A, 20, 1499 (1979).
10. E. Ikonen, P. Helisto, J. Hietaniemi and T. Katila, Phys. Rev. Lett. 60, 643 (1988).
11. C. B. Collins, S. Olarui, M. Petrascu, and I. Popescu, Phys. Rev. Lett, 42, 1397 (1979).
12. S. Olariu, I. Popescu, and C. B. Collins, Phys. Rev. C 23, 1007 (1981).
13. B. D. DePaola, S. S. Wagal, and C. B. Collins, J. Opt. Soc. Am. B2, 541 (1985).
14. T. H. O'Dell, Ferromagnetodynamics (J. Wiley, New York, 1981) Ch. 2.
15. C. Kittel, Phys. Rev. 110, 836 (1958).
16. P. C. Fletcher and C. Kittel, Phys. Rev. 120, 2004 (1960).
17. E. Schlömann, J. Appl. Phys. 31, 1647 (1960).
18. R. W. Damon and J. R. Eshback, J. Appl. Phys. Supp. 31, 1045 (1960).

19. H. A. Mook, J. W. Lynn, and R. M. Nicklow, Phys. Rev. Lett. 30, 556 (1973).

20. P. Grünberg, J. Appl. Phys. 51, 4338 (1980).

CHAPTER 3

INSTRUMENTATION AND PROCEDURES

The Mössbauer Spectrometer

In this chapter the fundamental aspects of the experimental design are presented which describe how the Mössbauer effect is used to study the influence of an rf magnetic field on the energy levels of the nucleus. Since a variety of experimental results are presented in this dissertation, a general overview of the experimental appartus and techniques will be presented in this chapter. The specific details pertaining to individual experiments which deviate from what is discussed here will be presented in the appropriate chapters covering the experimental results. The basic spectrometer used in all experiments consisted of an electromechanical transducer and its driving system, a gamma-ray detector with its associated electronics and a computer used as a multichannel scalar to collect and analyze the data. In addition to the above components, to apply the rf magnetic field to the absorber required a MHz signal generator, power amplifier, in-line power meter and a tuneable LC circuit.

The basic experimental arrangement is schematically shown in Fig. 3.1. The spectrometer consisted of an Austin Science Associates (ASA) model S-600 controller, an ASA linear motor and a multichannel scalar. The Mössbauer source was mounted on the motor which serves as an electromechanical velocity transducer to Doppler shift the frequency of the recoilless γ-radiation. The motion of the transducer is enslaved to a velocity reference signal (VRS) generated by the S-600. It could be operated in either a constant acceleration or a constant velocity mode. The Mössbauer resonance spectrum was generated by storing counts registered by a nuclear detector as a function of the velocity in an Apple II+ computer which served as a 1024 channel analyzer.

The S-600 requires a bistable signal from the MCA to properly time the drive waveform with the channel sweep. The memory channels were sequen-

Figure 3.1

Block diagram of the standard Mössbauer spectrometer used in all experiments.

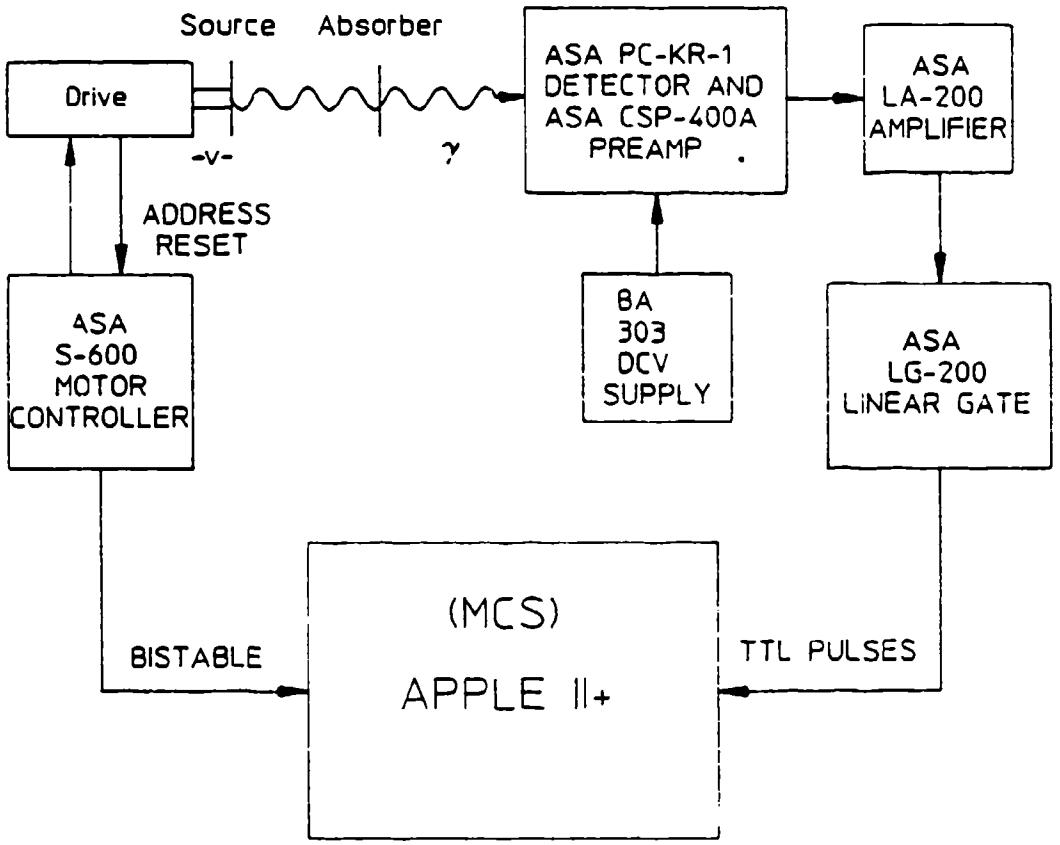
Source
Absorber
Drive
-v-
γ
ASA PC-KR-1
DETECTOR AND
ASA CSP-400A
PREAMP
ASA
LA-200
AMPLIFIER
ADDRESS
RESET
ASA
S-600
MOTOR
CONTROLLER
BA
303
DCV
SUPPLY
ASA
LG-200
LINEAR GATE
(MCS)
APPLE II+
BISTABLE
TTL PULSES

tially addressed with the velocity sweep using two triangular reference signals, 6 Hz and 24 Hz, to control both the channel advance and the velocity reference signal controlling the transducer.

For constant acceleration spectra the velocity of the motor was varied linearly with time in synchronism with the MCS. This was achieved by using a symmetric or asymmetric triangular waveform so that the VRS had a constant slope. In contrast, when the VRS had a constant voltage, the velocity of the motor was constant within a limited range. At the end-points of its motion, the motor required a flyback signal to bring the drive back to its starting position. Different review articles concerning this type of instrumentation used to study the Mössbauer effect have been published; two excellant examples are those by Cohen and Wertheim[1] and Herber and Hazony[2].

The velocity calibration of the spectrometer was usually done by measuring the peak positions of the six absorption lines of ^{57}Fe. The outer absorption peaks span ± 5.3 mm/sec while the inner lines are separated by ± 0.84 mm/sec. For velocity ranges greater than this it was convenient to use the rf sidebands produced in stainless steel driven by a nickel foil immersed in rf fields or by using an ultrasonic piezoelectric transducer to generate the sidebands. Since these sidebands appear at integral multiples of the driving frequency, their spacing from the parent transitions provides an ideal velocity calibration scale.[3,4] For absolute velocity calibration the velocity transducer was also equipped with an ASA LC-9A laser interferometer.

Mössbauer Sources

In this work two Mössbauer isotopes were used: ^{57}Fe and ^{119}Sn. Both of these isotopes have large recoil-free fractions at room temperature. The precursor nuclide for the 14.4-keV gamma radiation of ^{57}Fe is ^{57}Co. The

decay scheme and energy levels for this isotope was presented in Chapter II and will not be repeated here. The energy level diagram for ^{119}Sn is shown in Figure 3.2. This nuclide is produced by the (n,γ) reaction of ^{118}Sn (24.01% natural abundance), using the thermal neutron flux of a nuclear reactor. The Mössbauer transition at 23.875-keV from the first excited state (3/2 - 1/2), is populated by the decay of the more energetic metastable $^{119}Sn^{m}$ which has a half-life of 245 days. The ^{119}Sn was embedded in a $CaSnO_3$ matrix which gave it a recoilless fraction of 0.6 at room temperature. The initial activity of the source was 2.1 mCi.

A variety of ^{57}Co sources in Pd and Rh lattices were availble for use, with activities ranging from 2-25 mCi. Furthur details will be presented along with the experimental results.

Nuclear Detection System

To detect the 14.4-keV γ-rays in ^{57}Fe a Kr gas-filled proportional counter, ASA PC-KR-1, was used. A biasing voltage of 1.8 kV was supplied from a Bertran Associates model 303 dc voltage power supply. Krypton gas has a K-edge at 14.32-keV, so it is preferred for ^{57}Fe work despite an efficiency of only 50%. The resolution of a proportional counter is determined by the statistics of the conversion of the energy of the γ-rays into an electrical signal which scale as $2N^{-1/2}$, where N is the number of primary electrons. A charge sensitive preamplifier, ASA CSP-400A, amplified the signals from the proportional counter and delivered them to an ASA LA-200A linear amplifier. The amplifier output was then routed to an LG-200A linear gate which included upper and lower descrimination to allow the selection of pulses produced by the desired γ-rays. It also produced a TTL pulse used by the MCS for counting.

Because of the presence of a parasitic 25.8-keV x-ray line in the energy spectrum of the decay of $^{119}Sn^{m}$ it was necessary to use a different

Figure 3.2

Decay scheme and energy levels for the production of the 23.875-keV Mössbauer line of ^{119}Sn. Note the parasitic 24.8 x-ray line which can be electronically filtered out by using a high resolution Ge(Li) solid state gamma-ray detector.

$^{119}_{50}Sn$ (23.875 keV)

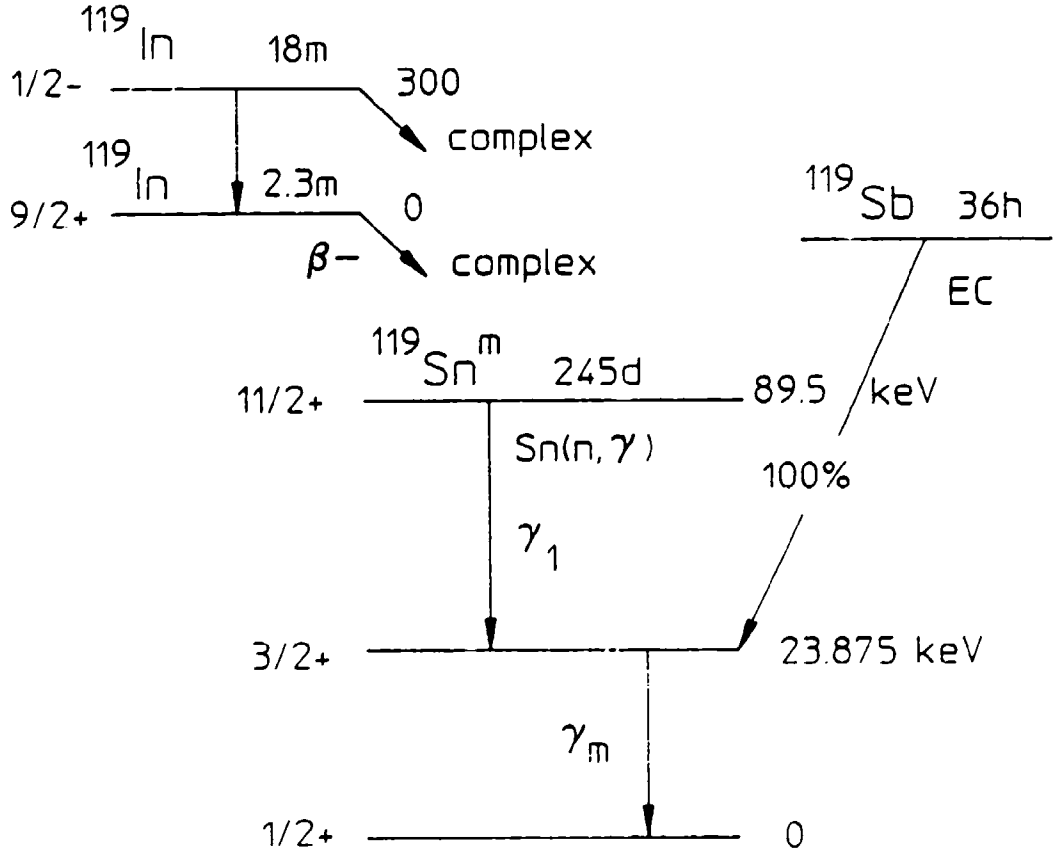

type of nuclear detector to detect the 23.875-keV Mössbauer line. The problem of resolving low energy lines in the presence of a background radiation caused by higher energy x-ray or γ-ray is best solved by using a high resolution semiconductor detector.[2] Therefore, to resolve the 23.875-keV Mössbauer transition from the 25.8-keV x-ray line an EG&G high purity Ge(Li) drift detector was used to collect the ^{119}Sn absorption spectra. In a semiconductor detector the incident γ-rays produce electron-hole pairs in the depletion layer of a pn junction of the semiconductor. In a Ge(Li) detector, lithium is drifted through the germanium to enlarge the depletion layer of this junction. The electrons and holes are collected at opposite terminals due to the influence of a negative bias across the pn junction.

Solid state detectors are highly sensitive, requiring only a few eV of energy to create electron-hole pairs. The statistical factor that contributed predominately to the resolution in a proportional counter is of much less importance for solid-state detectors. The lower limits on the resolution of the semiconductor detector are due to thermal noise and defects in manufacturing. These detectors must be operated at liquid nitrogen temperatures because of the large thermal noise present at room temperature which causes spurious pulses due to thermal excitations in the crystal.

The Rf Apparatus

The rf apparatus consisted of a signal generator for operation in the MHz range, amplifier, in-line power meter, and a parallel-series resonant circuit as shown in Figure 3.3. A Wavetek model 3510 frequency synthesizer with a very low intrinsic frequency modulation of only ± 100 Hz with an 500 Hz/(10-min) stability supplied the rf signal and was tunable over a frequency range of 1-1000 MHz. The output of the signal generator was then

amplified by an ENI model 550L linear amplifier which had a flat frequency response over the range of operation. The amplified signal was monitored by a Bird directional power meter. With the use of different elements both the forward and reflected rf power could be accurately measured. A more detailed discussion of the rf apparatus may be found in reference 8.

The magnetic field strength inside the induction coil in the absence of any magnetic material is approximated by[9]

$$H_{rf} = 6(PQ/V\nu)^{1/2} \quad , \qquad (3.1)$$

where P is the rf power in watts, Q is the Quality factor of the circuit ($Q = \omega/\Delta\omega$), V is the volume of the coil in cm^3 and ν is the resonance frequency in MHz. It is clear from Eq. (3.1) that if the product PQ is held constant, the rf current in the coil of such a circuit is also constant and, hence, different absorber arrangements could be subjected to applied fields of the same intensity, H.

Oxide Reduction of Absorbers

In experiments where the applied rf power exceeded more than about 5 watts cw, great care had to be taken to avoid oxidizing the absorber foils. This was particularly troublesome for experiments with tin absorbers. Stannic oxide, SnO_2, forms when metallic tin is heated and exposed to oxygen. The resonance absorption of the 23.875-keV γ-rays of ^{119}Sn in SnO_2 shows considerable line broadening over that calculated from the known lifetime of the 3/2 state ($\tau_{1/2} = 2.75 \times 10^{-8}$ sec, $\Gamma = 2.4 \times 10^{-8}$ ev). It has been shown that this broadening of the absorption spectrum of SnO_2 is due to an unresolved quadrupole doublet with splitting $\Delta = 0.50 \pm 0.02$ mm/sec.[5,6]

Figure 3.3

Modification to the Mössbauer spectrometer to allow the application of an rf magnetic field to the absorber foils. Proper rf shielding of the Doppler motor was a required to prevent rf interference from entering into the velocity drive wave form.

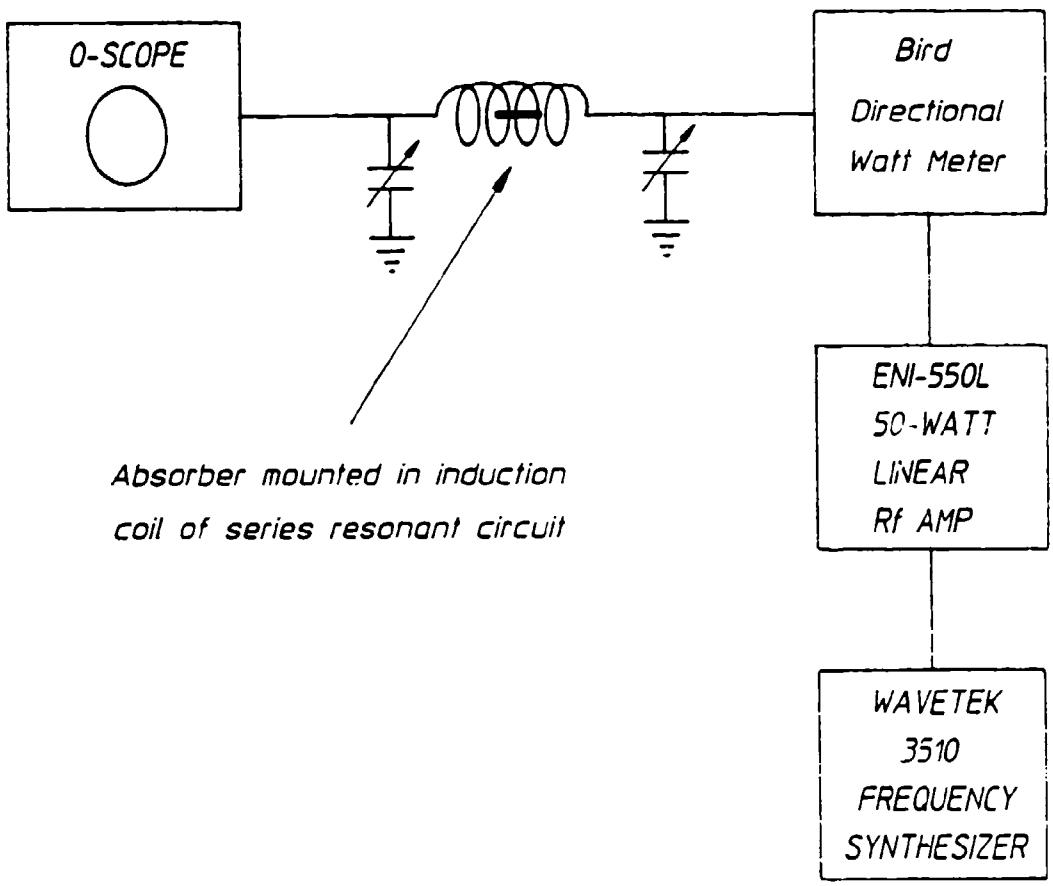
O-SCOPE
Bird
Directional
Watt Meter
ENI-550L
50-WATT
LINEAR
Rf AMP
WAVETEK
3510
FREQUENCY
SYNTHESIZER
Absorber mounted in induction
coil of series resonant circuit

Rf joule heating in the ferromagnetic iron foils causes excessive temperatures leading to the formation of iron oxides, in particular Fe_2O_3. The formation of ferric oxides can change the value of the hyperfine fields at the nuclear sites as well as induce quadrupole effects in the resonance spectra. Therefore, it was necessary to reduce the oxidized foils of iron and tin to their pure metallic forms by heat treating in a purified hydrogen atmosphere.

The chemical reaction for the reduction of Fe_2O_3 and SnO_2 are[7]

$$SnO_2 + 2H_2 = Sn + 2H_2O \qquad (3.2)$$

$$Fe_2O_3 + 3H_2 = 2Fe + 3H_2O \qquad (3.3)$$

The rates of these reactions are highly temperature dependent and are given by the logarithmic equation[7]

$$\log T + \log M = C \qquad (3.4)$$

where T is the absolute temperature, M is the time in hours and C is a constant. The time-dependent curve for the reduction of ferric and stannic oxide is shown in Fig. 3.4. From the figure, the shape of the curve indicates that the most advantageous temperatures at which to operate are those over 750°C. Hydrogen gas reduction of the iron foils was usually done around 1000°C; however, tin which has a low melting point (250°C) required lower reduction temperatures for extended periods of time. This was necessary to maintain the integrity of the foils.

As will be discussed in Chapter 5, some of the tin experiments involved using binary metallic alloys of iron/tin and nickel/tin. Since the reduction of ferric oxide is easier than stannic oxide for a mixture of these oxides the reduction would proceed as follows.[7] First, a reduction of the ferric oxide would occur followed by a period where both oxides were

undergoing a reducion. Finally, after a time all of the iron would be reduced with some SnO_2 remaining. The process would then continue until all of the tin oxide was reduced to its metallic form.

The H_2 gas reduction of oxides was accomplished by using a Lindberg 54000 series tube furnace. The maximum operating temperature was 1200°C. The temperature of the oven was monitored by measuring the EMF (millivolt) output of a Platinell II thermocouple which terminated inside the core of the furnace. The oxidized foils were placed in a quartz vessel and inserted into a one inch diameter quartz sleeve that fit into the center bore of the furnace. The flow rate of the hydrogen gas was approximately 4 ft^3/hour. After passing through the furnace the excess hydrogn gas was burned off using a modified bunsen burner.

To circumvent the oxidization of the absorber foils two techniques were used. First, the rf could be pulsed on and off to allow for radiational cooling of the absorber. This radiational cooling of the absorber could be expedited by using a small fan to blow a stream of cool air across the absorber mounted in the induction coil of the LC circuit. A second technique, used primarily in the tin experiments, was to perform the rf experiment inside a sealed plexi-glass box which was filled with an inert gas and held at positive pressures. Performing the tin experiments in this atmospheric isclation chamber in combination with rf pulsing and a cooling fan eliminated most of the oxidation problems.

Ultrasonic Transducer Assembly

Two of the experiments reported in this work involved the use of a quartz pieozelectric transducer to generate ultrasonic sidebands. The absorbers were bonded by a gel or epoxy to the transducer. X-cut quartz crystals were used to generate longitudinal waves, and AT-cut transducers were used to generate transverse waves.[4] The transducers were purchased

Figure 3.4

Oxide reduction for ferric and stannic oxides in a purified hydrogen atmosphere as a function of temperature (after reference 7).

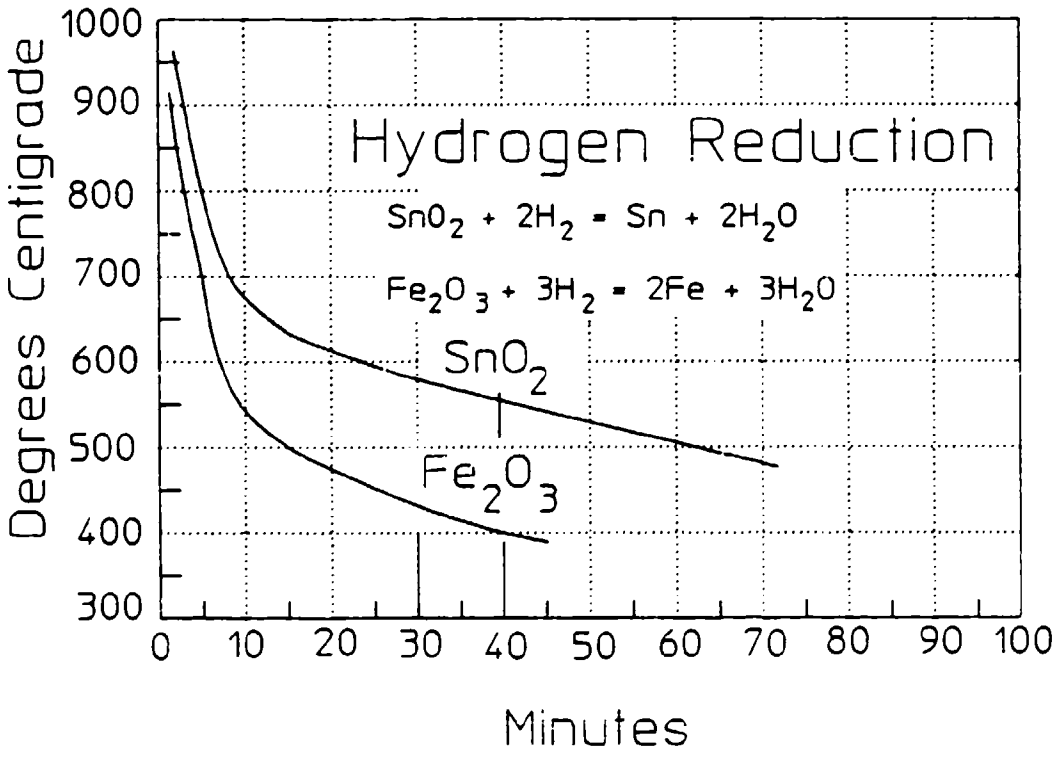
Hydrogen Reduction
$SnO_2 + 2H_2 = Sn + 2H_2O$
$Fe_2O_3 + 3H_2 = 2Fe + 3H_2O$
SnO_2
Fe_2O_3
Degrees Centigrade
1000
900
800
700
600
500
400
300
0
10
20
30
40
50
60
70
80
90
100
Minutes

from Valpey-Fisher and were cut to have their resonance frequency near 25 MHz. The electrodes were vacuum deposited chrome/gold and the transducer was one inch in diameter. A critical concern was to maintain the total thickness of the transducers to a value smaller than the range for the relatively soft γ-rays used in these experiments.

The absorber-transducer assembly was mounted in an aluminum holder to provide mechanical rigidity to the transducer and to allow a means of connecting the output of the rf generator/amplifier to the transducer electrodes. A schematic of the acoutic assembly is shown in Fig. 3.5.

The piezoelectric quartz transducer was driven from the ouput of the rf signal generator and amplifier described earlier. An rf impedance matching network was not necessary since all the experiments were performed at the natural frequency of the quartz transducer. The resonance frequency of the transducer could be "tuned" through a small range of frequencies by changing the dimensions and, hence, the mass of the absorber foils. The added mass would change the load on the transducer and, hence, its resonant frequency would shift slighty.

The mechanical resonance of quartz pieozelectric transducers are very high with typical Q values of about 400 being reported in the literature.[4] The vibrational resonance is Lorentzian with line widths dependent upon the attenuation of the ultrasound in the transducer material.[4]

Data Analysis

Several computer programs were available for processing Mössbauer data. The software used was from Coherent Technologies and basically treated the data as vectors representing the counts stored as a function of their channel address. Basic arithmatic operations such as addition or subtraction of data sets and running averages could be easily performed. Figure 3.6a shows an example of an unprocessed spectrum. The signal to

noise ratio could be improved by a factor of $(5)^{1/2}$ by performing a running average of the data from five successively resolved channels.[8] An example of a five point running average is shown in Fig. 3.6b.

Since the data is stored as a function of the channel address of the MCS and not as a function of the source velocity (mm/sec) it is necessary to know the calibration constant of the spectrometer (mm/sec/channel). This is calculated from a Mössbauer spectrum with known peak positions by dividing the separation of the peaks in mm/sec by the number of channels spanning the same range. The spectra could also be converted from counts versus mm/sec to frequency units by calculating

$$\nu = \frac{vE_\gamma}{\hbar c} \quad . \tag{3.5}$$

Although the work presented in this dissertation is not concerned with the absolute determination of the Mössbauer parameters for a given sample, there are, none-the-less, certain instrumental errors present due to the Doppler motion of the source which should be noted. They are: Parabolic distortion of the base line due to the inverse square law and Compton scattering; and cosine smearing and channel width broadening of the spectra.[10] The distortion of the baseline, due to the inverse square law, is noticable for a moving source when the source/absorber separation is small. Since the intensity of the γ-rays fall off as $1/r^2$, this distortion may be corrected by increasing the source to absorber separation.

Parabolic distortion of the baseline due to Compton scattering occurs when higher energy radiation is emitted by the source. This can be particularly troublesome when ^{57}Co is the source because of the 137-keV line due to the 5/2 - 1/2 transition.

The two remaing sources of instrumental error are cosine smearing and channel width broadening. Cosine smearing is a natural consequence of the

Figure 3.5

Schematic diagram of the ultrasonic transducer assembly used to mechanically modulate the gamma-ray energies of the 14.4 and 23.875-keV Mössbauer lines of ^{57}Fe and ^{119}Sn respectively.

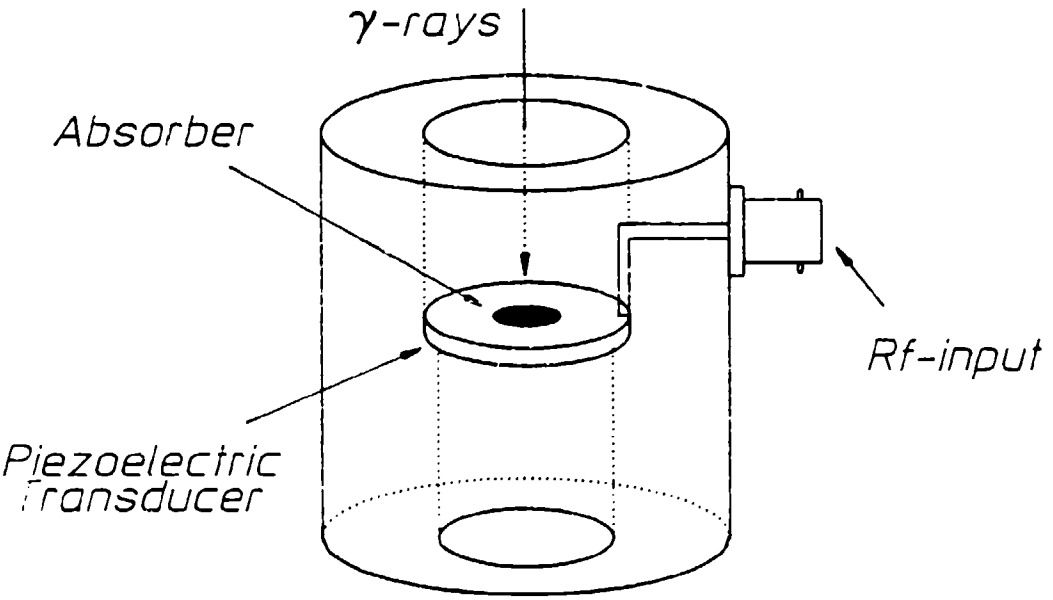
γ-rays
Absorber
Rf-input
Piezoelectric
Transducer

Figure 3.6

Raw data plot of a Mössbauer spectrum of an iron foil (b) the same data set after performing a five point running average which improves the signal to noise ratio by a factor of $(5)^{1/2}$.

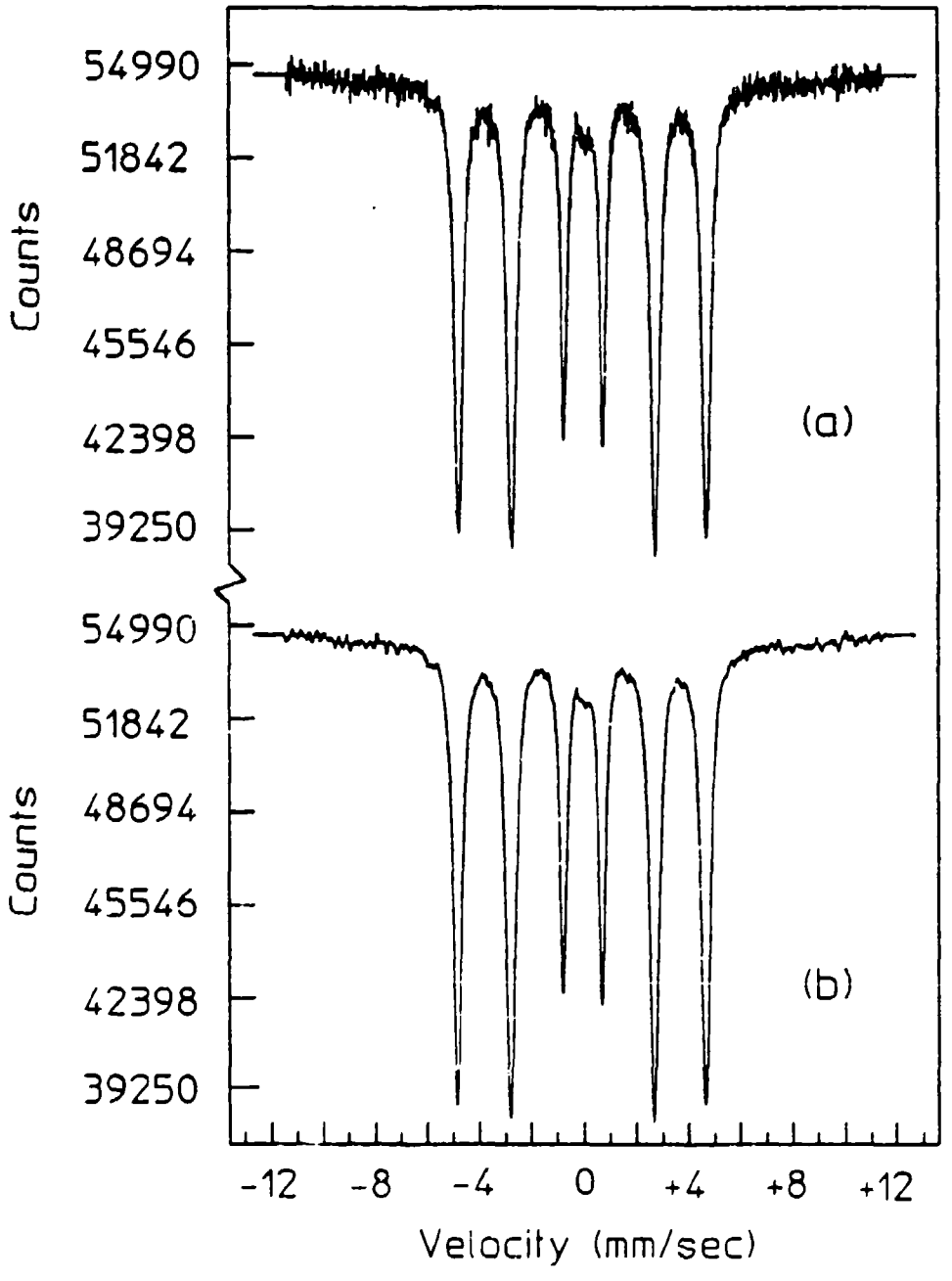
54990
51842
48694
45546
42398
39250
Counts
(a)
54990
51842
48694
45546
42398
39250
Counts
(b)
-12
-8
-4
0
+4
+8
+12
Velocity (mm/sec)

angular dependence of the Doppler effect and will produce a spectrum which shifted toward higher velocities. This velocity shift is given by $dv = vD^2/16d^2$, where D is the detector diameter and d is the source-detector separation.[10,11] Channel width broadening is due to a change in the velocity of the source while counts are still being accumulated in a channel. The magnitude of the effect is solely dependent upon the calibration constant of the spectrometer (mm/sec/channel).

REFERENCES

1. R. L. Cohen and G. Wertheim, in Methods of Experimental Physics, R. V. Colman ed., Solid State Physics, (Academic Press, New York, 1974), Vol II, p. 307.
2. R. H. Herber and Y. Hazony, in Techniques of Chemistry. A. Weissberger and B. Rossiter eds., (Wiley Interscience, New York, 1972), Vol. IIID, p. 215.
3. T. E. Cranshaw and P. Reivari, Proc. Phys. Soc. (London) 90, 1059 (1967).
4. J. Mishory and D. I. Bolef, in Mössbauer Effect Methodology, I. J. Gruverman ed., (Plenum Press, New York, 1968), Vol. 4, p. 13.
5. R. H. Herber and J. Spijkerman, J. Chem. Phys. 42, 4312 (1965).
6. K. P. Mitrofanov, M. V. Plotnikova, and V. S. Shpinel, Sov. Phys. JETP 21, (3) 524 (1965).
7. C. L. Mantell, Tin: Its Mining, Production, Technology, and its Applications, American Chemical Society Monograph Series, 2nd ed. (Reinhold Publishing Corporation, New York, 1949).
8. B. D. DePaola, Experimental Studies of the Interaction of the Nucleus with Long Wavelength Radiation, (unpublished Ph.d. Thesis, University of Texas at Dallas, 1984).
9. W. Gilbert Clark, Rev. Sci. Instrum. 35, (3), 316 (1964).
10. Jon J. Spijkerman, in An Introduction to Mössbauer Spectroscopy, Leopold May ed., (Plenum Press, New York, 1971), p. 23.
11. R. Riesenman, J. Steger, and E. Kostiner, Nucl. Instr. Methods 72, 109 (1969).

CHAPTER 4

EXPERIMENTAL RESULTS I

Introduction

In this chapter the results of two experiments are presented. Each yields strong evidence which contradict the accepted hypothesis that magnetostriction is the primary cause of radiofrequency sidebands. The first experiment reexamines the results of Chien and Walker[1] who demonstrated that sidebands could be propagated from a ferromagnetic driver foil into a nonmagnetic sample. The data presented here conclusively demonstrates that the effect of two foils varied from two to four times the effect produced by a single foil, depending upon the static magnetic bias applied; a result inconsistent with the magnetostrive-acoustic model of sideband generation. The second experiment involves a study of radiofrequency modulation of the hyperfine fields of ^{57}Fe in a nonmagnetostrictive iron-nickel alloy. Here it is found that the sideband development corresponds with the permeability of the sample and not with its magnetostriction.

Coherence Experiment

From a current perspective it is the experiment reported by Chien and Walker[1] in 1976 that forms the bulwark of the magnetostrictive-acoustic explanation of Mössbauer sidebands. In that experiment an absorbing foil composed of ferromagnetic and nonmagnetic layers was used to study transport of the causitive agent from the ferromagnetic layer into the nonmagnetic region where the sidebands were produced upon Mössbauer transitions of embedded ^{57}Fe nuclei. Very clear evidence showed that the cause did arise in the ferromagnetic Ni layers, producing sidebands in the nonmagnet-

ic stainless steel layers. The most ready explanation at that time was a transport of phonons from one layer to the next with a high acoustic Q. Those experiments were repeated in the work reported here, but with extensions which contradict the classic interpretation of Chien and Walker.[1]

Although not unique for all sidebands in a spectrum,[1] the idea of a modulation index m as a measure of the strength of the development of the sidebands offers practical convenience for descriptions. For a magnetostrictive origin,[1]

$$m = x_0/\lambda \quad , \tag{4.1}$$

where x_0 is the amplitude of the periodic displacement of the nuclei and λ = 0.137 A for the 14.4-keV line of ^{57}Fe. In the corresponding magnetodynamic model[2]

$$m = bH \quad , \tag{4.2}$$

where H is the applied magnetic field and b provides proportionality between M_s, the saturation magntization of the medium, and H. For relatively small m, the ratio of the magnitude of the first order sidebands to the intensity in the original parent line is proportional to m^2, which in turn is proportional to P, the applied radiofrequency power.

One of the most compelling results presented by Chien and Walker[1] was a demonstration supposed to show the enhancement of m^2 afforded by tighter acoustic coupling of the layers. They found that electroplating Ni upon a stainless steel foil produced much higher values of m^2 in absorption experiments than could be obtained by gluing a Ni foil to the stainless foil. They attributed the difference to the obviously poorer acoustic properties of the glue. However, as part of this dissertation it is

observed that their stainless steel foil was electroplated on both sides with Ni while the epoxied bond was used to join a single Ni foil to one side of the stainless absorber. While the m defined by Eq. (4.1) for a single foil could not be additive if produced in different magnetostrictive layers, in principle the M_s upon which m depends in Eq. (4.2) could add coherently. Two sources of m arising from distinctly separate sources could give a resulting modulation of $4m^2$ in a magnetodynamic model. Chien and Walker failed to recognize[1] that even in the magnostrictive model two sources of m generated in the two electroplated layers should give a modulation index of $2m^2$ in the absorber foil. Instead, they attributed the increased sideband intensity developed by the two plated sources in comparison to the one glued source only to the advantage they assumed for a plated contact over a glued interface. They reported no comparison of the effects of gluing or plating the *same number of ferromagnetic layers to the absorber foil.* Reported here is a repetition of the Chien and Walker experiment which showed that the effect of two foils varied from two to four times that produced by a single foil joined in the same fashion, depending upon the static magnetic bias applied.

In this experiment the absorber was a 2.5 μm paramagnetic stainless steel (SS) foil with 90.6% enrichment of ^{57}Fe. For the nonabsorbing ferromagnetic drivers, 2.5 μm Ni foils were used, all of which were cut from a single sheet of polycrystalline Ni. The stainless-steel absorber was sandwiched between two Ni foils and held in rigid contact by mounting the foils between glass cover slides of 100 μm thickness. A conventional Mössbauer spectrometer, modified for rf experiments, as shown in Fig. 4.1, utilized a 25 mCi source in a Rh matrix to obtain the ^{57}Fe absorption spectra. The 14.4-keV gamma rays were detected with a Kr gas filled proportional counter biased with 1.8 kV.

A 25 MHz rf magnetic field was applied by mounting the foils in the cylindrical induction coil of an LC tank circuit. In obtaining data for a

Figure 4.1

Schematic drawing of the experimental arrangement used in the coherence experiments. Note the position of the rare earth magnets which are used to apply a magnetic bias to the absorber.

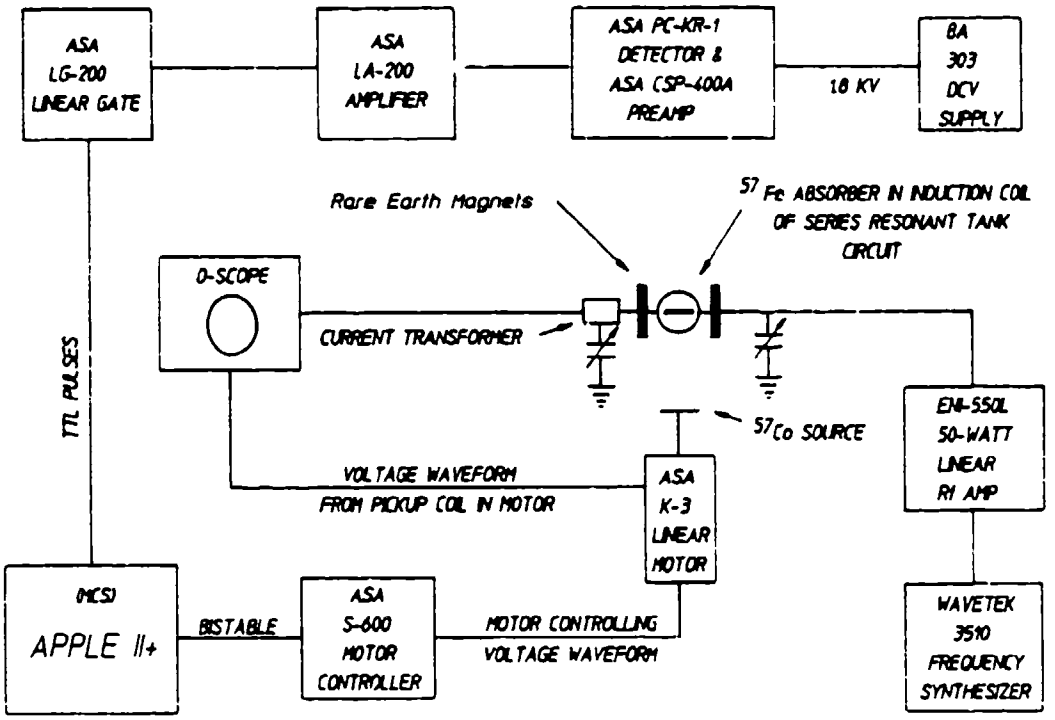
ASA
LG-200
LINEAR GATE
ASA
LA-200
AMPLIFIER
ASA PC-KR-1
DETECTOR &
ASA CSP-400A
PREAMP
18 KV
BA
303
DCV
SUPPLY
Rare Earth Magnets
57 Fe ABSORBER IN INDUCTION COIL
OF SERIES RESONANT TANK
CIRCUIT
O-SCOPE
CURRENT TRANSFORMER
TTL PULSES
57Co SOURCE
EMI-550L
50-WATT
LINEAR
RF AMP
VOLTAGE WAVEFORM
FROM PICKUP COIL IN MOTOR
ASA
K-3
LINEAR
MOTOR
(MCS)
APPLE II+
BISTABLE
ASA
S-600
MOTOR
CONTROLLER
MOTOR CONTROLLING
VOLTAGE WAVEFORM
WAVETEK
3510
FREQUENCY
SYNTHESIZER

direct comparison between the effect of one Ni driver versus two, the product of the applied rf power P and the electrical Q of the circuit containing the rf induction coil was maintained at constant values. Elementary analysis shows that if PQ is constant the rf current in the coil of such a circuit is also constant and, hence, the two absorber arrangements are subjected to applied fields of the same intensity H. The results of the first experiment verified the linearity of the first order sideband amplitudes at 25 MHz for SS with two Ni drivers with PQ products of 75, 150, and 300 W producing the data shown in Fig. 4.2. The spectra are scaled so that the intensity of the central Mössbauer absorption peak of ^{57}Fe in SS is held constant in order to make direct comparisons of the sideband amplitudes.

Having established the linearity of the first order sidebands in the Ni-SS-Ni sandwich, one of the Ni drivers was removed and the experiment was repeated with the same PQ products as before. Figure 4.3 shows a comparison of the sideband amplitude for two Ni drivers versus one; in this configuration two Ni drivers give twice the effect of one driver foil.

In the next experiment a comparison is made between the effect of one source of excitation with that from two sources when both were biased with a static magnetic field. Rare earth magnets were placed about the induction coil such that the static magnetic field was mutually orthogonal to the rf magnetic field and the direction of gamma-ray propagation.

The linearity of the sideband amplitudes at 25 MHz as a function of PQ was again established as seen in Fig. 4.4 in order to insure that the introduction of the static magnetic field did not introduce any nonlinearities to the system. The scale, thus established, was used to measure the decrease in the sideband amplitude when one of the sources of excitation was removed from this biased sandwich. As is clearly shown in Fig. 4.5, the sideband amplitudes obtained with two driver foils are four times the

amplitudes obtained with one driver foil. Therefore, with the application of a static B-field, two sources of excitation give four times the effect.

The results of this reexamination of the Chien and Walker experiment support only the first conclusion reached in that original work, namely that the causitive agent of rf sidebands can be produced in a ferromagnetic layer and then transported into a nonmagnetic layer. Their other conclusion is completely refuted by this demonstration because the effects they attributed to the type of coupling between layers most probably resulted from the relative numbers of magnetic and nonmagnetic layers.

These new results go beyond the propositions tested by Chien and Walker[1] and display behaviors completely inconsistent with the traditional magnetostrictive-acoustic origin of Mössbauer sidebands. In experiments such as these, acoustic phonons are the bosons associated with vector fields driven by tensor forces, *not vector forces*. Without invoking stimulated emission, there seems to be no way in which tensor sources which are physically separated can produce coherent vector fields in a space between them, even if they are temporally synchronized. As the fields increase, the magnetostrive foils will become stressed along parallel axes which are displaced by the thickness of the stainless layer between them. There is no mechanism to produce a displacement vector in a particular direction as a consequence of the resulting strains in the Ni foils. Only a small scale buldging or buckling of each Ni foil is to be expected and this is usually described as the scattering of phonons at right angles to the source. Without the stimulated emission of such phonons, there is no way to insure that one foil buckles toward the stainless layer at a particular point while the other buckles away.

The stimulated emission of phonons that would be necessary to produce coherent additions of the displacements arising from the different sources would imply the existence of a threshold of power, above which two modulation indices of m would give an effect of $4m^2$ and below which only $2m^2$. No

Figure 4.2

Experimental verification of the linearity of the first order sidebands at 25 MHz as a function of the applied rf power. The product of the applied rf power, P, and the quality factor, Q, of the circuit are used to insure reproducibility of the rf field strengths.

Linearity of First Order Sidebands

as a Function of Rf Power

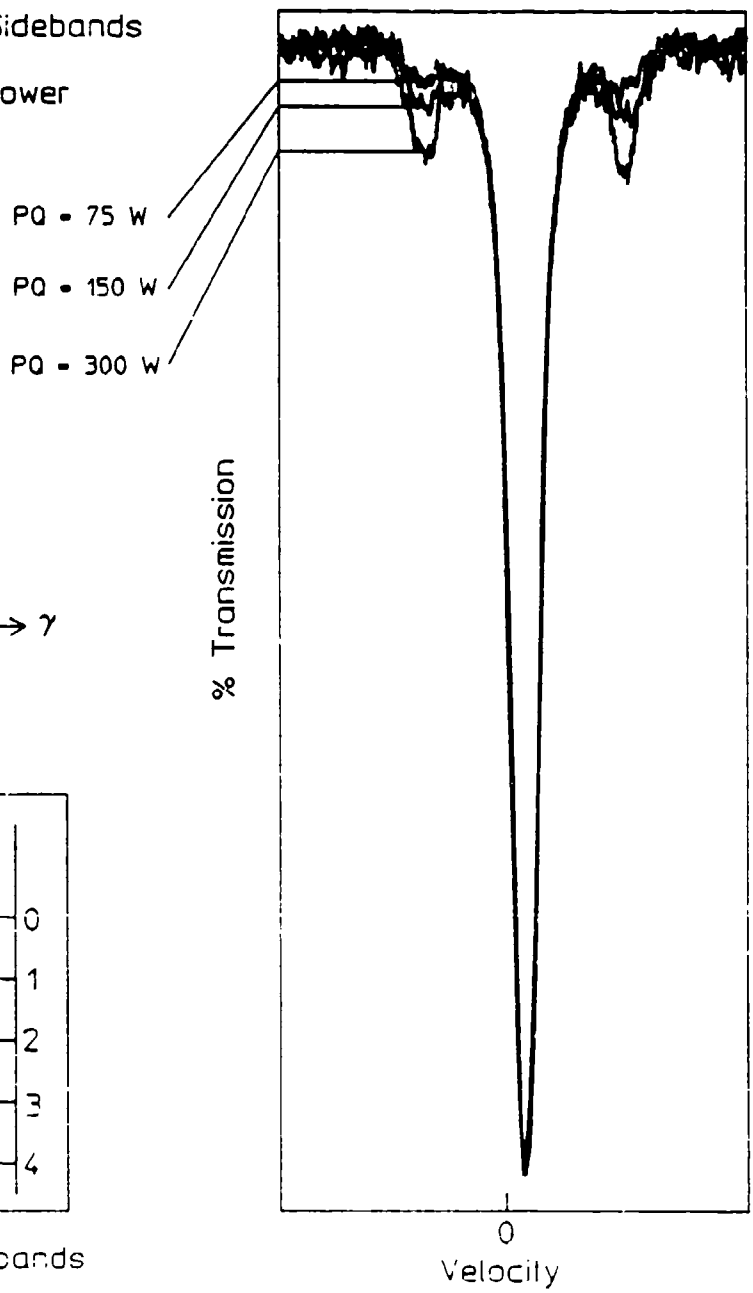

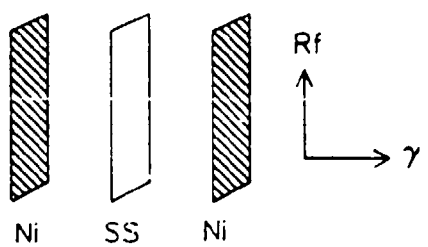

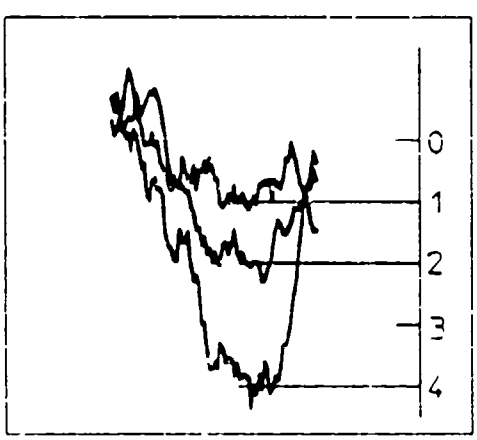

Details of First Order Sidebands

Figure 4.3

Comparision of the first order sideband amplitudes for one Ni driver foil versus two at 25 MHz with a PQ product of 300 W.

Comparison of Sideband Amplitudes
for One Driver Foil vs Two
PQ = 300 W

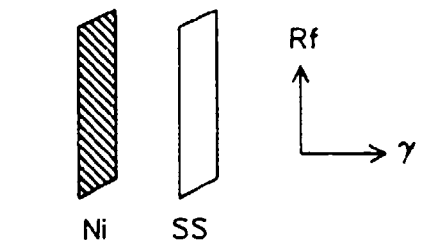

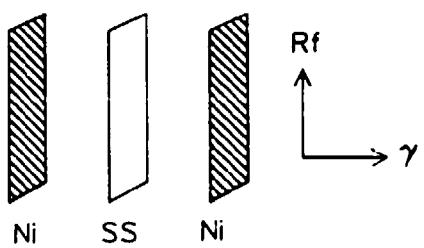

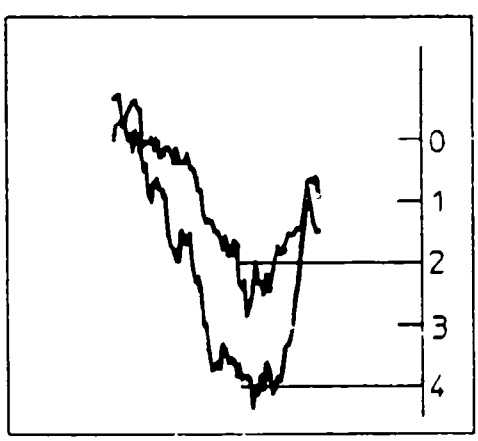

Details of First Order Sidebands

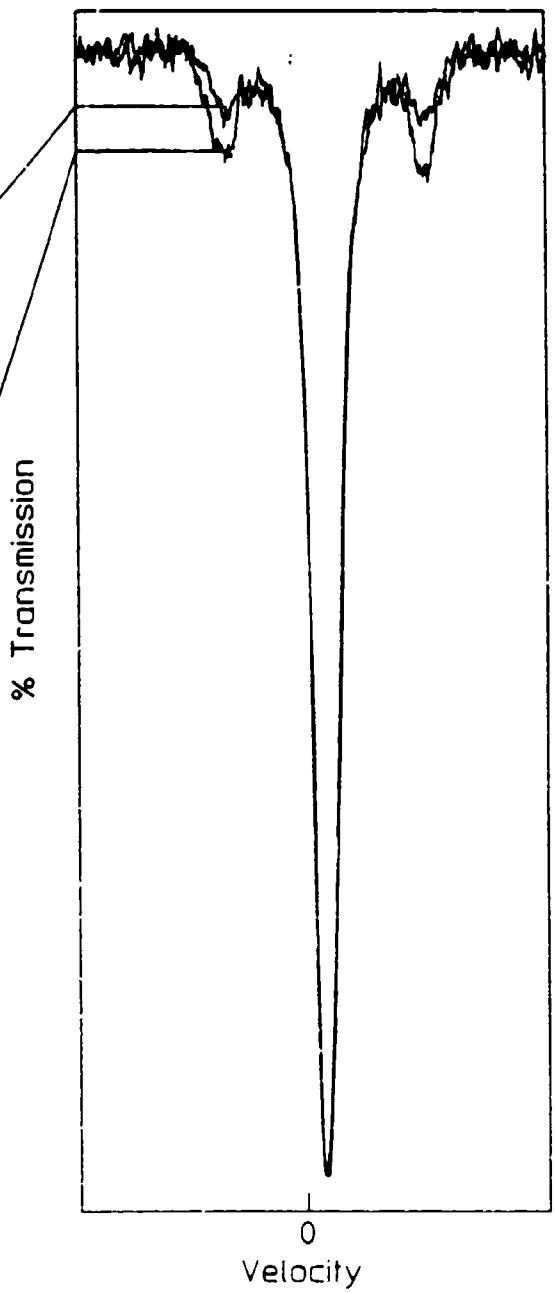

Figure 4.4

Establishment of linearity of the first order sidebands at 25 MHz with PQ = 75, 150 and 300 W when the foils are biased with a static magnetic field.

Linearity of First Order Sidebands
Under the Influence of a Static B-Field

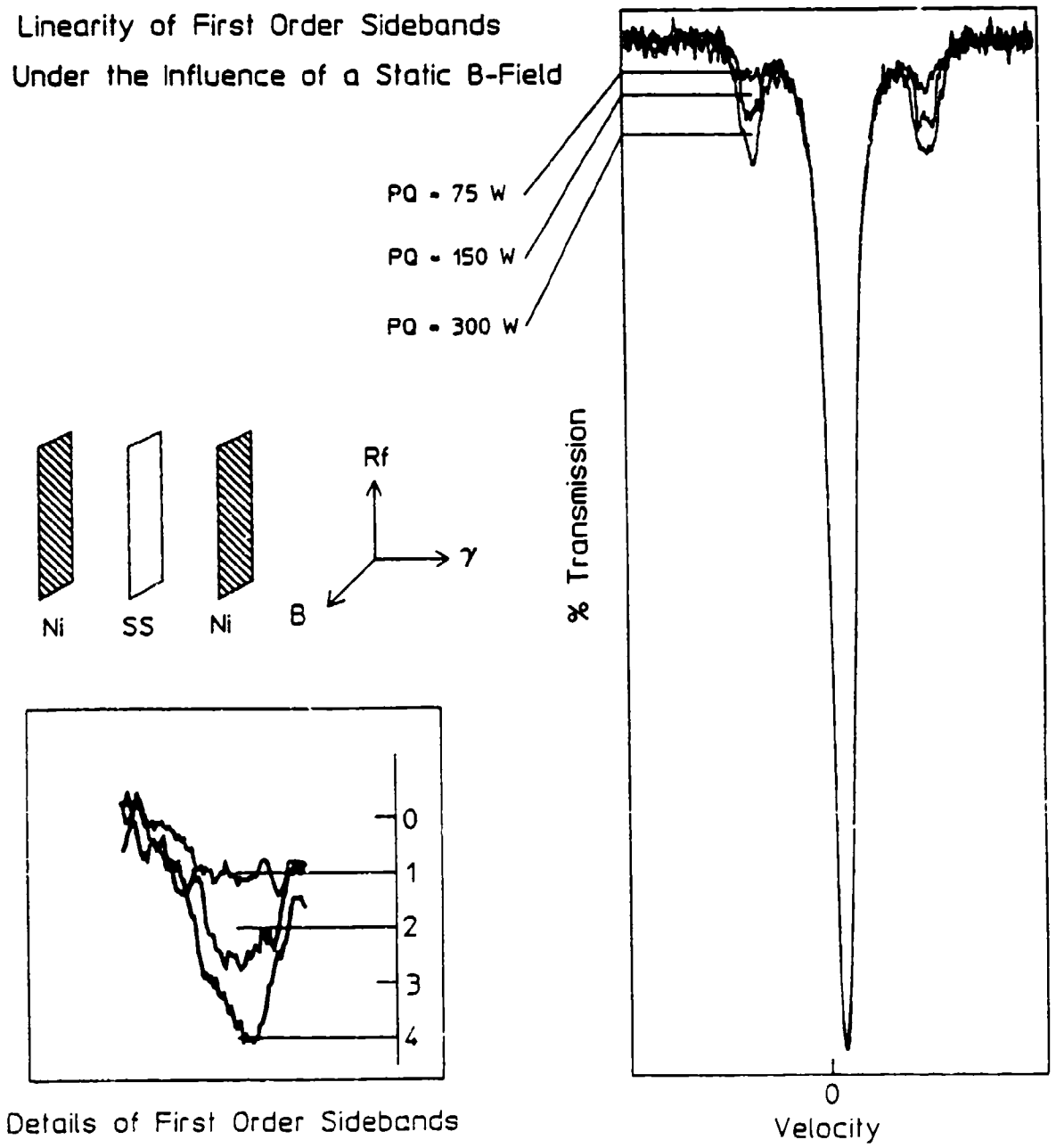

Details of First Order Sidebands

Figure 4.5

Comparision of sideband amplitudes for one driver foil versus two when both are biased by a static B-field with PQ = 300 W. Here two foils give four times the effect of one thus giving a modulation index of $\frac{1}{4}m^2$.

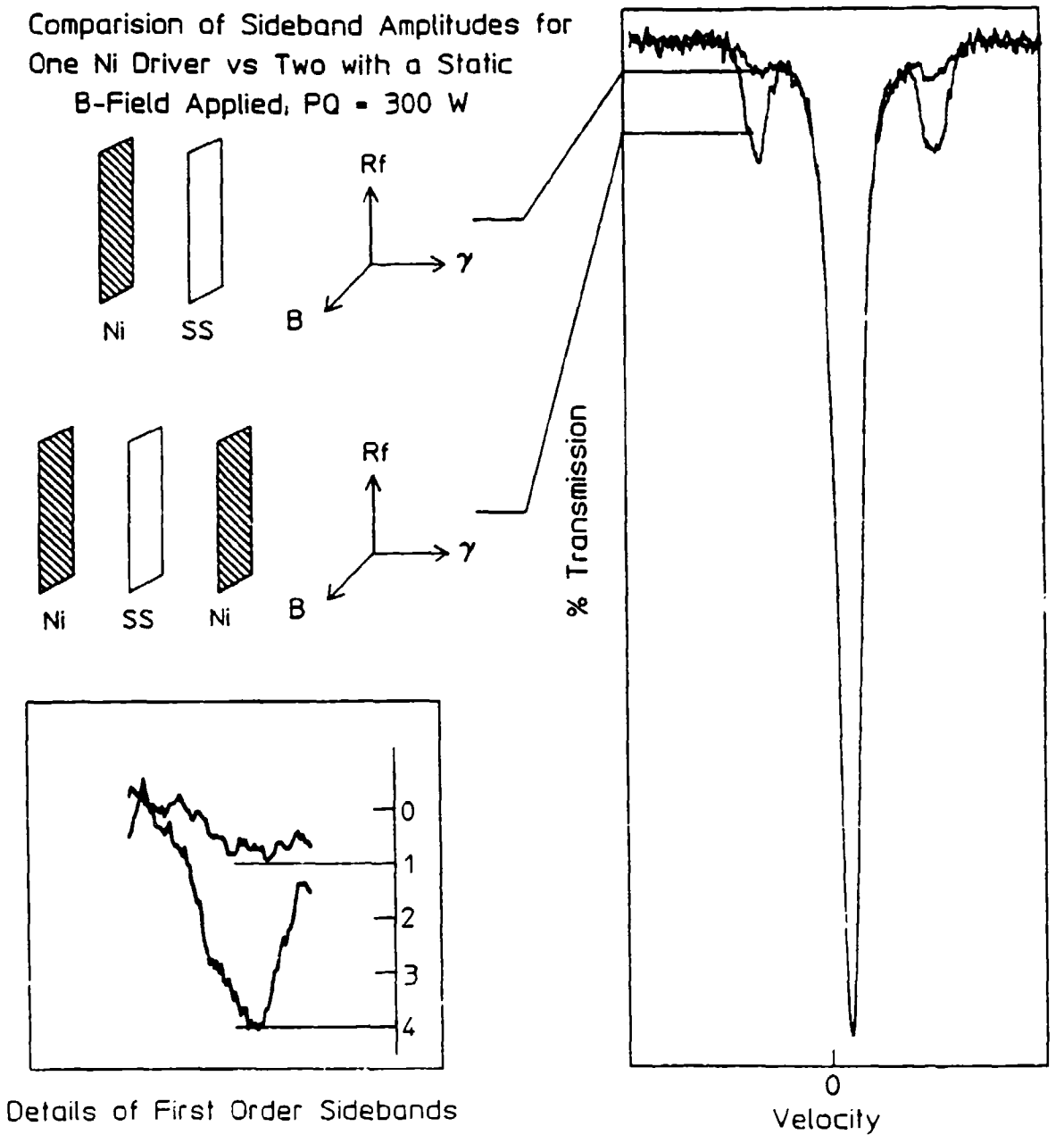

Details of First Order Sidebands

such threshold was suggested by data similar to that of Fig. 4.5 which was obtained over an adequate range of powers.

Magnetic Phase Modulation in Nonmagnetostrictive Permalloys

In both the ^{181}Ta and ^{67}Zn experiments, which were discussed in Chapter 1, the observed effects were small and required the application of large fields. An enhancement of the amplitude of the rf magnetic field acting on the Mössbauer nuclei would clearly result in a larger effect. However, joule heating and other effects make simply increasing the rf power unattractive. A more elegant technique, which can be used to enhance the magnitude of the field seen by the nucleus, is to embed the nuclei under investigation in a thin ferromagnetic foil[2-4]. In this case the magnetization of the foil is then controlled by the internal magnetic field B_0 and a perpendicular radiofrequency field B_{rf}. The applied radiofrequency field at the nuclear site is then enhanced by the ratio of the hyperfine magnetic field to the static field.

Unfortunately, in thin ferromagnetic foils there exists a coupling between the magnetic and elastic energy of the lattice which manifests itself as time-dependent magnetostrictive oscillations of the foil when it is subjected to a radiofrequency field. It is generally believed that this magnetostrictive-acoustic coupling introduces a Doppler motion of the iron nuclei and leads to a mechanical frequency modulation of the recoilless γ-radiation which is great enough to produce sidebands to each of the six allowed magnetic dipole (parent transitions) in the ^{57}Fe Mössbauer spectrum.[5-7] However, in view of the recent observations of magnetically induced transitions in the spectra of ^{181}Ta and ^{67}Zn it seems clear that this phenomena should be observable in ^{57}Fe as well and perhaps play a dominant role in magnetically soft materials, provided that the contribu-

tions to the sideband intensities due to mechanical effects can be eliminated.[8]

In this experiment the first clear evidence of radiofrequency modulation of the hyperfine fields of ^{57}Fe in a nonmagnetostrictive iron-nickel alloy is presented. Iron-nickel alloys, or permalloys as they are called, are of great scientific and technical interest because of their unusual magnetic properties. Permalloys are characterized by their high permeabilities and low magnetostriction. The magnetostriction of a polycrystalline permalloy passes through zero when the composition of the permalloy approaches 81 percent nickel.[9-11] More specifically, Mckeehan[9] established that to a first approximation the net magnetostriction should be a linear function of the concentration of either component (Fe or Ni) with a smooth passage of the magnetostriction through zero at 81 percent nickel. At this critical compositon in well annealed alloys, hystersis losses are at a minimum and the permeability is near maximum. The effect of composition versus magnetostriction is shown in Fig. 4.6.[12] Clearly, an 81 percent nickel permalloy is the ideal candidate in which to look for magnetically induced transitions in the Mössbauer spectrum of ^{57}Fe. With this goal in mind two permalloy foils were specially prepared for us by ONRL, one foil with 81 percent nickel and the other with 82 percent nickel. Each foil has a thickness of 2.5 μm with an ^{57}Fe-enrichment of 92.8 percent of the iron component of the alloy.

A conventional Mössbauer spectrometer using a 2.9 mCi source in a Pd matrix was used to obtain the ^{57}Fe absorption spectra. A Wavetek 3510 signal generator with a frequency range of 1 MHz to 1GHz and a 100-Hz resolution was used along with an ENI 550L 50-W linear amplifier, to generate the rf field at the absorber. Prior to taking the Mössbauer absorption spectra of the permalloys, with and without the presence of an rf field, the permalloy foils were annealed in dry hydrogen at a temperature of 1000°C for six hours.

Figure 4.6

Magnetostriction of the class of magnetically soft iron-nickel alloys, known as permalloys at various fractions of saturation versus the percent nickel in iron (after reference 12). The magnetostriction passes through zero when the composition of the permalloy approaches 81% Ni.

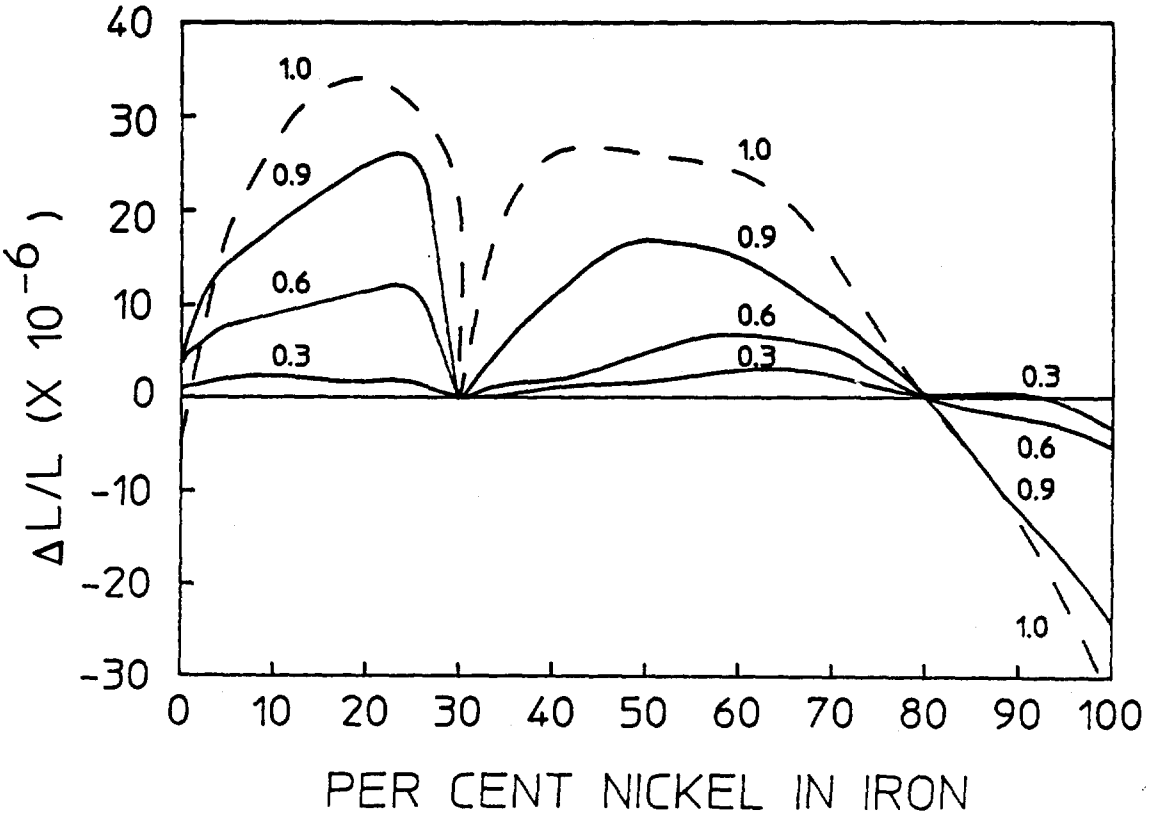
40
30
20
10
0
-10
-20
-30
ΔL/L (X 10⁻⁶)
1.0
0.9
0.6
0.3
1.0
0.9
0.6
0.3
0.3
0.6
0.9
1.0
0
10
20
30
40
50
60
70
80
90
100
PER CENT NICKEL IN IRON

Mössbauer spectra of the 81 and 82 percent permalloy were taken with and without rf, as shown in Fig. 4.7 and 4.8 respectively. The frequency of the applied rf field was 60 MHz and the product of power and Q-factor (PQ) of the resonator in which the foil was mounted was 12.5 watts. This PQ product is proportional to the intensity of the rf field acting on the absorber. Within the context of previous experiments on Mössbauer sidebands this is an extraordinarily low level of input corresponding to only 1.2 Watts of rf power into a Q of 10.42. This is to be contrasted with results reported in the literature[7] to require input powers approaching 1 kW at comparable frequencies.

As is shown by Fig. 4.7, sideband development is greatest in the foil in which there is little or no magnetostriction. Assay results from ORNL, obtained by mass spectrometry and in-house permeability measurements, confirm that the 81 percent Ni foil has characteristics reported in the literature necessary for the foil to have a minimum or zero in the magnetostriction.

Taking advantage of the unusual magnetic properties of a class of iron-nickel alloys known as permalloys we have, for the first time, demonstrated a direct interaction of the Mossbauer nucleus ^{57}Fe with a periodically oscillating magnetic field. The result of such an interaction is to generate a spectrum in which the six lines (parent transitions) in a normal absorption spectrum of ^{57}Fe are accompanied by additional absorption peaks (rf induced sidebands) when the absorber is subjected to a radiofrequency field.

Figure 4.7

(a) Mössbauer absorption spectrum of the 81% Ni permalloy showing the six parent lines resulting from a magnetic interaction of the dipole moment with the strong internal hyperfine fields present in the foil. (b) Rf spectrum of the same foil subjected to a radiofrequency field oscillating at 60 MHz and a PQ product of 12.5 W. Note the strong sideband development present in the spectrum even though the foil has negligible magnetostriction.

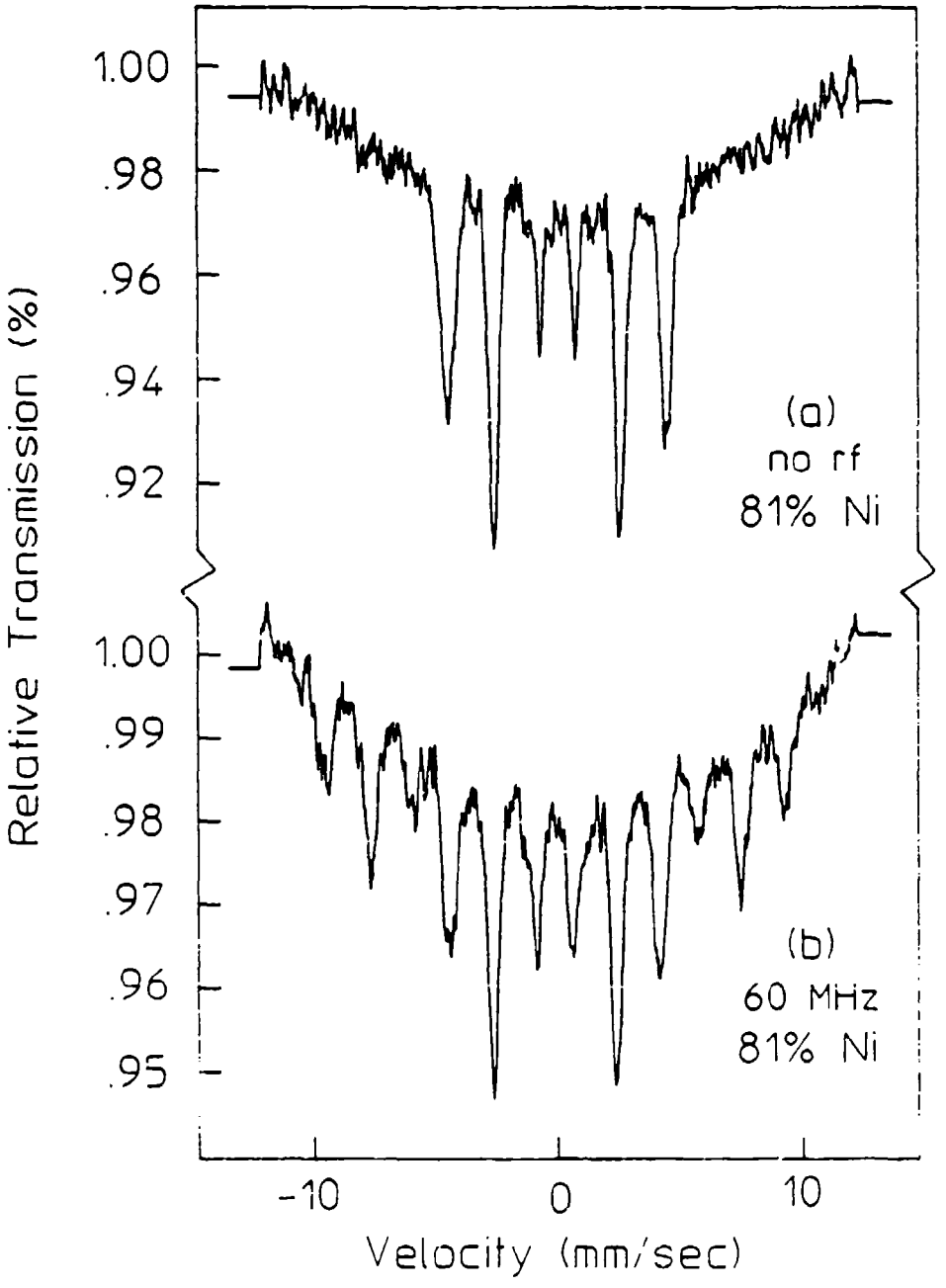
1.00
.98
.96
.94
.92
(a)
no rf
81% Ni
1.00
.99
.98
.97
.96
.95
(b)
60 MHz
81% Ni
Relative Transmission (%)
-10
0
10
Velocity (mm/sec)

Figure 4.8

(a) Mössbauer absorption spectrum of the 82% Ni permalloy foil. (b) Rf spectrum showing weak sideband development under identical rf conditions as that used to obtain the data of Fig. 4.7b. Even though this foil has a non-negligible magnetostriction, the permeability is lower in the 82% Ni permalloy than in the 81% Ni foil; hence, phase modulation effects are also weaker.

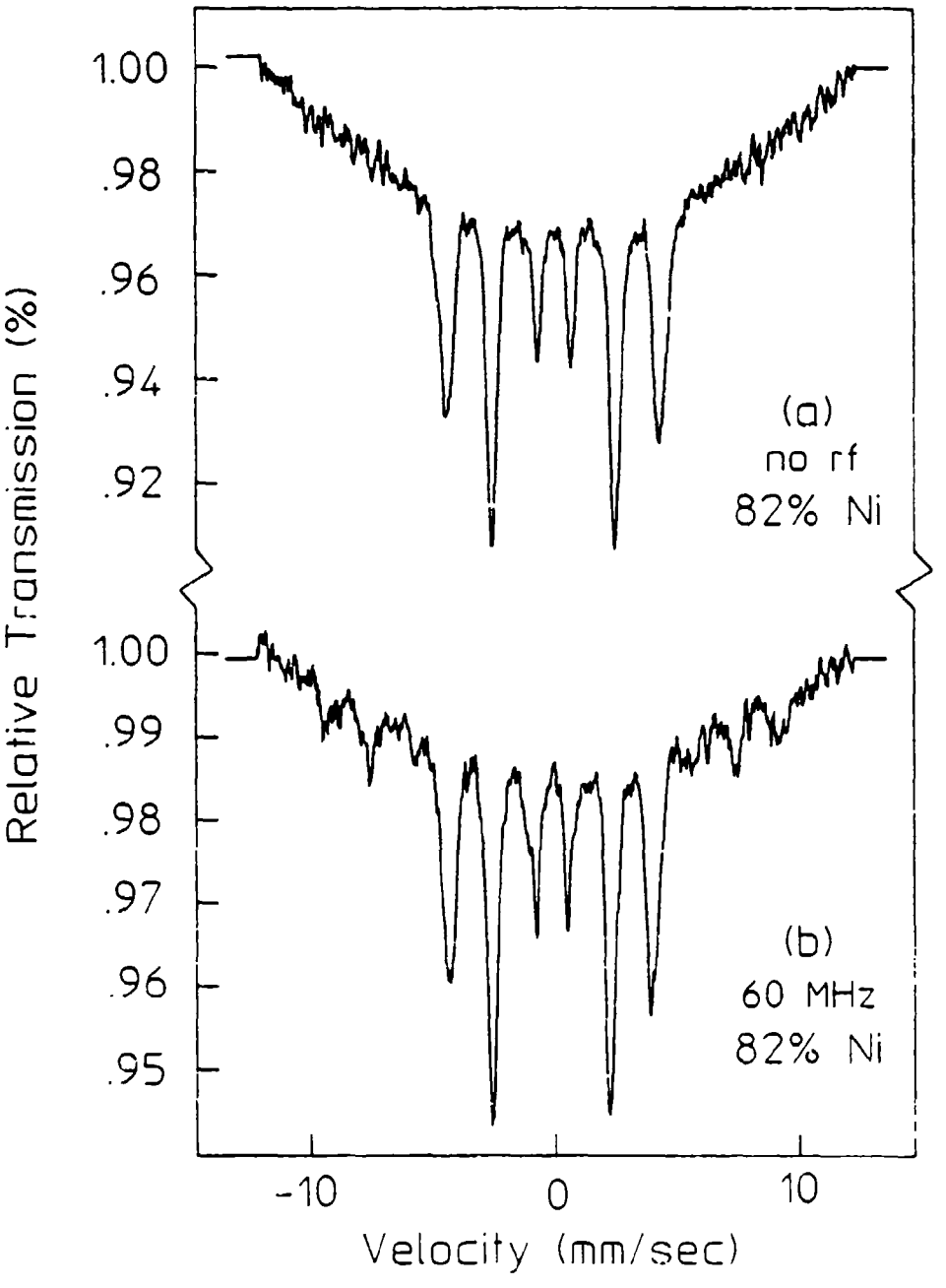
Relative Transmission (%)
1.00
.98
.96
.94
.92
(a)
no rf
82% Ni
1.00
.99
.98
.97
.96
.95
(b)
60 MHz
82% Ni
-10
0
10
Velocity (mm/sec)

REFERENCES

1. C. L Chien and J. C. Walker, Phys. Rev. B 13, 1876 (1976).
2. C. B. Collins and B. D. DePaola, Optics Lett. 10, 25 (1985).
3. B. D. DePaola and C. B. Collins, J. Opt. Soc. Am. B 1, 812 (1984).
4. B. D. DePaola, S. S. Wagal, and C. B. Collins, J. Opt. Soc. Am. B 2, 541 (1985).
5. N. D. Heiman, L. Pfeiffer, and J. C. Walker, Phys. Rev. Lett. 21, 93 (1968).
6. N. D. Heiman and J. C. Walker, Phys. Rev. 184, 281 (1969).
7. L. Pfeiffer, N. D. Heiman, and J. C. Walker, Phys. Rev. B 6, 74 (1972).
8. E. Ikonen, P. Helistö, J. Hietanieni, and T. Katila, Phys. Rev. Lett. 60, 643 (1988).
9. L. W. Mckeehan, Phys. Rev. 28, 158 (1926).
10. M. Kersten, Z. tech. Physik 12, 665 (1931).
11. R. Lichtenberger, Ann. Physik 15, 45 (1932).
12. R. M. Bozorth, Ferromagnetism, (D. Van Nostrand Co. Inc., Princeton New Jersey, 1964), p.556.

CHAPTER 5

EXPERIMENTAL RESULTS II

Introduction

During the last three decades there has been a tremendous number of publications dealing with ultrasonic and radiofrequency sidebands in Mössbauer spectroscopy. Nearly all of these used ^{57}Fe as the Mössbauer isotope. The only exception to this for ultrasonic sidebands is an experiment performed in 1962 by Burov et. al.,[1] on the ultrasonic splitting of the absorption line of $^{119}SnO_2$. Radiofrequency sidebands have been reported in only two isotopes other than ^{57}Fe;[2,3] they are ^{181}Ta and ^{67}Zn. In this chapter the results of an experimental investigation of ultrasonic and radiofrequency sidebands in ^{119}Sn are presented.

Chien and Walker Experiment with a Diamagnetic Tin Absorber

During the course of preliminary investigations into rf sidebands, one experiment of considerable importance was the demonstration of the inability to produce rf sidebands in the absorption spectrum of ^{119}Sn by using ferromagnetic drivers. By the magnetostrictive hypothesis it should be possible to transfer the sidebands into the tin absorber from ferromagnetic drivers, similar in technique to the Chien and Walker[4] experiment.

In the initial attempts to develop rf sidebands in tin, the absorber consisted of a 5 μm tin foil with 89.90% enrichement of ^{119}Sn sandwiched between two ferromagnetic non-absorbing nickel drivers of either 2.5 or 5 μm thickness. This composite sample was pressed together and rigidly held in contact by mounting the foils between two glass cover slides each of 100 μm thickness. This arrangement replicated the one used to transfer sidebands to stainless steel. The radiofrequency field was applied by

mounting the foils in a flat coil of about eight turns in an L-C circuit. To reduce the rf heating of the sample, the rf power was pulsed with a duty cycle of 1:3 and a pulse duration of 200 msec. Additional cooling of the sample was accomplished by mounting a small cooling fan above the absorber in the L-C tank circuit. Since tin is easily oxidized, the experiments were performed in a nitrogen atmosphere.

A conventional Mössbauer spectrometer using a 2 mCi source in a $CaSnO_3$ matrix was used to obtain the ^{119}Sn absorption spectra. To detect the 23.875-keV gamma-rays of the tin, a high resolution EG&G Ge detector and pre-amplifier which was negatively biased with 1000 V was used. With the use of an EG&G 552 PSA/T-SCA discriminator, it was possible to filter out electronically the 25.8-keV characteristic x-ray line of the tin source.

Experiments with a PQ product of up to 800 W were performed with no clear evidence of sideband development (where P is the applied rf power and Q is the quality factor of the L-C circuit). To make a comparison with a Ni-SS-Ni absorber, we note that pronounced sidebands are propagated into a stainless-steel absorber from the nickel driver foils with PQ products of only few watts.

The failure to transfer rf sidebands into a 5 μm tin foil from a pair of ferromagnetic driver foils is a very significant result. According to the magnetostrictive model, acoustic waves should exist in the ferromagnetic foils when they are subjected to an rf magnetic field. When placed in contact with the tin foil these acoustic vibrations should be detected in the tin Mössbauer spectrum as sidebands. The fact that this is not observed, even with the application of large rf fields, can be explained by assuming: (a) the ultrasonic properties of the Ni-Sn-Ni foils are not conducive to the transport of acoustic vibrations from the nickel to the tin or (b) the magnetostrictive-acoustic model is incorrect. If the conclusions drawn by Chien and Walker are even qualitatively correct this experiment should work. To assure that this failure is not due to extreme-

ly poor acoustic coupling between the driver foils and the tin, a brief discussion of the ultrasonic properties of the foils will now be presented.

Ultrasonic Properties of the Ni-Sn-Ni Absorber

The transfer of ultrasound from one material to another is analogous to the passage of light through materials with different refractive indices. Both phenomena are described by wave equations which are identical in form. For ultrasonic waves, instead of a refractive index to characterize the medium it is the acoustic impedence that is of importance. The acoustic impedence of a material is defined by

$$Z = \rho c \quad , \tag{5.1}$$

where ρ is the density of the material in g/cm^3 and c is the velocity of ultrasound in the material. The acoustic impedence is different for longitudinal (l) and shear (s) waves, so it is necessary to specify the type of wave when discussing impedence values of materials.

Closely following the analogy with light waves, the power transmission coefficient, α_t, can be calculated for the transmission of ultrasound from a material with a high impedence, Z_1, into a material with a lower impedence, Z_2. The power transmission coefficient has been given for ideal materials at normal incidence as[5]

$$\alpha_t = \frac{I_t}{I_i} \frac{4Z_1Z_2}{(Z_1 + Z_2)^2} \quad . \tag{5.2}$$

where I_t/I_i is simply the ratio of the transmitted intensity of the acoustic wave to the incident intensity. For longitudinal acoustic waves evaluation of Eq. (5.2) yields for a Ni-SS interface (Z_{Ni} = 49.5 g/cm^3sec

and Z_{SS} = 45.4 g/cm^{3}sec) a value of 99.81% for α_t. The same calculation for a Ni-Sn interface (Z_{Sn} = 24.2 g/cm^{3}sec) yields a value of 88.2% for the power transmission coefficient. For this idealized calculation, we see that even though the Ni-Sn interface is not as efficient for transport of ultrasonic waves, as is the Ni-SS foils, it is none-the-less not so poor as to prevent the formation of sidebands in the tin absorber. Clearly, the transfer of acoustic vibrations into the tin foil is sufficient for sidebands to develop if magnetostrictive-acoustic oscillations of the driver foils are the source of the sidebands in a Ni-SS-Ni absorber. However, even PQ products in excess of 800 W failed to produce the sidebands in tin.

Ultrasonic Sidebands in Tin

For completeness it was decided to repeat the experiment of Burov et al.[1] to determine if tin might have unusual ultrasonic properties making it particularly difficult to develop acoustic sidebands. The experiment was performed using the ultrasonic assembly described in Chapter 3. The absorber was a 1 cm^2 piece of tin with a thickness of 5 μm. The foil, which was annealed in a purified hydrogen atmosphere for six hours at 200°C, was acoustically bonded to an X-cut quartz pieozelectric transducer (PZT). The resonant absorption of ^{119}Sn without rf is shown in Fig. 5.1a. From the figure we see that the resonance is displaced from zero by 2.2 mm/sec. This is the isomer shift due to differing monopole interactions experienced by the tin nuclei in the source ($CaSnO_3$) and the absorber (metallic tin). The Mössbauer resonance is also very broad, with a FWHM of about 18 MHz. Figure 5.1b shows the rf spectra taken at the resonant frequency of the quartz PZT which was 24.0 MHz. Strong first order sidebands developed in the absorption spectra, as shown by the figure, with an applied rf voltage of only 6 mv corresponding to an applied power of

only 60 mW. Similar ultrasonic experiments performed using 310 SS and iron foils, as shown in Fig. 5.2, demonstrated that ultrasonic sidebands develop in tin with power level comparable to that necessary to develop them in stainless steel and iron foils.

The failure to produce rf sidebands in tin with ferromagnetic drivers can easily be explained in the context of magnetic phase modulation theory presented in Chapter 2. Tin is a diamagnetic material with a magnetic susceptibility of $\chi_{Sn} = -31 \times 10^{-6}$ (cgs units). Also, since tin has no uncoupled electrons there is no net spin to allow the propagation of the large amplitude spin waves generated in the ferromagnetic drivers in the the tin foil.

Iron-Tin Layered Alloys

Since ^{57}Fe and ^{119}Sn both have excellant Mössbauer properties, it is not suprising that there exists an abundance of Mössbauer data on Fe-Sn alloys and compounds. In this section we are interested in alloying tin with iron so that the tin nuclei experiences a nonzero internal hyperfine magnetic field which can be coupled to an rf magnetic field to modulate the quantum phases of the nuclear states.

When thin foils of iron and tin are placed in contact and heated, an interphase layer forms at the interface between the foils. The compounds which form in this layer are contingent upon the temperature and duration of the heat treatment. Vertes et al.,[6] demonstrated that at low temperatures (< 300°C) the interface layer will consist primarly of Fe_3Sn_2. At higher temperatures (> 400°C)the interphase layer will consist mainly of $FeSn_2$. Vertes et al.[6] also reports that the thickness of the interphase region will change according to $\Delta x^2 = k\Delta t$, where k is proportional to the diffusion coefficient for tin into iron and t is the time. From their

Figure 5.1

The Mössbauer absorption spectrum of a 5 μm tin foil enriched with 89.90% ^{119}Sn. (a) Unperturbed spectrum and (b) spectrum of the same foil acoustically bonded to an X-cut piezoelectric transducer oscillating at a frequency of 24.0 MHz. Clear first order sidebands due to mechanical frequency modulation are shown to have developed.

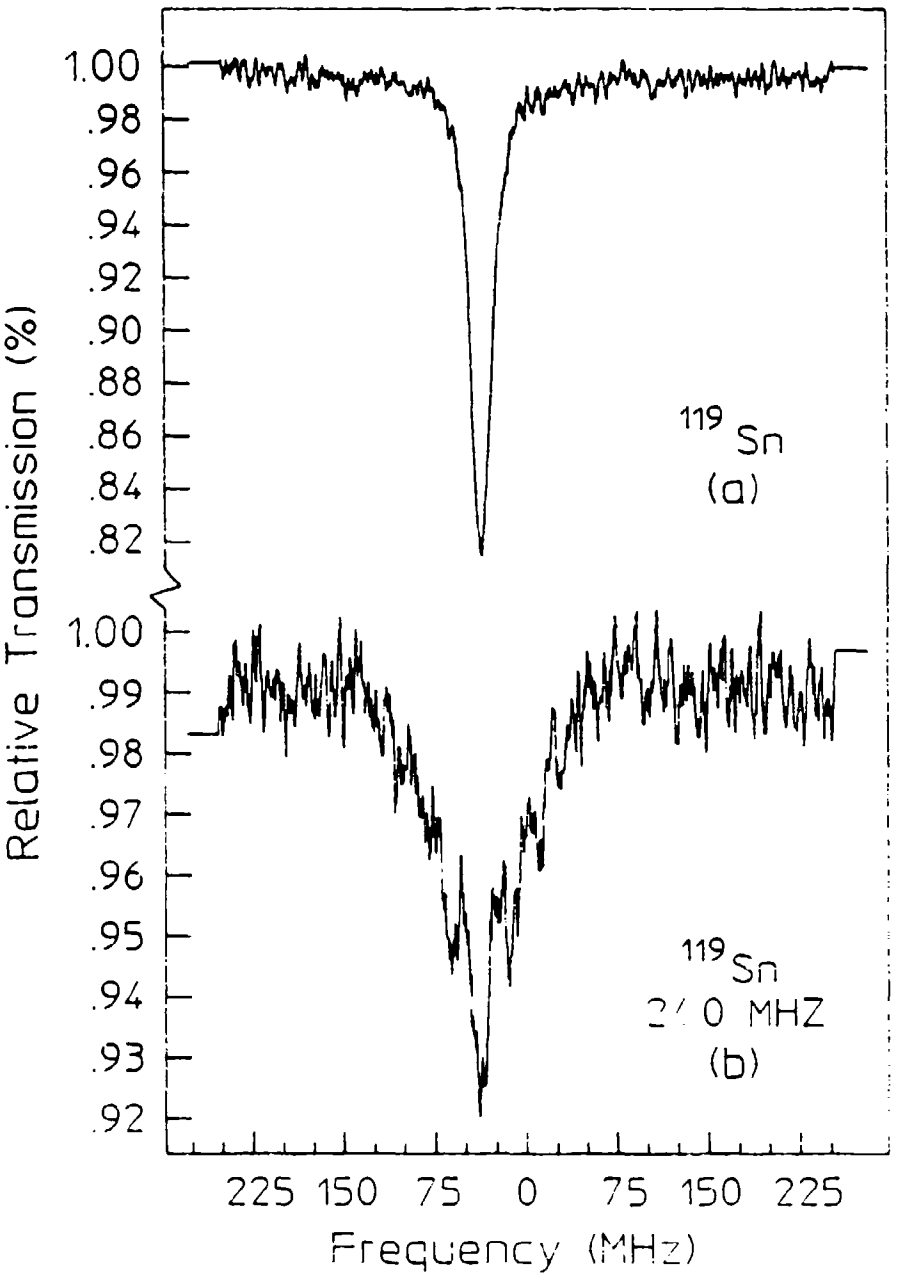
1.00
.98
.96
.94
.92
.90
.88
.86
.84
.82
1.00
.99
.98
.97
.96
.95
.94
.93
.92
Relative Transmission (%)
119 Sn
(a)
119 Sn
2 0 MHZ
(b)
225 150 75 0 75 150 225
Frequency (MHz)

Figure 5.2

Ultrasonic sidebands generated in (a) a 2.5 μm foil of 310-SS and (b) a 2.5 μm iron foil. Both absorbers were enriched with 90.89% ^{57}Fe. The sidebands were generated using an X-cut quartz piezoelectric transducer oscillating at 24 MHz.

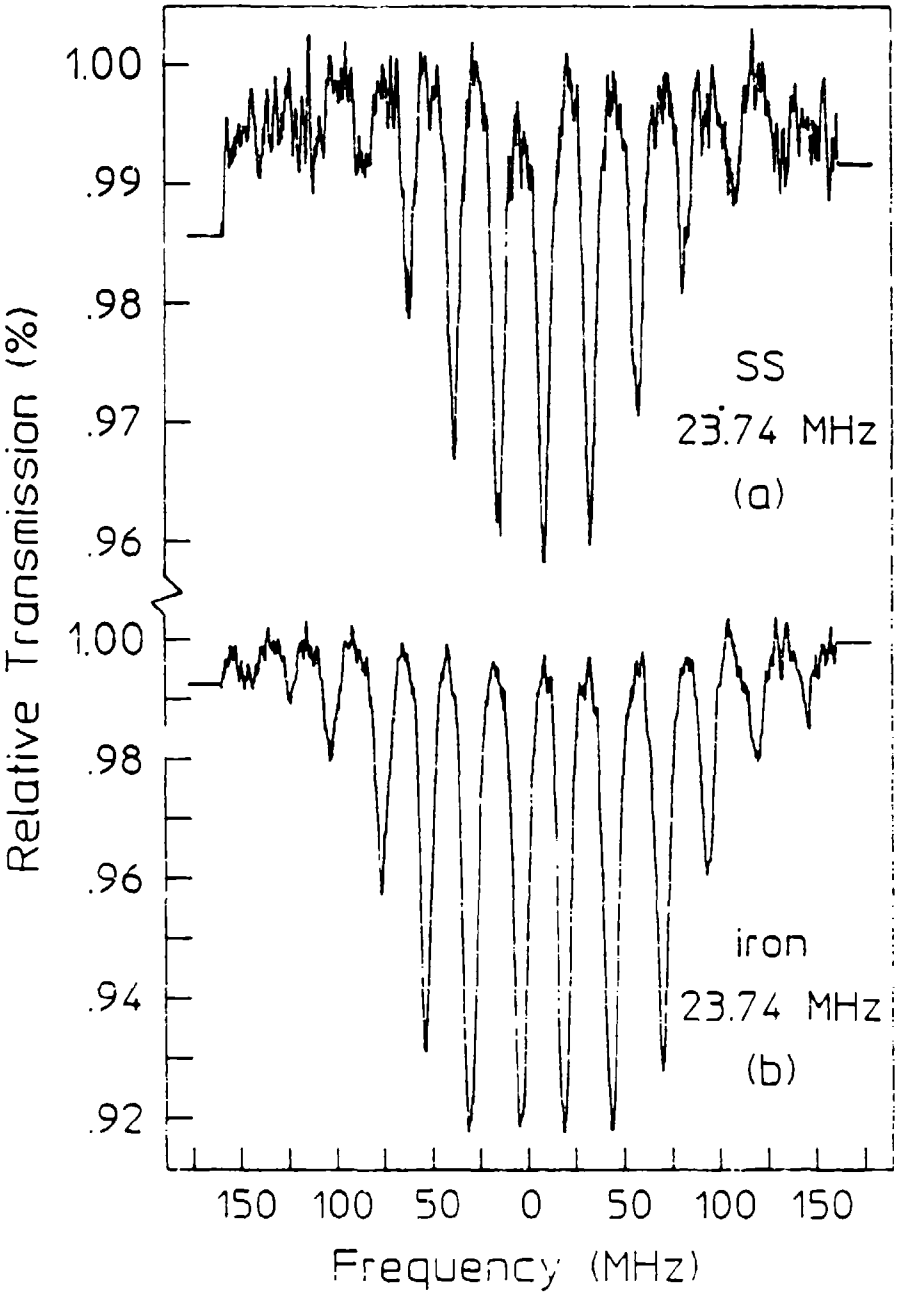
1.00
.99
.98
.97
.96
1.00
.98
.96
.94
.92
Relative Transmission (%)
SS
23.74 MHz
(a)
iron
23.74 MHz
(b)
150 100 50 0 50 100 150
Frequency (MHz)

experimental data they concluded that the thickness of the alloyed layer could be calculated from the Mössbauer absorption spectrum by

$$x = \frac{d}{1 + RS_\beta/S_\alpha} \frac{C_\beta}{C_\alpha} \quad , \tag{5.3}$$

where d is the original thickness of the tin layer, S_β and S_α are the corresponding areas under the Mössbauer resonance for both the alloyed and unalloyed tin. The values C_β and C_α are the concentrations of the unused tin and the alloyed tin and R is the ratio of the recoilless fractions.

The construction of the iron-tin layered alloys is as follows. A 6 μm foil of natural iron was held in rigid contact with a 5 μm foil of ^{119}Sn and placed in an oven and baked at 425°C for six hours in a purified hydrogen atmosphere to reduce any oxides present in the foils. Under these conditions a layered alloy was formed with the composition Fe + $FeSn_2$ + Fe_3Sn + Sn. Figure 5.3a shows the resulting absorption spectra of this composite absorber. The compond $FeSn_2$ is antiferromagnetic with a Neel temperature, T_N of 393 K.[7] The absorption spectrum consist of a paramagnetic component and hyperfine structure of magnetic origin in the form of an unresolved doublet which is characteristic of $FeSn_2$ with $T < T_N$. With increasing temperature, the separation of the lines would decrease until $T > T_N$, at which point they would coalesce into a single line.[8] The observed spectrum corresponds to an incomplete resolution of the hyperfine pattern. The isomer shift of the center of gravity of the doublet is + 2.2 ± 0.1 mm/sec. In the literature it is reported that the cross-section for the absorption of the 23.875-keV γ-rays of $FeSn_2$ is approximately the same as that for SnO_2.[8]

A study of the magnetic structure of $FeSn_2$ by neutron diffraction has been reported by G. Le Caër et al.,[9] who found that at room temperature the magnetic structure is collinear and characterized by ferromagnetic (100)

planes coupled to [100] directions. The hyperfine magnetic field felt by the tin nuclei can be calculated from the splitting of the absorption line by using Eq. (2.9). From the spectrum in Fig. 5.3a this calculation yields a magnetic field of approximately 25 kOe at the nuclear tin sites.

The rf spectrum of this layered iron-tin absorber is shown in Fig. 5.3b. The absorber was mounted in a flat coil of a L-C circuit and an rf magnetic field was applied. With a PQ product of 620 W and a frequency of 75 MHz, sidebands up to third order were observed in the ^{119}Sn absorption specrum.

Nickel-Tin Layered Alloys

Many Mössbauer studies have been carried out on the intermetallic compounds of FeSn and $FeSn_2$, but limited studies have been carried out on the intermetallic compounds of nickel and tin. The work of Leideiser et. al.,[10] represents the first such attempt to study the Mössbauer properties of nickel-tin systems.

Tin and nickel alloy readily, forming compounds such a Ni-Sn, Ni_3Sn_2 and Ni_3Sn_4. Which compound actually forms again depends upon the temperature and duration of the heat treatment. Nickel-tin alloys have a ^{119}Sn absorption spectrum similar to that of $FeSn_2$ (Fig. 5.4a) both of which are due to magnetic dipole interactions. The NiSn alloys have much narrower line separation than that for the $FeSn_2$ spectra (30 MHz vs. 70 MHz); therefore, lower rf frequencies could be applied without sacrificing the clarity of the spectrum (i.e. no overlapping resonances), resulting in sideband development at much lower powers (sideband generation requires lower rf power at lower frequencies). The magnetic field at the tin nuclear sites in the NiSn absorbers indicate that they experience an internal hyperfine field of about 8 kOe. The rf Mössbauer spectrum of the NiSn layer of the composite absorber is shown in Fig. 5.4b.

Figure 5.3

The Mössbauer absorption spectum of an $FeSn_2$ interphase region of a layered absorber constructed by pressing thin foils of iron and tin together and heat treating in a purified hydrogen atmosphere. The doublet structure is due to a magnetic dipole interaction.

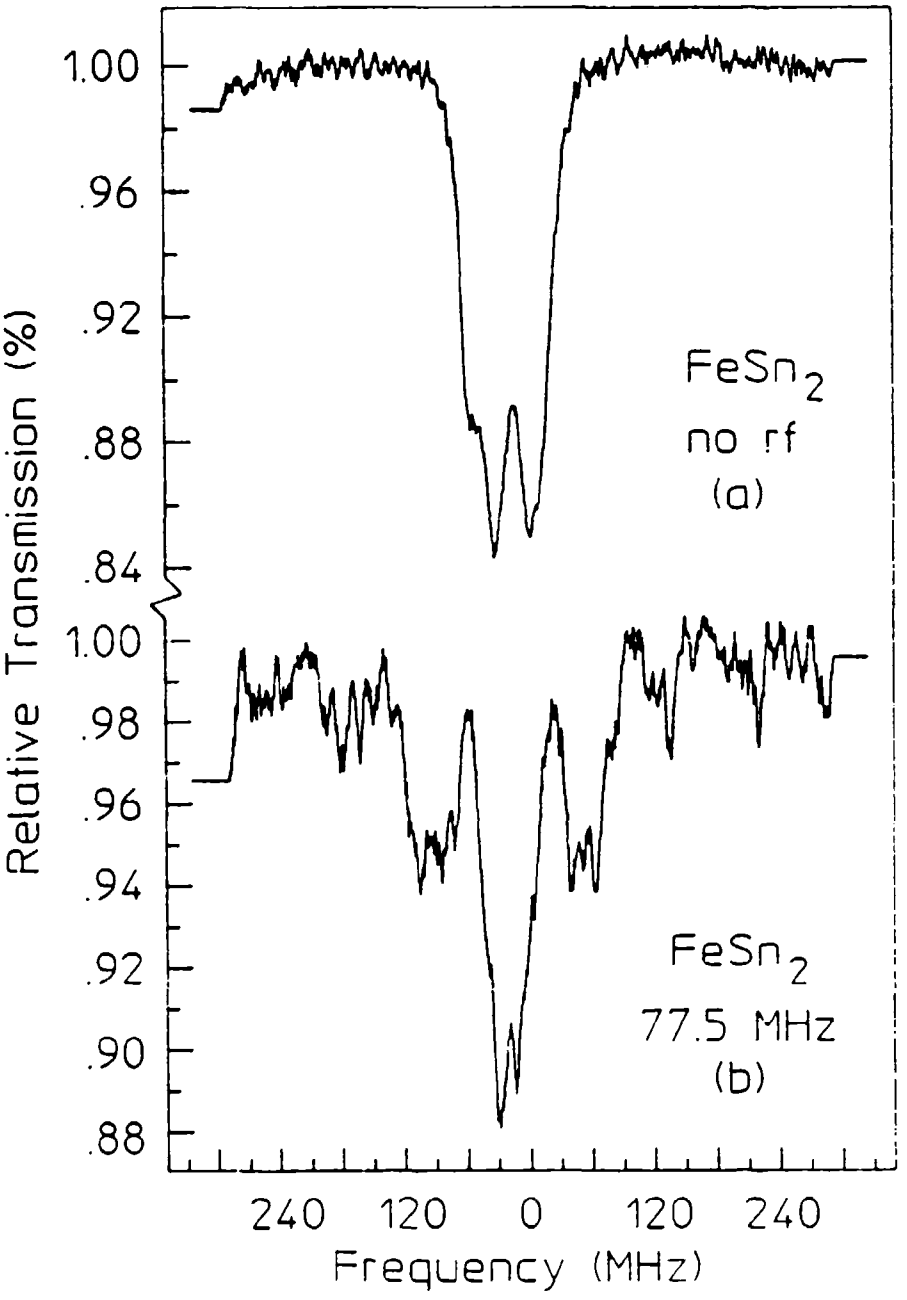
1.00
.96
.92
.88
.84
1.00
.98
.96
.94
.92
.90
.88
Relative Transmission (%)
FeSn2
no rf
(a)
FeSn2
77.5 MHz
(b)
240
120
0
120
240
Frequency (MHz)

Figure 5.4

Mössbauer spectra of the NiSn interphase region of a composite absorber constructed by pressing thin foils of nickel and tin together and heat treating in a purified hydrogen atmosphere. The doublet is characteristic of the compound NiSn as reported by Leidheiser et. al.,[10] and is the result of a magnetic dipole interaction. The separation of the two peaks is 30 MHz. (b) Rf spectrum at 75 MHz showing strong sideband development.

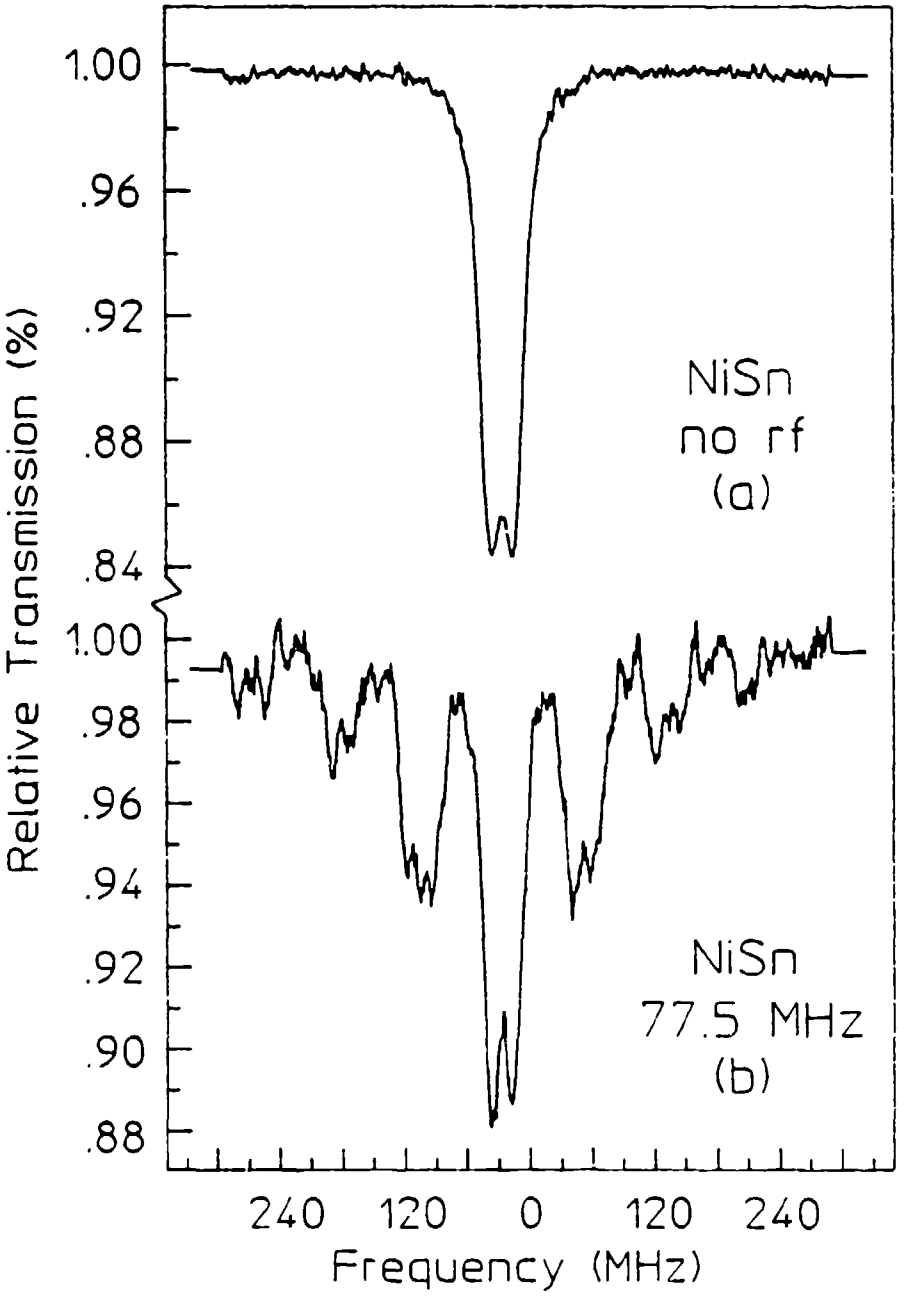
1.00
.96
.92
.88
.84
1.00
.98
.96
.94
.92
.90
.88
Relative Transmission (%)
NiSn
no rf
(a)
NiSn
77.5 MHz
(b)
240
120
0
120
240
Frequency (MHz)

The magnetostrictive hypothesis would explain the above experiments if it were assumed that the acoustic coupling between the tin and driving foils were greatly increased by the alloying, thereby producing acoustic waves in the sample. However, the dramatic failure of a Chien and Walker experiment with a tin absorber sandwiched between ferromagnetic Ni foils rules out this possibility. Since hyperfine structure is present in the spectra of the alloys, the sideband development must result from the modulation of the interaction energy of the applied radiofrequency field with the nuclear magnetic moments, thereby resulting in nuclear phase modulation of the nuclear states.

REFERENCES

1. V. A. Burov, V. A. Krasil'nikov, and O. Yu Sukharevskaya, Sov. Phys. JETP 43, 837 (1962).
2. E. Ikonen, P. Helisto, J. Hietanieni, and T. Katila, Phys. Rev. Lett. 60, 643 (1988).
3. P. J. West and E. Matthias, Z. Phys. A 288, 369 (1978).
4. C. L. Chien and J. C. Walker, Phys. Rev. B 13, 1876 (1976).
5. Lawrence E. Kinsler and Austin R. Frey, Fundamentals of Acoustics, 2nd ed., (John Wiley & Sons, Inc., New York, 1962), Chp. 6, p. 128.
6. A. Vertes, S. Nagy and M. Z. Awas, Nuclear Instrum. and Methods 199, 367, (1982).
7. V. A. Varnedk, L. I. Strugova, and E. G. Avvakumov, Sov. Phys. Solid State 16, 1186 (1974).
8. V. I. Nikolaev, Yu.I. Slacherbina, and A. I. Karchevskii, Sov. Phys. JETP 44, 775 (1963).
9. G. Le Caër, B. Malaman, G. Venturini, D. Fruchart and B. Roques, J. Phys. F: Met. Phys. 15, 1813 (1985).
10. H. Leidheiser, I. Czako-Nagy, M. L. Varsanyi, and A. Vertes, J. Electrochem. Soc. 126, 204 (1979).

CHAPTER 6

EXPERIMENTAL RESULTS III

Introduction

The excitation of coherent transients in Mössbauer spectra has been previously limited to a low range of frequencies by the high powers required to modulate the nuclear phases.[1] Reported in this chapter is an eleven orders-of-magnitude increase in the efficiency through which such phenomena can be produced. Magnetic modulation of the quantum phases of ^{57}Fe nuclei has been produced by magnetostatic spin waves excited at large amplitudes in paramagnetic stainless steel foil. Transport of the waves allowed the observation of coherent effects in a region where spurious acoustic vibrations were absent. Sidebands were found on the 14.4-keV line of ^{57}Fe with less than a 1% contribution from the phonons.

The propagation of magnetoelastic waves is a complex problem which has been intensively studied since 1958.[2] For many magnetic media the dispersion equation for such waves displays several branches[3,4] which can be individually identified with spin waves, magnetostatic waves or elastic waves, as shown in Figure 6.1. Mixed waves coupling magnons and phonons occur principally when branches intersect, so that the frequencies and wavelengths for both are nearly equal.[2] Away from those values of parameters magnetic and acoustic waves can be separated. In principle this offers a means to propagate only the former to a sample in which it is desired to magnetically modulate the phases of the states of the nuclei to be observed there without the concomitant introduction of acoustic noise.

The most convenient of the Mössbauer transitions for modulation experiments is the 14.4-keV transition of ^{57}Fe diluted in a thin metal foil. The propagation of magnetic waves in conductive foils presents a special problem because of eddy current losses and Kittel has given an approximation[2] which would limit the mean free path for a magnon to a few wavelengths for the frequencies of tens of MHz which would be interesting for use with ^{57}Fe. For this reason the preferred choices for the propaga-

Figure 6.1

Dispersion curve showing a plot of the wavevector k of spin waves as a function of energy (after reference 4).

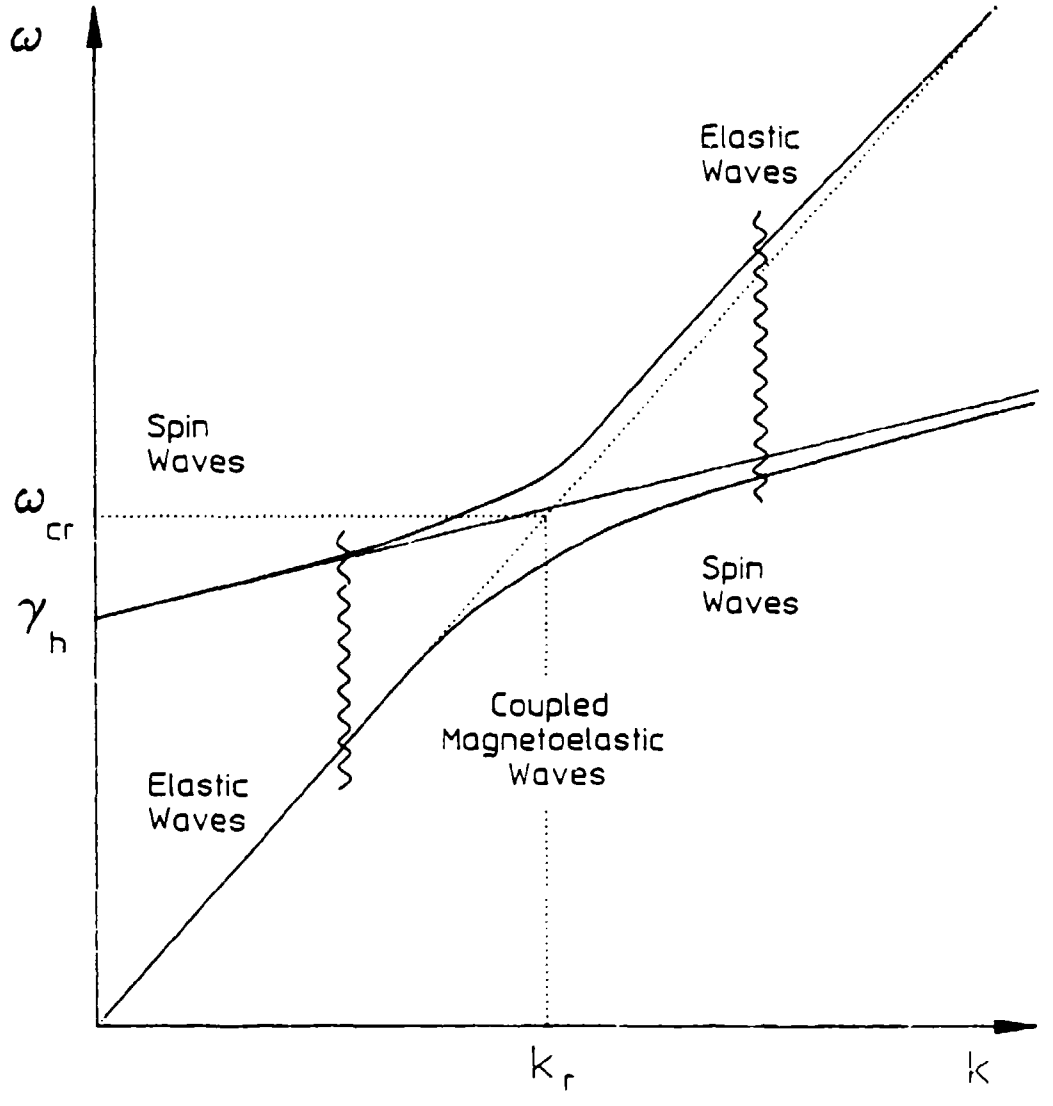
ω
Elastic
Waves
Spin
Waves
ω cr
γ h
Spin
Waves
Coupled
Magnetoelastic
Waves
Elastic
Waves
k r
k

steel foil of 2.5 μm thickness was acoustically bonded to the transducer. The remaining length of the 10 mm × 20 mm stainless foil was gently curved, forming a 90 degree angle with the plane of the transducer. Mechanical support was provided for the transverse section of foil by mounting it between glass cover slides which were then fastened to the transducer cell.

In the usual longitudinal geometry for a transmission experiment, a convenient level of input power of 0.06 W produced the reference level of sideband development seen in Fig. 6.3 in which the 4th order contained 34% of the intensity remaining in the parent transition. In the transverse geometry, the effect of phonons transported in the foil about 1 cm around a bend of 90 degrees could not be detected even with a tenfold increase in power above the reference level. Such an absence of phonons seems consistent with the difficulties expected in propagating transverse vibrations through a medium thin in comparison to a wavelength of sound. This experiment was performed with both X- and AT-cut quartz crystals for transducers as shown in Figs. 6.2a and 6.2b. Sidebands were not observed in the transverse geometry in either case, and the AT-cut transducer required a larger input power of 2.9 W in the longitudinal geometry in order to obtain the same reference level of sideband development.

In the second experimental arrangement, the piezoelectric transducer was replaced with a pair of 2.5 μm foils of ferromagnetic Ni (8 mm × 10 mm) which were periodically magnetized as shown in Fig. 6.2c. The foils (Ni-SS-Ni) were held in rigid contact by sandwiching them between glass cover slides. The protruding section of the stainless foil was again bent at an angle of 90 degrees and enclosed between glass cover slides in the same way as before. Mechanical rigidity was provided to the absorber assembly by a plastic frame.

An rf magnetic field of 0.07 mT was applied to the absorber via a flattened induction coil of a tuned L-C circuit. In the longitudinal geometry for observation the rf power level was adjusted to give about the

Figure 6.2

Schematic representation of the mounting arrangements used in the excitation of sidebands on the Mössbauer absorption line of ^{57}Fe in a 2.5 μm thick stainless steel (SS) foil shown as shaded. The optical path from gamma source to detector is shown by the dotted arrow for the orthogonal directions marked as longitudinal and transverse. Excitation is injected into the horizontal face of the SS-foil and the vertical face is mechanically stabilized by the 100 μm thick glass cover slides sandwiching the absorber foils.

(a) Vibrational excitation injected by the X-cut quartz crystal transducer connected to a radiofrequency oscillator.

(b) Vibrational excitation injected by the AT-cut quartz crystal transducer connected to a radiofrequency oscillator.

(c) Spin waves injected by the periodic oscillation of the Ni foils pressed onto the absorber foil by additional cover slides not shown and excited by the magnetic field in an inductor containing the Ni foils. The vertical section protrudes from the coil between windings.

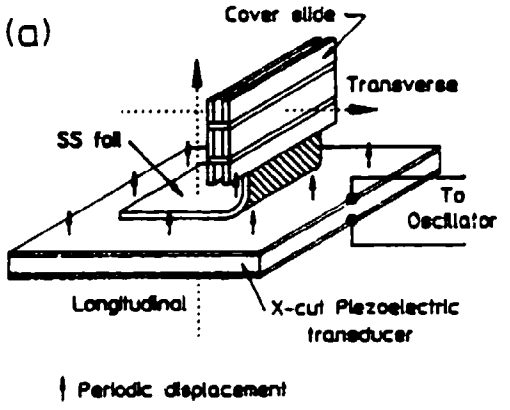
(a)
Cover slide
Transverse
SS foil
To
Oscillator
Longitudinal
X-cut Piezoelectric
transducer
Periodic displacement

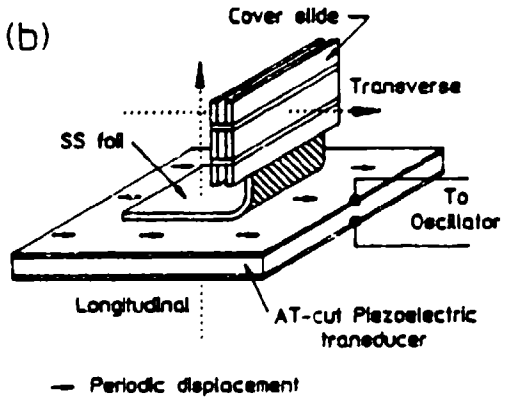
(b)
Cover slide
Transverse
SS foil
To
Oscillator
Longitudinal
AT-cut Piezoelectric
transducer
Periodic displacement

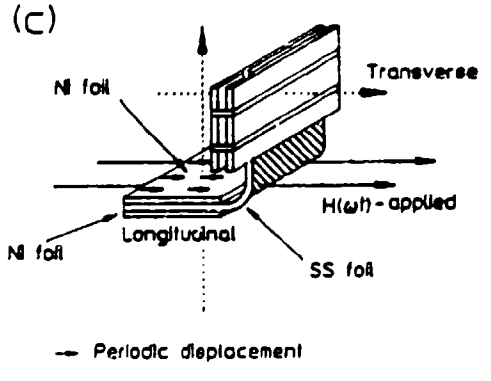
(c)
Ni foil
Transverse
H(ωt) - applied
Longitudinal
Ni foil
SS foil
Periodic displacement

same reference level of sideband development as had been generated with the piezoelectric transducer, thus facilitating a direct comparison of the propagation of ultrasonic sidebands with those induced by phase modulations generated by magnetostatic waves.

The spectra obtained in the longitudinal and transverse geometries of Fig. 6.2c are shown in Fig. 6.4. In the transverse geometry at this same level of input power, first order sidebands containing about 22 percent of the intensity of the parent line developed. This represents a level 10 times the threshold for detection and hence 100 times any component contributed by acoustic phonons as determined from the data of Fig. 6.3 obtained with the experimental arrangement of Fig. 6.2a. It seems that these experiments have shown that an oscillating alignment of spins can be propagated through such a stainless foil better than mechanical vibrations can be transported under the same condition.

Excited on one end by the oscillating magnetization of a strip of ferromagnetic Ni, the absorber foil showed the strong development of sidebands at the other end where mechanical vibrations were shown to contribute less than 1% of the signal. In these experiments the driving amplitude, H_o in the Ni, was only 0.07 mT while the frequency was 23.74 MHz. Without the excitation of spin waves the effect should have been smaller by at least the ratios of the scaling parameters,[1] $(B_o/\omega)^2$, a factor of 10^{11} for this case. Even with some attenuation of the spin waves during transport, the great enhancement in the effects of coherent modulation which they produced in this arrangement makes possible the examination of many predicted coherent phenomena over practical ranges of tuning at accessible levels of input powers.

Bridging Experiments

In the previous section it was shown that radiofrequency sidebands induced in a paramagnetic stainless foil from a pair of ferromagnetic drivers could be transported away form the source foil along a length of stainless tape. It was demonstrated that the acoustic vibrations in the foils contributed less than 1% of the signal of the transported sidebands. Without the excitation of spin waves the effect should have been smaller by at least the ratios of the scaling parameters, $(B_0/\omega)^2$, a factor of 10^{11} for this case. If indeed spin waves are the transport mechanism for these magnetically induced sidebands then it should be possible to transport this effect through any paramagnetic material. In this section the results of a series of experiments designed to qualitatively verify that spin waves are the transport mechanism of magnetic sidebands in paramagnetic materials and also provides the remarkable amplification of the phase modulation of nuclear states observed in the last section.

Spin waves (or magnons) are low-lying excitations that occur in ordered magnetic materials. In ferromagnetic or anitferromagnetic materials the long-range magnetic ordering decreases as the temperature increases until eventually there is a phase transition to a disordered (paramagnetic) state. This critical temperature is known as the Curie temperature T_C in ferromagnets and as the Neel temperature T_N in antiferromagnetic materials.

The concept of spin waves, as the lowest lying magnetic states above the ground state, was introduced by Bloch in 1930. He hypothesised the spin waves as deviating slightly from their ground state, and that these disturbances would then propagate with a wavelike behavior through the material.

Several techniques are used to study spin waves. Light scattering from magnons and inelastic neutron scattering are the most useful techniques for studying the dispersion of magnons. Electron energy loss

Figure 6.3

Absorption spectra of ^{57}Fe in stainless showing sidebands developed by phonons present in the sample foil.

(a) Reference spectrum observed in the longitudinal geometry at a level of excitation of 0.06 W in the piezoelectric crystal.

(b) Sidebands observed in the transverse geometry of Fig. 6.2a for an excitation level of 0.7 W. Only the unsplit parent line is seen.

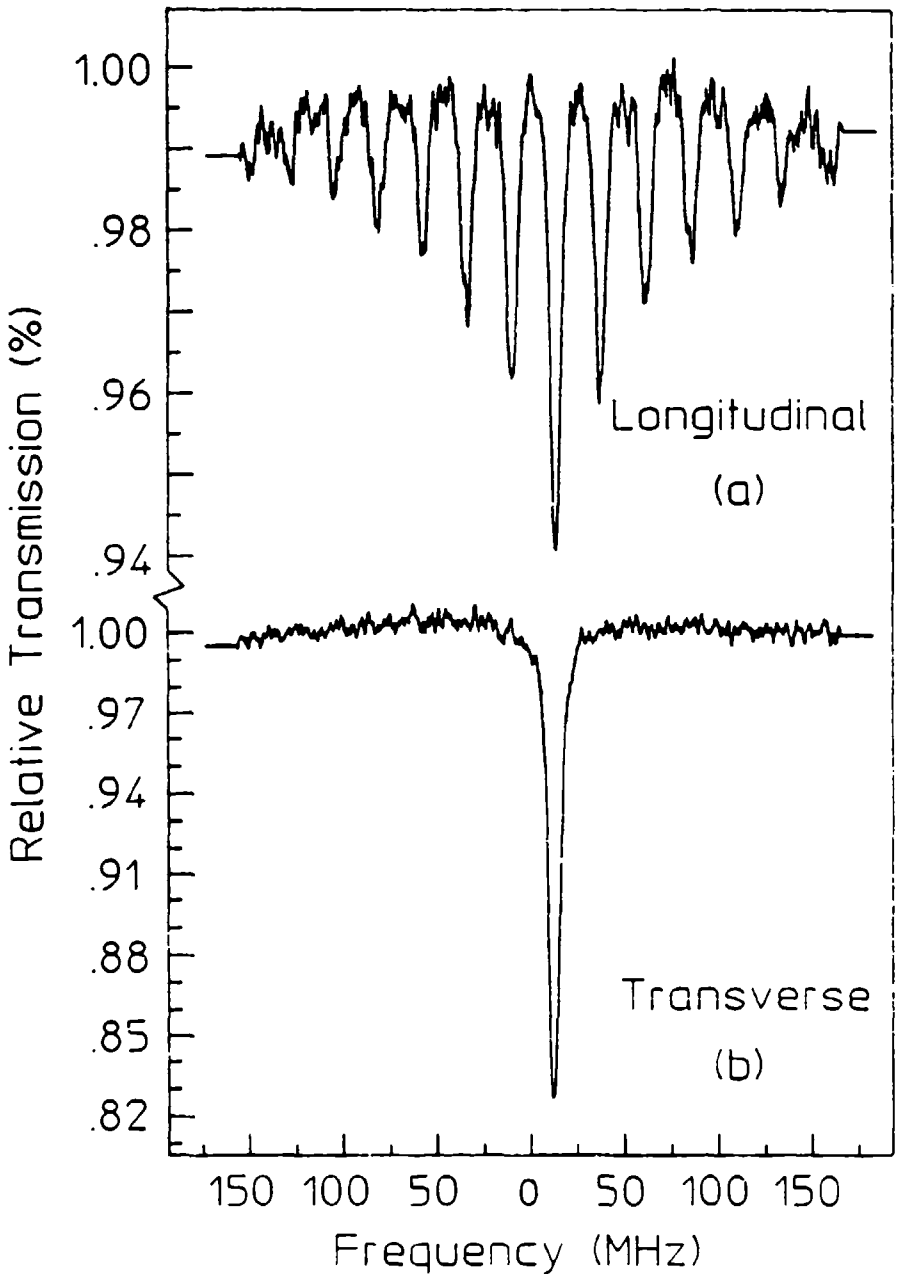
1.00
.98
.96
.94
1.00
.97
.94
.91
.88
.85
.82
Relative Transmission (%)
Longitudinal
(a)
Transverse
(b)
150 100 50 0 50 100 150
Frequency (MHz)

Figure 6.4

Absorption spectra of ^{57}Fe in stainless showing sidebands resulting from the modulation of nuclear phases by spin waves present in the sample foil.

(a) Reference level of excitation observed in the longitudinal geometry of Fig. 6.1b at a field amplitude of 0.07 mT.

(b) Sidebands observed in the transverse geometry for the same driving field of 0.07 mT.

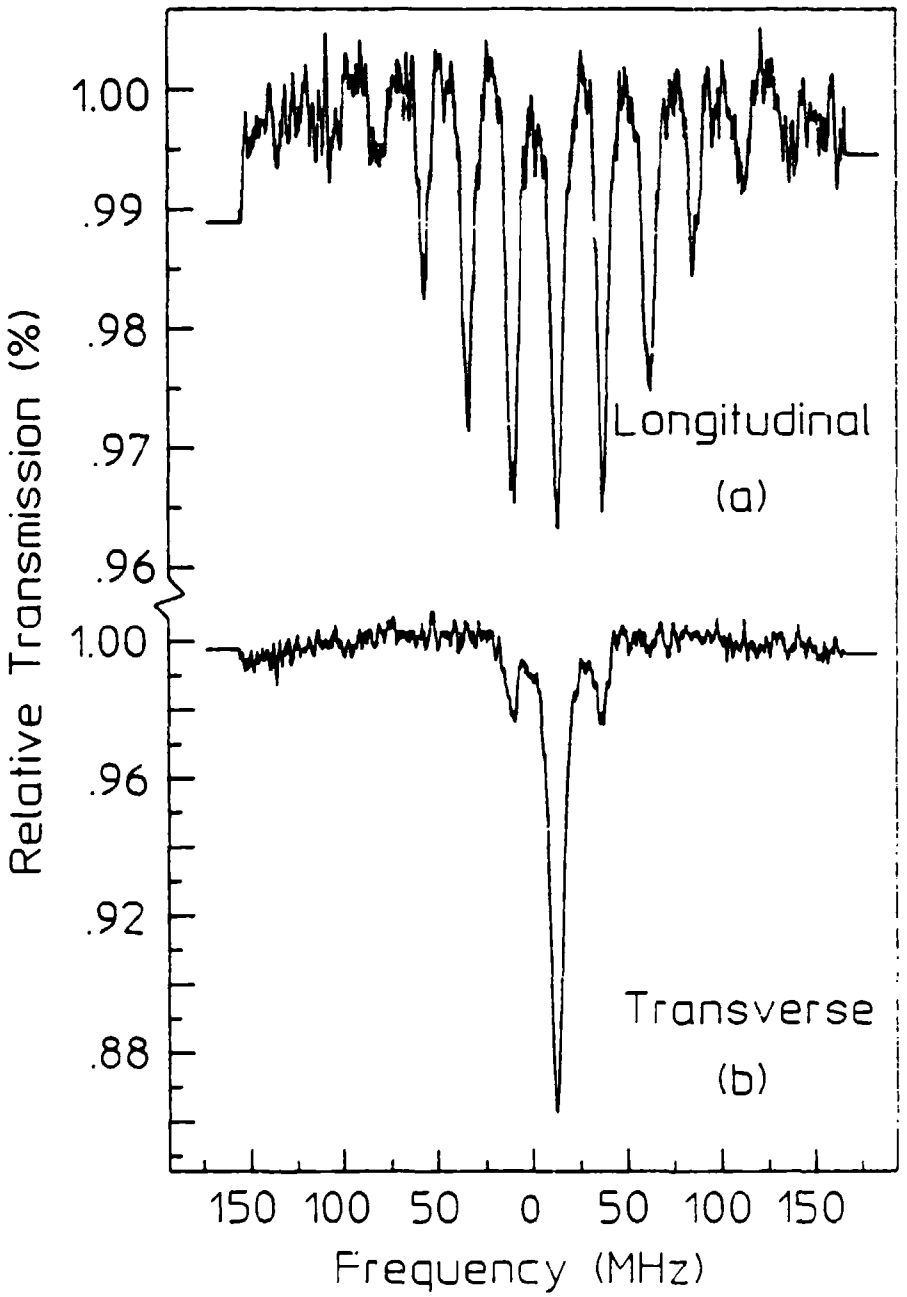
1.00
.99
.98
.97
.96
1.00
.96
.92
.88
Relative Transmission (%)
Longitudinal
(a)
Transverse
(b)
150 100 50 0 50 100 150
Frequency (MHz)

spectroscopy is another scattering technique used to study excitation on crystal surfaces. Magnetic resonance spectroscopy can also be used.

The absorber arrangement for the sideband transport experiments reported in this section is shown in Figure 6.5. A 2.5 μm, ferromagnetic nickel foil with a surface area of 1 cm^2 was used as the source of large amplitude magnetic oscillations which were injected into a variety of foils with varying magnetic susceptiblilites. The bridging foils were chosen on the basis of whether or not they have a positive or negative magnetic susceptibility which would indicate whether the material is paramagnetic ($\chi > 0$) or diamagnetic ($\chi < 0$). If spin waves are the transport, medium then large amplitude spin waves generated in the nickel foil should propagate across a paramagnetic bridge which connects the nickel and stainless foils. In diamagnetic materials where there are no unpaired electrons, the medium for spin wave transport is nonexistent and the waves of oscillating magnetization quickly die out once they enter the material. The resulting phase modulation of the nuclear states is then detected in the 310 SS paramagnetic absorber enriched with 90.82% ^{57}Fe of the iron component of this alloyed foil.

The results of these experiments for a variety of bridging materials is summarized in Table 6.1. The second column of the table gives the magnetic susceptibility of the bridging material. A cursory examination of table reveals the mechanism responsible for the transport of nuclear phase modulation effects can propagate only through paramagnetic bridging foils, a result consistent with the spin wave hypothesis.

As a basis of comparision the acoustic impedences of the bridging foils are also given in Table 6.1. The acoustic impedance, as was discussed in Chapter 5, is simply a measure of how well acoustic vibrations can be propagated through a material. As can be seen from the table there is no correlation between the acoustic coupling between the foils and the transport of the effect, whereas the correlation between the transport of

the effect and the magnetic properties of the bridging foil is excellent. For example, consider the case for Al which has a magnetic susceptibliity of + 16.5 ($\times 10^{-6}$ cgs) and shows a strong transport of sidebands as seen in Figure 6.6a, yet it has very poor acoustic properties compared to the nickel source and the stainless absorber. In contrast, Cu which has very good acoustic matching with the Ni and SS foils does not transport the effect as is clearly seen in Figure 6.6b. From the results of these bridging experiments it is possible to conclude that the sidebands transported across a paramagnetic bridging foil is the result of nuclear phase modulation and not mechanical frequency modulation. The results of this experiment furthur supports the spin wave transport hypothesis in the previous section.

Figure 6.5

Absorber configuration of the rf bridging experiments. The foils were mounted between glass cover slides for mechanical rigidity. The rf field was applied to the foils by mounting the assembly in the induction coil of a tuned LC-circuit.

Absorber Arrangement for

Sideband Transport Experiments

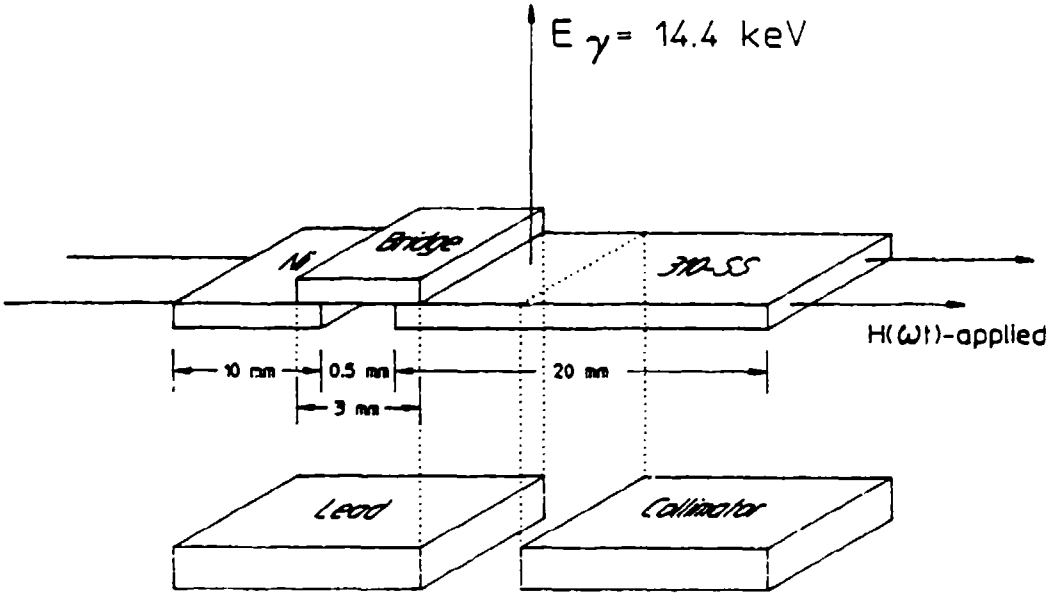

Table 6.1

Summary of experimental results for the rf bridging experiments. As can be seen the mechanism responsible for transporting the magnetically induced sidebands from the nickel source to the stainless steel absorber can be propagated only by paramagnetic materials. The transport of this effect is also independent of the acoustic coupling between the foils. The results of the bridging experiments are consistent with the spin wave hypothesis discussed in the text.

Bridging Material (25 μm)	Susceptibility χ (10^{-6} cgs)	Acoustic Impedence $Z = \rho c$ (10^5 g/cm^{2}sec)	Effect Transported
Aluminum	+ 16.5	17.33	yes
Copper	- 5.46	44.74	no
Silver	- 19.5	37.96	no
310-SS	+ 4000	45.4	yes
Tin	- 37.0	24.24	no
Titanium	+ 153.0	27.32	yes

Figure 6.6

Representative data sets showing (a) the transport of sidebands across a paramagnetic Al bridge and (b) no transport of the effect across a diamagnetic Cu bridge. The bridging foils were both 25 μm thick.

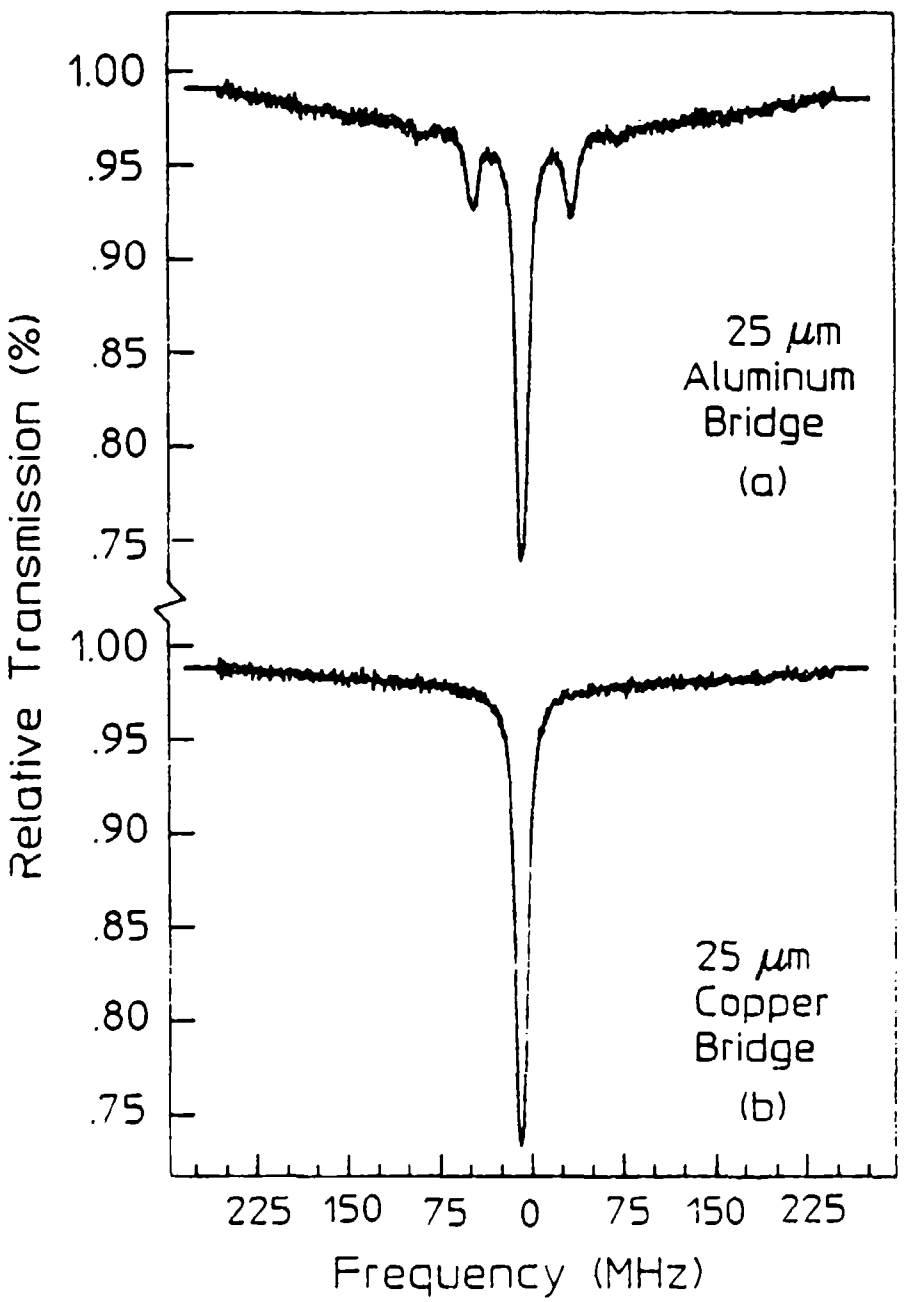
1.00
.95
.90
.85
.80
.75
1.00
.95
.90
.85
.80
.75
Relative Transmission (%)
25 μm
Aluminum
Bridge
(a)
25 μm
Copper
Bridge
(b)
225 150 75 0 75 150 225
Frequency (MHz)

References

1. E. Iko. P. Helisto, J. Hietaniemi and T. Katila, Phys. Rev. Lett. 60, 643 (1988).
2. C. Kittel, Phys. Rev. 110, 836 (1958).
3. P. C. Fletcher and C. Kittel, Phys. Rev. 120, 2004 (1960).
4. E. Schlömann, J. Appl. Phys. 31, 1647 (1960).
5. R. W. Damon and J. R. Eshback, J. Appl. Phys. Supp. 31, 1045 (1960).
6. H. A. Mook, J. W. Lynn, and R. M. Nicklow, Phys. Rev. Lett. 30, 556 (1973).
7. T. Lyman, Metals Handbook, 8th ed. (Am. Soc. for Metals, Ohio, 1961), Vol. I, p. 793.
8. P. Grünberg, J. Appl. Phys. 51, 4338 (1980).

CHAPTER 7

SUMMARY AND CONCLUSIONS

The interaction of the nucleus with long wavelength (rf) radiation has been studied using the Mössbauer effect for more than two decades. As first proposed by Mitin,[1] this interaction could result from a multiphoton interaction where a quantum of rf is simultaneously absorbed along with a quanta of gamma-ray energy under Mössbauer conditions. These multiphoton effects should be observed as sidebands accompanying the usual Mössbauer transitions. While probably observed for 20 years[2] the effects, however, were initially confused with mechanical frequency modulation first reported by Ruby and Bolef[3]. Later researchers,[4-5] studying the influence of rf magnetic fields on the Mössbauer transitions in iron foils enriched with ^{57}Fe, incorrectly assumed that the rf sidebands thus observed were the result of a periodic displacement of the Mössbauer nuclei driven by the magnetostrictive oscillations of the foils. This conceptual error was later compounded by the work of Chien and Walker[7] who developed a scheme where sidebands could be transfered into nonmagnetic absorbers from ferromagnetic driver foils. They incorrectly assumed that under the influence of rf magnetic fields acoustic waves were set up in the ferromagnetic foils and then transferred in to the absorber foil. The acoustic vibrations could then be detected as sidebands on the Mössbauer transitions. This dissertation reports the reexamination of rf sidebands in various absorber arrangements and concludes that the magnetostiction model of rf sideband development is incorrect.

In chapter 4 the results of two experiments were presented which demonstrate that the magnetostrictive model of rf sidebands does not explain the new experimental evidence reported in this work. The first experiment reexamined and extended the Chien and Walker experiment which from current perspective was considered to be the bulwark of the magnetostrictive-acoustic hypothesis. The results of this experiment supported

only the first conclusion reached in that original work, namely that the causitive agent of rf sidebands can be produced in a ferromagnetic layer and then transported into a nonmagnetic layer. Their other conclusion was completely refuted by data presented in Chapter 4 because the effects they attributed to the type of coupling between layers was seen to result from the relative number of magnetic and nonmagnetic layers. In this dissertation it was found that the effect of two ferromagnetic source foils varied from two to four times the effect produced by a single foil, depending upon the static magnetic bias applied, a result not explained by the magnetostrictive-acoustic hypothesis.

The second experiment reported in Chapter 4 demonstrated that the magnetostrictive properties of the absorber foils do not correlate with the observed sideband development. In this experiment two professionally prepared alloys of iron and nickel served as the absorber foils. These alloys or permalloys possessed unusual magnetic properties in that at a composition near 81% Ni the magnetostriction of the foil passed through zero in at least two crystalographic directions. By comparing the sideband development in two foils with compositions near this critical point it was demonstrated that sideband development anticorrelated with magnetostriction and correlated with the higher permeability of the nonmagnetostrictive foil.

In Chapter 5 the results of an experimental investigation into the rf sideband development in the absorption spectra of ^{119}Sn were reported. Here it was found that sidebands could not be propagated into a diamagnetic tin foil from a pair of ferromagnetic drivers, even with the application of rf powers nearly three orders of magnitude greater than that necessary to induce sidebands in a paramagnetic 310 stainless steel foil. Even considering the slightly poorer acoustic coupling between the nickel and tin, as compared to a nickel-stainless interface, the magnetostrictive-acoustic model cannot explain this failure.

In the remaining two experiments reported in Chapter 5, tin was alloyed with iron and nickel forming the magnetic compounds $FeSn_2$ and NiSn. Here it was found that sidebands easily developed with application of reasonable rf powers. The results were explained using nuclear phase modulation theory presented in Chapter 2. By coupling the naturally occuring hyperfine magnetic fields at the nuclear sites with the rf fields, large scale phase modulation effects were observed in these binary metallic compounds.

The experimental results of Chapter 6 represent the most convincing argument against the magnetostrictive-acoustic model. In the first experiment discussed, a direct comparision between ultrasonic and magnetic sidebands was made. As a basis for comparision, sidebands were excited upon the unsplit absorption line of ^{57}Fe nuclei embedded in a paramagnetic 310 stainless steel foil by the sinusoidal vibrations injected with X and AT-cut transducers. In the usual longitudinal geometry for transmission experiments, a convenient level of input power produced a reference level of sideband development that resulted in sidebands up to 4th order, which contained 34% of the intensity remaining in the parent line. In the transverse geometry, the effect of phonons transported in the foil about 1 cm around a bend of 90 degrees could not be detected even with a tenfold increase in rf power above the reference level.

Replacing the piezoelectric source of ultrasonic phonons with a pair of 2.5 μm foils of ferromagnetic nickel subjected to an rf magnetic field, gave the opportunity to launch what is believed are large amplitude spin waves into the magnon fluid of the paramagnetic foil. The longitudinal geometry was used to set the same reference level of sideband development at the source. In the transverse geometry at this same level of input power, the first order sidebands were found to have 20% of the intensity of the parent transition, a level 10 times the threshold for detection and, hence, 100 times any component contributed by acoustic phonons. It is

believed that these sidebands are the result of nuclear magnetic phase modulation of the quantum phases of ^{57}Fe nuclei which were produced by spin waves of large amplitude transported from the ferromagnetic source. This represents an eleven orders-of-magnitude increase in the efficiency through which phase modulation effect can be produced.

The second experiment reported in Chapter 6 further strengthens the argument in favor of spin waves as the transport mechanism of the magnetically induced sidebands. Here it was shown that these sidebands could be propagated from a ferromagnetic source across a paramagnetic "bridge" and then detected in a stainless tape enriched with ^{57}Fe. It was found that sidebands could only be propagated through materials which have a nonzero spin, that is to say sidebands cannot be propagated across a bridge of diamagnetic material.

In summary, the results presented in this dissertation resolve a controversy which has existed in the literature for over 20 years. It was shown that nuclear magnetic phase modulation is indeed observed and that the effect can be transported a considerable distance through a foil by first coupling the rf field to the individual magnons in a material and then coupling to the nucleus, to modulate the quantum phases of the nuclear states.

REFERENCES

1. A. V. Mitin, Sov. Phys. JETP 25, 1062 (1967).
2. G. L. Perlow, Phys. Rev. 172, 319 (1968).
3. S. L. Ruby and D. I. Bolef, Phys. Rev. Lett. 5, 5 (1960).
4. N. D. Heiman, L. Pfeiffer, and J. C. Walker, Phys. Rev. Lett. 21, 93 (1968).
5. L. Pfeiffer, N. D. Heiman, and J. C. Walker, Phys. Rev. B 6, 74 (1972).
6. N. Heiman, R. K. Hester, and S. P. Weeks, Phys. Rev. B 8, 8 (1973).
7. C. L. Chien and J. C. Walker, Phys. Rev. B 13, 1876 (1976).